

Adsorption Study of CO₂ Capture using Date Pits in Continuous Fixed Bed Column

A Thesis submitted to the
University of Petroleum and Energy Studies

For the award of

Doctor of Philosophy

In

Chemical Engineering

By

Mohd Danish

July 2022

Supervisor (s)

Prof. Vijay Parthasarthy

Prof. Mohammed K. Al Mesfer



**Department of Chemical Engineering
School of Engineering (SOE)
University of Petroleum & Energy Studies
Dehradun- 248007: Uttarakhand (INDIA)**

Adsorption Study of CO₂ Capture using Date Pits in Continuous Fixed Bed Column

A Thesis submitted to the
University of Petroleum and Energy Studies

For the award of

Doctor of Philosophy
In

Chemical Engineering

By

Mohd Danish
(SAP-ID 500058054)

July 2022

Internal Supervisor

Prof. Vijay Parthasarthy

Professor, Chemical Engineering
University of Petroleum and Energy Studies

External Supervisor

Dr. Mohammed K. Al Mesfer

Professor, Chemical Engineering
King Khalid University, Saudi Arabia



**Department of Chemical Engineering
School of Engineering (SOE)
University of Petroleum & Energy Studies
Dehradun- 248007: Uttarakhand (INDIA)
July 2022**

DECLARARTION

I declare that the thesis “Adsorption Study of CO₂ Capture using Date Pits in Continuous Fixed Bed Column” has been prepared by me under the guidance of Dr.Vijay Parthasarthy, Professor of Chemical Engineering Department and Mohammed K. Al Mesfer, Professor, Chemical Engineering Department, King Khalid University, Saudi Arabia. No part of this thesis has formed the basis for the award of any degree or fellowship previously.



Mohd Danish

Lecturer, Department of Chemical Engineering

College of Engineering, King Khalid University

Abha 61411 Saudi Arabia

CERTIFICATE

I certify that **Mohd Danish** has prepared his thesis entitled “**Adsorption Study of CO₂ Capture using Date Pits in Continuous Fixed Bed Column**” for the award of PhD degree of the University of Petroleum & Energy Studies, under my guidance. He has carried out the work at the Department of Chemical Engineering, College of Engineering of King Khalid University, (Abha, Saudi Arabia) and Department of Chemical Engineering, University of Petroleum and Energy Studies (Dehradun, India).

It is certified that work has not been submitted anywhere else for the award of any degree of this or any other University.

Supervisor



Dr. Vijay Parthasarthy,

Professor,

Chemical Engineering – Energy Cluster

School of Engineering.



CERTIFICATE

I certify that Mohd Danish has prepared his thesis entitled "Adsorption Study of CO₂ Capture using Date Pits in Continuous Fixed Bed Column" for the award of PhD degree (Chemical Engineering) of the University of Petroleum & Energy Studies, under my guidance. He has carried out the work at the Department of Chemical Engineering, College of Engineering of King Khalid University, (Abha, Saudi Arabia) and Department of Chemical Engineering, University of Petroleum Studies (Dehradun, India).

It is certified that work has not been submitted anywhere else for the award of any degree of this or any other University.

External Co-Supervisor

Dr. Mohammed K. Al Mesfer

Professor, Department of Chemical Engineering

Dean, College of Engineering

King Khalid University, Abha 61411, Asir Saudi Arabia

Date:

ACKNOWLEDGEMENT

I would like to express my deepest gratitude to Prof. P. Vijay, supervisor and Prof. Mohammed K. Al Mesfer, co-supervisor for encouraging me to work on the Adsorption Study of CO₂ Capture using Date Pits in Continuous Fixed Bed Column. My supervisors have been a source of inspiration and motivation to me throughout this work. I am thankful to the to each and every faculty of Chemical Engineering at University of Petroleum and Energy Studies, Dehradun and King Khalid University, Abha for their support and cooperation.

I would like to thank Deanship of Scientific Research, King Khalid University Abha for financial support to carry out the work.

Thank You



Mohd Danish

King Khalid University

Abha, KSA

ABSTRACT

CO₂ increasing volume in the atmosphere is extremely causative to rise in average earth's surface temperature. The utmost overbearing problem is the alarming pace by which the CO₂ volume in the atmosphere is accelerating. The accessible CO₂-reducing techniques have the potential to cut CO₂ emission cost. Many suggested techniques can be adapted to existing plants those rely on non-renewable fuel sources. An adsorption is considered as prominent technology to separate CO₂ from emissions of post-combustion process.

The main aim of the current work is to synthesize activated carbon by suitable activation technique from the vastly available date pits-based biomass, characterize for surface and morphological characteristics and to access the adsorption performance using fixed bed adsorption system for CO₂ capture. The breakthrough response is to be analyzed in terms of feed mixture gas flow, temperature and initial CO₂ level. The different classes of adsorbents i.e. commercial activated carbon, molecular sieve and silica gel are to be examined for comparative adsorption performances. The adsorption performance is required to be investigated in terms of the various characteristics parameters.

The vastly available date pits-based biomass in Saudi Arabia needs to be utilized for synthesizing the porous adsorbent. The objective of the current work is to produce activated carbon for CO₂ capture and to access the adsorption performance in terms of different adsorption characteristics. The activated carbon from date pits have been produced by Physical activation technique using three-zone tubular furnace. The biomass is carbonized and activated at a temperature of 600 °C in the presence of CO₂. The produced activated adsorbent material has been characterized for surface area and surface morphology. The different characterization techniques e.g. BET, XRD, SEM and TGA are applied to characterize the produced activated carbon. The adsorption study of CO₂ capture from a mixture of CO₂/N₂ has been carried out using fixed bed continuous column.

This work reports the breakthrough profiles as a function of temperature, feed mixture flow rate and initial adsorbate concentration and these profiles have been analyzed by breakthrough and saturation periods. The adsorbent effectiveness is predicted as CO₂ adsorption capacity (mmol/g) determined under different set of operating conditions. The capacity utilization factor, column efficiency, length of mass transfer zone and usable bed height are the bed characteristics parameters evaluated to judge the adsorption system performance for CO₂ capture.

The three different type of adsorbents i.e. commercially available activated carbon (Norit-RB2), molecular sieve 3Å and silica gel have been used for CO₂ adsorption study to provide ease in comparison of adsorption capacity and to evaluate the effect of surface and morphological characteristics on adsorption capacity. These adsorbents have also been characterized by suitable technique. The exothermic nature of the CO₂ capture by adsorption is examined by temperature profiles produced using the temperatures measured by Type-K thermocouples positioned at fixed distances inside the column. The repeatability of the measured data is depicted in terms of mean error and coefficient of determination (R^2). The accuracy analysis of the all measuring instruments has been carried out.

Table of Contents

Topic	Page no.
Abstract	vii
Table of Contents	ix
List of Figures	xii
List of Tables	xv
Nomenclature	xvii
1. Introduction	1
1.1 Need of Research	2
1.2 Objectives of Research	3
1.3 Research Methodology	3
1.4 Thesis Outlines	4
2. Literature Review	5
2.1 Introduction to Literature review	5
2.2 CO ₂ emissions and global temperature rise	5
2.3 CO ₂ reduction technologies	6
2.4 Post-combustion reduction technologies	7
2.5 CO ₂ capture by adsorption	8
2.6 Adsorption using commercial adsorbents	9
2.7 Adsorption using modified commercial adsorbents	16
2.8 Adsorption using modified and biomass-derived activated carbon	20
3. Methodology	32
3.1 Materials	32
3.2 Experimental	32
3.3 Procedure	35
3.4 Adsorption isotherms, kinetics and modeling	36
3.4.1 Adsorption isotherms	36
3.4.2 Kinetics	38
3.4.3 Modeling	40
3.5 Physical activation of date based biomass	41
3.6 Adsorbent characterization	41
4. Results and discussion	42

4.1 Adsorption study using commercial Norit-RB2	42
4.1.1 Characterization of Norit-RB2	42
4.1.2 Breakthrough profiles of Norit-RB2	45
4.1.3 Adsorption capacity and column efficiency for Norit-RB2	49
4.1.4 Mass transfer zone and capacity utilization factor for Norit-RB2	53
4.1.5 Temperature profiles and repeatability measurement for Norit-RB2	56
4.2 Adsorption study using molecular sieve 3Å	58
4.2.1 Characterization of molecular sieve 3Å	58
4.2.2 Breakthrough profiles for molecular sieve 3Å	60
4.2.3 Adsorption capacity and column efficiency for molecular sieve 3Å	64
4.2.4 Mass Transfer zone and capacity utilization factor for molecular sieve 3Å	67
4.2.5 Temperature profiles and repeatability measurement for molecular sieve 3Å	68
4.3 Adsorption study using Silica gel type-III	70
4.3.1 Characterization of Silica gel type-III	71
4.3.2 Breakthrough profiles for Silica gel type-III	73
4.3.3 Adsorption capacity and column efficiency for Silica gel type-III	77
4.3.4 Mass Transfer zone and capacity utilization factor Silica gel type-III	80
4.3.5 Temperature profiles and repeatability measurement for silica gel type-III	81
4.4 Adsorption study using synthesized date pits based activated carbon AC-DS	83
4.4.1 Synthesis of activated carbon by physical activation AC-DS	84
4.4.2 Characterization of date-pits activated carbon AC-DS	85
4.4.3 Breakthrough profiles of date-pits based activated carbon AC-DS	91
4.4.4 Adsorption capacity and column efficiency for date-pits activated carbon AC-DS	96
4.4.5 Mass Transfer zone and capacity utilization factor for date-pits activated carbon AC-DS	102
4.4.6 Temperature profiles and repeatability measurement for AC-DS	104
4.5 Adsorption isotherms study	106
4.6 Comparative analysis of adsorption performances	109
4.6.1 Adsorption performances of investigated adsorbents	109

4.6.2 The comparative adsorption performances of current process with literature	113
4.7 Quantitative assessment of error	114
5. Conclusions and future recommendations	116
5.1 Conclusions	116
5.2 Future recommendations	117
References	118
Summary of published articles	131
Annexure I-Plagiarism report	132

LIST OF FIGURES

Fig.3.1(a) Sketch of continuous fixed bed adsorption column	33
Fig.3.1(b) Setup layout of continuous fixed bed unit	33
Fig.3.1(c) Top view of continuous fixed bed unit	34
Fig.3.1(d) Thermocouple positions in continuous fixed bed adsorption column	34
Fig.4.1 Commercial activated carbon Norit RB-2	42
Fig.4.2 N ₂ -adsorption isotherm and pore size distribution: (a) Experimental N ₂ adsorption isotherm for AC-Norit, (b) BJH pore size distribution for AC-Norit	44
Fig.4.3 SEM images of AC-Norit: (a) 2,500 x magnification and (b) 20,000 x Magnification	45
Fig.4.4 Temperature dependent breakthrough profiles for AC-Norit at F= 4 L/min, C _o =5%	46
Fig.4.5 Flow rate dependent breakthrough profiles for AC-Norit at T=298 K, C _o =5%	47
Fig.4.6 CO ₂ concentration dependent breakthrough profiles for AC-Norit at F= 4 L/min, T= 298 K	48
Fig.4.7 Adsorption breakthrough profile and shifting of MTZ	54
Fig.4.8 Temperature profiles along axial positions for AC-Norit at F= 4 L/min and C _o = 5%)	57
Fig.4.9 Molecular sieve 3Å (MS-3Å)	58
Fig.4.10 Scanning electron microscope characterization of molecular sieve MS-3Å	59
Fig.4.11 Temperature dependent breakthrough profiles for MS-3Å at F= 4 L/min, C _o =5%	60
Fig.4.12 Flow rate dependent breakthrough profiles for MS-3Å at C _o =5%, T= 298 K	62
Fig.4.13 CO ₂ concentration dependent breakthrough profiles for MS-3Å at F= 4 L/min, T= 298 K	63
Fig.4.14 Temperature curves for MS- 3Å at F= 4 L/min and C _o = 5%	69
Fig.4.15 Repeatability assessment utilizing MS-3Å at F= 4 L/min, C _o =5% and T= 328 K	70

Fig.4.16 Silica gel type-III used for adsorption study	70
Fig.4.17 N ₂ adsorption isotherms for silica gel type-III	72
Fig.4.18 BJH pore size distribution for silica gel type-III	72
Fig.4.19 Morphological image of Silica gel type-III	73
Fig.4.20 Breakthrough profiles at various temperatures at F= 4 L/min, C _o =5% for Silica gel type-III	74
Fig.4.21 Breakthrough profiles at various feed flow at T= 298 K, C _o =5% for Silica gel type-III	75
Fig.4.22 Breakthrough profiles at various CO ₂ level with F= 4 L/min and T= 298 K for Silica gel type-III	76
Fig.4.23 Temperature contours for Silica gel type-III at F= 4 L/min and C _o = 5%	82
Fig.4.24 Repeatability assessment utilizing SG at F= 4 L/min, C _o =5% and T= 308 K	82
Fig.4.25 Date tree with dates	83
Fig.4.26 Rinsed and cleaned date pits before size reduction	84
Fig.4.27 Produced activated carbon from date pits by physical activation	85
Fig.4.28 N ₂ adsorption isotherms and pore size distribution (a) Experimental adsorption isotherm	87
Fig.4.29 Morphological images of produced activated carbon AC-DS	88
Fig.4.30 Thermogravimetric analysis of (a) date stone biomass, and (b) porous AC-DS	89
Fig.4.31 XRD of date pits derived porous activated carbon AC-DS	90
Fig.4.32 Raman spectra for the produced activated carbon AC-DS in the spectrum range 0 – 3500 cm ⁻¹	91
Fig.4.33 Breakthrough profiles at various temperatures for activated carbon AC-DS at F= 4 L/min, C _o =5%	92
Fig.4.34 Breakthrough profiles at different feed flow rates for AC-DS at T= 298 K with C _o =5%	94
Fig.4.35 Breakthrough profiles at different CO ₂ level for AC-DS at F= 4 L/min and T= 298 K	95
Fig.4.36 Parametric dependence of CO ₂ uptake; (a) at different temperatures with C _o = 5%, F= 4 L/min, (b) at different feed flows with C _o = 5%, T= 298 K	101

and (c) at different initial levels with $T = 298 \text{ K}$, $F = 4 \text{ L/min}$	
Fig.4.37(a) Breakthrough profile and narrow MTZ, and (b) breakthrough profile and wide MTZ	103
Fig.4.38 Temperature profiles along axial positions inside the column for AC-DS	105
Fig.4.39 Repeatability measurement of adsorption-desorption data of AC-DS	106
Fig.4.40 (a) Langmuir Isotherms (b) Freundlich Isotherm (Experimental conditions: $T = 298 \text{ K}$, $Q = 4 \text{ L/min}$)	107
Fig.4.41 Error bar analysis of adsorption capacity, length of mass transfer zone and capacity utilization factor	115
Fig.4.42 Error bar analysis of efficiency based on column capacity and usable bed height	115

LIST OF TABLES

Table 2.1 Adsorption capacity for CO ₂ capture reported using commercial Adsorbents	15
Table 2.2 Adsorption capacity for CO ₂ capture reported using modified Adsorbents	20
Table 2.3 Adsorption capacity for CO ₂ capture reported using modified and biomass- derived activated carbon	30
Table 3.1 Sensitivity analysis of the sensors used for measurements	36
Table 4.1 BET Surface characterization results for commercial activated carbon AC-Norit	43
Table 4.2 The temperature dependent adsorption performances for AC-Norit (F= 4 L/min, C _o =5%)	51
Table 4.3 Feed rates dependence adsorption performance for AC-Norit (C _o =5%, T=298 K)	52
Table 4.4 CO ₂ concentration dependence adsorption performance (F= 4 L/min, T=298 K)	53
Table 4.5 Summary of characteristic parameters for CO ₂ capture of AC-Norit activated carbon	55
Table 4.6 BET Surface characterizations of molecular sieve MS-3Å	59
Table 4.7 Adsorption characterizations at different temperatures MS-3Å (F= 4 L/min, C _o =5%)	65
Table 4.8 Adsorption characteristics at various feed rates for MS-3Å (T=298 K, C _o =5%)	66
Table 4.9 Adsorption characteristics at different initial CO ₂ concentrations for MS-3Å (T=298 K, F= 4 L/min)	66
Table 4.10 Summary of characteristic CO ₂ capture parameters of MS-3Å	67
Table 4.11 BET Surface characterizations of silica gel type-III	71
Table 4.12 The dependence of temperature on CO ₂ capacity, column efficiency and usable bed height for SG at C _o =5% and F= 4 L/min	77
Table 4.13 The dependence of flow rate on CO ₂ capacity, column efficiency and usable bed height for SG at T=298 K and C _o =5%	78
Table 4.14 The dependence of initial CO ₂ level on capacity, column efficiency	79

and usable bed height for Silica gel type-III at T=298 K and F= 4 L/min	
Table 4.15 Characteristic parameters of CO ₂ adsorption for Silica gel type-III	80
Table 4.16 BET surface characterization of Date-pits derived activated carbon AC-DS	86
Table 4.17 Adsorption characterizations for AC-DS at different temperatures With F= 4 L/min and C _o =5%	96
Table 4.18 Feed rates dependence on adsorption performance for AC-DS at C _o =5%, T=298 K	98
Table 4.19 Adsorbate concentration dependence on adsorption performance for AC- DS at F= 4 L/min, T=298 K	99
Table 4.20 Characteristic parameters of CO ₂ adsorption for produced porous carbon AC-DS	104
Table 4.21 Langmuir and Freundlich isotherm constants for CO ₂ adsorption on AC-DS adsorbent	108
Table 4.22 Comparative breakthrough time and adsorption capacity obtained for various classes of adsorbents	109
Table 4.23 Comparative analysis of adsorption capacity, column efficiency and usable bed height	111
Table 4.24 Comparative analysis of length of mass transfer zone and capacity utilization factor	112
Table 4.25 Comparative adsorption performances of current process with literature	113

NOMENCLATURE

C	Column exit CO ₂ concentration, vol.%
C _o	Initial concentration of CO ₂ in feed, vol.%
F	Feed rate, L/min
L	Total bed height, cm
L _b	Usable bed height, cm
L _{MTZ}	Length of mass transfer zone, cm
P*	CO ₂ partial pressure, N/m ²
T	Column temperature, K
f	Capacity utilization factor
m _{ad}	Mass of adsorbent, g
t	Adsorption-desorption time, s
t _b	Breakthrough time, s
t _{st}	Stoichiometric time, s
t _s	Saturation time, s
q	Adsorption capacity, mmol/g
q _u	Column capacity upto breakthrough, mmol/g
η	Efficiency based on column capacity

Subscript

MTZ	Mass transfer zone
ad	Adsorbent
b	Breakthrough
o	Initial
st	Stoichiometric
u	Usable

CHAPTER 1: INTRODUCTION

Continuously increasing concentration of CO₂ in the environment is very contributory to increase in average surface temperature of earth. It is the major contributor to global warming. The paramount domineering problem is the worrying pace at which the CO₂ amount is accelerating in the atmosphere [1]. Global warming is mostly due to the carbon dioxide amongst all the greenhouse gases. The burning of fossil fuels during power generation, industrialized processes and transportation are the core sources accountable for CO₂ discharge into the environment. The 81% of world's commercial energy requirement is fulfilled by the incineration of fossil fuels with the emission of 3.0×10^{13} Kg CO₂ on yearly basis [2]. The available CO₂ reduction techniques have the prospective to reduce cost of CO₂ emission into the atmosphere.

As the necessity of the electricity is projected to rise in developed and developing countries, the power generation will add to nearly half rise in over-all emissions between 2000 and 2030 years [3]. The thermoelectric and industrial plants are imperative source of CO₂ release which amount to 45% of global CO₂ release in the atmosphere [4]. The level of carbon dioxide concentration has increased from 280 ppm to 370 ppm with an inclusive earth temperature increase from 273.6 K to 274 K (0.6 °C to 1 °C) through the same period. An increase in global temperature greater than 275 K (2 °C) will leads to extensive consequences and therefore, the overall greenhouse gases required to be reduced at least 50% by 2050 year [5]. The reasonable increase of CO₂ concentration level in the environment is becoming a significant environmental problem [6].

The carbon dioxide lessening technologies are viewed as decisive alternatives to make economical cuts in greenhouse gas emissions. Physical and chemical

absorption, cryogenic separation, membrane based and adsorption are the leading technologies in use to separate CO₂ from the emissions of fossil fuel based power plant. The chemical or physical absorption banks on the reaction between carbon dioxide and aqueous solutions of mono-, di-and tri-amine etc. [7].

In situation, where feed stream has CO₂ composition greater than 50%, the cryogenic separation is normally applied [8]. The membrane based separation systems are greatly applicable for CO₂ amount greater than 20% [9]. Depending on the plant configurations, the CO₂ release into the atmosphere can be regulated by any one of the three methods - a) oxy-fuel combustion, b) post-combustion, and c) pre-combustion [10]. The pre-combustion includes with treatment of synthesis gas having majority of H₂ and CO₂ in the mixture [11]. In oxy-fuel combustion, the emissions largely consist of H₂O and CO₂ in 70-95% range [12]. The 1.5 times extra energy is needed in post-combustion compared to pre-combustion [13]. Capturing of CO₂ applying post combustion technique is well-thought-out as high thermal efficiency process.

1.1 NEED OF RESEARCH

An adsorption is foreseen as prime potential options to adsorb CO₂ from flue gases due to its low energy constraint, simplicity from application viewpoint over varied range of temperature/pressure and cost benefits. The CO₂ decrease through post-combustion includes the adsorption of CO₂ from the emissions of combustion process. The lesser amount of CO₂ (13-15 %: coal based plant, gas based plant: 7-8%) requires higher volume of gas in turn needs bigger equipment size and high capital costs. The fixed percentage of CO₂ is always accompanied with post-combustion flue gases depending on the feed stock. The Kingdom of Saudi Arabia has plenty of date pits-based biomass and it is the need of hour to utilize the vastly available date-based biomass for useful purpose.

The Kingdom positions at 11th in the rank of CO₂ discharging countries with the release of 5.17×10^8 tons CO₂ in the year 2016. Consequently, there is necessity to synthesize activated carbon for CO₂ capture adopting suitable technology. An

adsorption is well-thought-out as established technology to separate CO₂ by adsorption in post-combustion process [14-15]. The post-combustion CO₂ reduction is primarily a convincing process due to the fact that various suggested technologies can be retrofitted to prevailing plants based on fossil fuel [16-18]. The adsorbent favorably adsorbs CO₂ and subsequently regenerates to release CO₂ irrespective of process configuration [19-20]. There is no byproduct such as H₂O in carbon dioxide capture by adsorption and assumed as dry process.

1.2 OBJECTIVES OF THE RESEARCH

The chief objectives of the current work for CO₂ capture using date pits-derived activated carbon in continuous fixed bed column are summarized as follows:

- To develop porous activated carbon from date pits based biomass for CO₂ capture by physical activation technique.
- To produce and analyze breakthrough profiles for all the adsorbents i.e. developed activated carbon, commercial activated carbon, molecular sieve 3A and silica gel as function of temperature, feed flow and CO₂ initial concentration.
- Analyzing the adsorbent in terms of breakthrough and saturation periods for CO₂ adsorption.
- Estimating adsorption performance i.e. CO₂ adsorption capacity (mmol/g) under different operating conditions.
- Predicting the performance characteristics in terms of capacity utilization factor (f) and length of mass transfer zone (L_{MTZ}).
- Determining the adsorbent characteristics in terms of column efficiency ($\eta\%$) and usable bed height (L_b).

1.3 RESEARCH METHODOLOGY

The numerous investigations have been carried on the synthesis of carbon adsorbent from biomass based material for CO₂ capture. Most of study for CO₂ capture has been conducted in batch mode based on activated carbon obtained

from date pits. The investigations on the CO₂ capture using continuous fixed bed column with date pits based activated carbon are rare. In the present work, vastly available date pits based biomass is converted to activated carbon using physical activation. The produced activated carbon in addition to other class of adsorbent e.g. commercial activated carbon Norit RB-2, molecular sieve MS-3Å and silica gel (SG) have been characterized by TGA, BET, XRD, Raman and SEM for surface, morphological and structural properties. All four types of adsorbent have been tested for dynamic adsorption in continuous fixed bed column for adsorption performances. The breakthrough data of column exit concentration measured with adsorption time. An adsorption temperature, feed rate, and initial CO₂ amount in feed are the operating conditions examined. The CO₂ adsorption performances have been analyzed in terms of breakthrough/saturation time (s), adsorption capacity (mmol/g), length of mass transfer zone (cm), utilization factor (f), efficiency based on column efficiency (η) and usable bed height (L_b). The extend of adsorption is explained by temperature rise above the set point during adsorption phenomenon. The repeatability of the CO₂ adsorption data was measured to check the reliability of measurement.

1.4 THESIS OUTLINES

The thesis contains the following sections:

- Chapter 1 Introduction
- Chapter 2 summarizes the literature review that illustrate the general know-how of activation of different biomass specially date pits-based biomass for CO₂ capture application in addition to the adsorption study conducted utilizing commercial and modified adsorbents.
- Chapter 3 includes the detailed description of apparatus, materials and methodology for experimental purpose.
- Chapter 4 describes the results along with detailed description.
- Chapter 5 includes the conclusions and recommendations for future work.

CHAPTER 2: LITERATURE REVIEW

2.1 INTRODUCTION TO LITERATURE REVIEW

The current chapter covers literature review on different types of adsorbents: modified, synthesized or commercially available for CO₂ capture and other similar applications. Section 2.2 gives an overview of CO₂ emissions and global temperature rise. Section 2.3 describes the literature review on the available technologies for CO₂ capture. The technologies for post-combustion CO₂ capture by adsorption very well explained in Section 2.4. The Section 2.5 specifically dedicated to adsorption. An adsorption using commercial adsorbents has been explained under the Section 2.6 whereas Section 2.7 covers literature review on adsorption using modified commercial adsorbents. The literature on the adsorption study using modified and biomass-derived activated carbon has been extensively reviewed under the section 2.8 in detail.

2.2 CO₂ EMISSIONS AND GLOBAL TEMPERATURE RISE

The surge of CO₂ quantity in atmosphere has become the core factor in the stride of global temperature increase [1]. It is the chief causative to global warming condition. The role and adsorption performance of various classes of adsorbents for anthropogenic CO₂ from combustion emissions preceding to emission into an atmosphere have been examined and reviewed. The continuously rising level of CO₂ in the atmosphere is assumed as severe problem for all manhood on the earth. Amongst all the greenhouse gases, CO₂ is the single largest donor to global warming resulting in rise in earth temperature. The 81% of world's overall energy requirement is met by the incineration of fossil fuels with discharge of 3.0×10^{13} kg CO₂ on yearly basis [2]. The technique of capture CO₂ and separation of

harmful gas from main sources e.g. fossil-fuel based power plants need to be industrialized to decrease the quantity emitted to the environment through human related actions. The available CO₂-reducing techniques have the prospective to cut the cost of CO₂ emissions in the atmosphere. As the necessity of the electricity is projected to surge in developed and developing countries, the power generation will attribute to nearly half rise in over-all emissions between 2000 and 2030 [3]. The growth will require substantial reduction in gross global emissions by 2030-2050 years to evade considerably high volume of CO₂ in the atmosphere. The Kingdom of Saudi Arabia has blessed with an abundance of date pits-based biomass and it is advantageous to utilize the date-based biomass for useful purpose. The Kingdom stands at 11th position in the rank of CO₂ emitting countries with the release of 5.17×10^8 tons CO₂ in the year 2016.

2.3 CO₂ REDUCTION TECHNOLOGIES

The progress and advancement in CO₂ separation and capture technologies have been reviewed thoroughly and various technologies i.e. absorption, adsorption and membrane separation have been described in detail [16]. The CO₂ emission into an atmosphere can be reduced by any one of three routes i.e. reducing energy intensity, decreasing carbon intensity and augmentation of carbon sequestration of CO₂. The initial option can be achieved by effectual utilization of energy. The 2nd alternative requires moving to non-fossil resources like renewable and hydrogen energy. The last route includes an improvement in technologies for CO₂ capture and sequesters more and more CO₂.

In an international standpoint, amongst all the activities releasing carbon dioxide, the power plants utilize fossil fuel yield the highest volume of CO₂ emissions contributing to almost 30-40 % of the total emissions [21-22]. The carbon dioxide desired to be captured from flue gas before of such source in advance to sequestration. For such power plant, carbon dioxide separation/capture is distributed into three dissimilar situations: pre-combustion process, post-combustion process, and oxy-fuel processes. Chemical combustion looping (CLC)

which is newly developed technology significantly decreases the intricacy of separating CO₂ from gaseous stream.

The CO₂ is captured from combustion emissions environs comprising SO₂ and NO_x under post-combustion method. This technique is commonly applied in processing of chemical. In the pre-combustion process, initially a mixture of CO₂/H₂ is produced from fuels through reforming process and succeeding shift-reaction. The CO₂ later, segregated from product stream and H₂ then incinerated in gas turbine or utilized in fuel cell. The clean O₂ is segregated from air and afterwards directed to energy conversion section and mixes with partly recycled flue gas of concentrated CO₂ to maintain the temperature of furnace below the permissible point in oxy-firing process. The combustion occurs in the environs of CO₂ and O₂. This separation method is beneficial due to: i. simpler to integrate into the existing plant without significant change to plant layout. ii. more appropriate for gas plants. iii. flexible as its repairs/maintenance does not discontinue the process of the running plant.

2.4 TECHNOLOGIES FOR POST-COMBUSTION CARBON CAPTURE

The numerous technologies for post-combustion application described in detailed with emphasis on physical adsorption of carbon dioxide [23] and it is well-thought-out as most efficient and least interfering way of carbon capture from emissions of post-combustion process. A few and largely post-combustion separation technologies are: a) absorption [24], b) membrane based, c) cryogenic, and d) adsorption.

Absorption of CO₂ is a separation process in which CO₂ is separated from combustion emissions by an absorbent solution preferably amine through reaction leaving the residual gas to move into the column [25]. The less-concentrated absorbent is yet again-concentrated for re-use in the process. CO₂ capture by absorption utilizing amine type solvents offer a number of drawbacks e.g. high heat/power requisite for regeneration of the solvent, necessity control measures for corrosion and solvents sensitivity loss in chemical purity/quality owing to

permeations from by-products into the flue gas stream yielding to reduction in efficiency.

The usage of membranes prepared from polymer/ceramic to screen out the greenhouse gas from combustion emissions is involved in membrane based separation process. The polymer/ceramic materials are utilized to make these membranes and their structures are planned for higher selectivity of CO₂. Tasks are still being tackled to use these membranes on commercial level to fabricate membrane that would operate competently for required objective at reasonably increased temperatures. The CO₂ separation using cryogenic applies the concept of liquid state temperature and pressure differential in constituent gases of the combustion emissions. In this method, CO₂ is cooled and condensed, consequently recovered from the flue gas stream [26].

2.5 CO₂ CAPTURE BY ADSORPTION

The principle of variances in adsorption/desorption characteristics of the components of mixture is applied in adsorptive separation. The term “adsorption is described as the adhesion of atoms, ions or molecules from a gas, liquid or solid in dissolve form to a solid surface [23]. The attached atoms, ions or molecules develop thin layer on the materials’ surface to which they are attached and are named as an adsorbate whereas the material on which they are adhered is branded as an adsorbent. An adsorption might take physically and this includes weak van der Waals forces called as physi-sorption. It might occur chemically, which will include covalent bonding termed as chemi-sorption. It possibly will take place owing to electrostatic attraction. Some absorption limitations such as lesser gas-liquid contact area, small CO₂ loading, and adsorbent losses have moved the attention toward the adsorption [27].

Several studies have been dedicated on utilizing different class of adsorbent for CO₂ capture. A number of chief biomasses have been utilized to develop activated for CO₂ capture by adsorption based separation. By and large, two-step and one-step procedure is realistic to produce activated carbon using physical activation

method. Biomass is initially carbonized to produce char and thereafter produced char is activated with steam/ CO_2 to develop high surface area and porous activated carbon under two-step process. Two-step activation procedure may possibly be combined into one-step procedure by evading separate carbonization step. The biomass materials are first impregnated by dehydrating agents and after that, carbonized at preferred conditions usually with activating agents e.g. $\text{H}_3\text{PO}_4/\text{HNO}_3/\text{ZnCl}_2$ and base for example KOH and NaOH under chemical activation technique. The process simplicity and capability to develop activated carbon of high porosity and improved physical characteristics ascribed to physical activation and appropriate for large scale production of adsorbent. The requirement of time consuming washing stage to remove an activating agent from carbon, is chief drawback of technique of chemical activation.

2.6 ADSORPTION STUDY USING COMMERCIAL ADSORBENTS

A commercial activated carbon with average diameter of 3 mm was utilized for CO_2 capture by adsorption [14] from a mixture of $\text{CO}_2/\text{H}_2/\text{N}_2$ to yield clean H_2 gas. The surface response methodology was applied to investigate the collective influence of CO_2 pressure and temperature on CO_2 loading and breakthrough period in the temperature range of 298 - 338 K with system pressure ranging from 1 to 3 bars. The mass of adsorbent equivalent to 3.22 g was utilized for the study. The highest CO_2 loading of 3.98 mmol/g was attained at 3 bars and reduced to 2.46 mmol/g with reduced pressure to 1 bar. It was observed that there is certainly no interaction influence between the variables on the adsorption response.

An experimental study of pure/binary equilibrium of CO_2 and CH_4 adsorption for the commercial porous carbon RB2 at 293 K and 298 K has been carried out [28]. The mass of adsorbent equivalent to 1 g was used for an investigation. The effect of pressure in the range of 0 - 3.5 MPa specifically for pure gases and 0 - 0.1 MPa for mixture of gases applied was examined to assess the system performance. The capture capacity of 10.7 mmol/g was attained at 273 K and reduced to 9.4 mmol/g at 298 K under constant pressure of 3 MPa. Also, the single-gas isotherms

investigated applying equation known as Dubinin-Astakhov with 3-parameters related with the micro-texture of carbon based adsorbent.

An experimental study of CO₂ capture for CO₂/CH₄ mixtures on an activated carbon at a temperature of 293 K was performed and experimental data were equated with Ideal adsorption solution theory and also, with an Extended Langmuir model [29]. The adsorbent mass equivalent to 2.48 g was used in the study. The highest adsorption capacity of pure CO₂ adsorption was tabulated equal to 10.5 mmol/g at 1.5 MPa and reduced to 8.4 mmol/g at 1 MPa at a fixed temperature of 293 K. Increased CO₂ loading was exhibited for CO₂ as compared to that for CH₄ under the same and constant operating conditions of temperature and pressure.

Higher selectivity was obtained at 0.1 MPa with a maximal selectivity of 8.7 for nearly equimolar mixture of CO₂ /CH₄. Sound supported fluidized bed was experimented for CO₂ separation on fine grade activated carbon [30]. The influence of CO₂ partial pressure, sound intensity/frequency, and fluidization velocity was examined. The adsorption performance was examined by capture capacity and portion of bed utilized at breakthrough period. The highest adsorption capacity of 0.55 mmol/g and a breakthrough time of 169 s were obtained at ambient temperature and pressure at 1cm/s superficial velocity. It was established that acoustic field positively influence an adsorption efficiency as a function of prolonged breakthrough period, CO₂ loading and fraction of bed used.

The impact of temperature and adsorbate pressure on CO₂ capture by temperature swing adsorption has been investigated [31]. The breakthrough and regeneration experiments were conducted in lab scale sound aided fluidized column to calculate the CO₂ working capacity. The utmost adsorption capacity of 0.43 mmol/g was determined at 298 K with 20% adsorbate in the feed mixture. Six commercial zeolites were used for CO₂ adsorption from a mixture of CO₂/CH₄ at atmospheric pressure [32] and NaX adsorbent exhibited the maximal adsorption performance for CO₂ at 0.1 MPa. The selectivity exhibited by ideal adsorbed

solution theory (IAST) model was 76 for NaX type zeolite. It was also determined that moisture considerably decreases the separation performance of zeolites and pre-drying of zeolites is essential step for enhanced adsorption performance. It was also perceived that thermal desorption is appropriate for zeolites regeneration.

The pure and binary adsorption profiles of CO₂ and methane adsorption using zeolite 5A of 3 mm apparent diameter were examined at various temperatures with maximal pressure of 10 bars [33]. An adsorption capacity of 4.5 mmol/g was determined at 273 K with a pressure of 273 K and reduced to 3.8 mmol/g at 5 bars under similar constant temperature. It was also suggested that adsorption capacity decreased significantly with augmented temperature. The experimental pure data for carbon dioxide and methane were very well described by the Langmuir-Freundlich and Toth isotherms, respectively. The vacancy solution theory (VST) and Ideal adsorbed solution theory (IAST) which adopts idyllic performance of mixture, do not give adequate estimate for CO₂/CH₄ adsorption system.

The fixed bed adsorption investigation was conducted for temperature in the range of 313 K to 473 K with 5 atm total pressure and the maximal loading equivalent to 4.7 mmol/g was determined for CO₂ at 313 K in 1:1 equimolar mixture of both the components [34]. The selectivity ranges from 37 at low pressure of 0.667 bars to 5 with an increased temperature at 423 K. The binary isotherm profiles were very well fitted by extended Fowler model that assumed interaction affect among molecules at adsorption spots. The calculated interaction parameter recommends reasonable repulsion between adsorbed CO₂ and CH₄ molecules.

An experimental and thermodynamic modeling of adsorption of CO₂ on zeolite 13X was performed at various temperatures ranging from 273 K to 343 K with pressure upto 10 bars for pure component [35]. The determined pure isotherms were regressed using various isotherm equations. The real adsorbed solution theory (RAST) that includes activity coefficient as describing parameter for non-ideality exhibited improved results for the binary equilibrium. The adsorption cell

was made-up of SS adsorption column with a diameter of 2.8 cm. The CO₂ loading of 6.1 mmol/g was achieved at 273 K temperature with 10 bar pressure and capacity decreased to 5.7 mmol/g by reducing the pressure to 6 bars. The vacuum swing adsorption (VSA) was applied for CO₂ removal to upgrade methane using Zeolite 13X with average diameter of 0.7 mm at various temperatures and pressure upto 5 bar [36]. The experimental isotherm of CO₂ was defined by Toth equation and the isotherms of CH₄ and CO₂ were very well described by Langmuir equation. The highest CO₂ capacity of 6 mmol/g was determined at 308 K and decreased to 5.5 mmol/g at 323 K under constant pressure of 5 bars. A 4-step VSA cycle was recommended and authenticated experimentally to adsorb CO₂ upto 3.7 % level in the stream of methane.

The CO₂ adsorption and kinetics on numerous microporous materials have been investigated at three different temperatures and pressure upto 100 kPa [37]. Different porous materials i.e. Zeolites, MOFs, activated carbons and clays were examined for the adsorption study. The non-isothermal and isothermal diffusion models were applied to determine diffusion time constant from breakthrough curves. It was observed that zeolites have the highest affinity for CO₂ and the isotherms exhibited maximal saturate loading. The lowest adsorption capacity was obtained for clay-type adsorbent. It was also proposed that the Darken equation exhibits good prediction of diffusion time constant for all examined adsorbents.

The maximal CO₂ uptake of 5.4 was achieved for 13X at 273 K and 1bar pressure. The kinetics of pure gases including CO₂ and an adsorption equilibrium on 13X adsorbent were investigated via volumetric method at various temperatures with a pressure upto 10 bars [38]. Isotherms were correlated with different models and Ship model exhibited a lesser deviation than Langmuir model. An adsorption loading of 5.6 mmol/g was determined at an adsorption temperature of 273 K and 10 bars and reduced to 5 mmol/g under constant temperature at 1 bar pressure. The minimal adsorption capacity was reported for H₂ under the same operating conditions of temperature and pressure.

A study of CO₂ capture for flue gas (dry) was performed to meet the requirement of carbon capture and sequestration (CCS) using 13X zeolite [39]. Temperature swing adsorption (TSA) and two stage vacuum swing (VPSA) adsorption were designed, equated and simulated at lab-scale. It offered a great benefit in terms energy consumption and productivity with a value of and 0.79 MJ/Kg_{CO2} and 3.8 mmol/g/h, respectively. A study on the determination of sustainable CO₂ and H₂O adsorption on zeolite 13X was performed for CO₂ adsorption [40] in the range of 295 K to 373 K for temperature applying volumetry and gravimetry. The equilibrium data was found to fit with dual-site Langmuir isotherm. The equilibrium data showed maximal 98% loading reduction for CO₂ at 74% RH while H₂O exhibited no reduction equated to its single component loading.

The kinetics and adsorption equilibria for N₂, N₂O, CO₂, and O₂ using Silica gels with adsorbent average size 3.3 mm were determined at different temperatures using volumetric method upto 10 bars [41]. The results obtained for Silica gel were compared with activated carbon. The maximal CO₂ loading of 4.8 mmol/g was determined at a temperature of 293 K with 10 bars pressure. Breakthrough curves and adsorption isotherm were very well described by diffusion model for non-isothermal condition and Sips model, respectively. The equilibrium and kinetics of CO₂ adsorption onto carbon molecular sieve, zeolites and activated carbon were investigated over varied range of operating conditions [42]. Amongst all the six adsorbents examined, the activated carbon exhibited maximal capacity where zeolites 4A provide lowest adsorption capacity.

The comparative pressure swing adsorption study of investigating adsorption performances for CO₂-N₂ and CO₂-CH₄ separations using zeolites and activated was carried out to gauge selectivity, adsorption capacity and reusability [43]. The temperature was adjusted in the range of 273 K to 348 K with pressure upto 8 bars. At a pressure above 4 bars, the adsorption loading determined for activated carbon is greater than that obtained for zeolites and maximal CO₂ capacity of 10.5 mmol/g was reported at 8 bars and 298 K temperature.

The performance of CO₂ and CO adsorption at 303 K was examined using different adsorbents for potential separation of syngas [44]. Two activated aluminas, 20 zeolites, 2 silica gels and 3 activated carbons were utilized to determine pure gas isotherms and the loading of CO₂ and CO were investigated independently by system based on gravimetry. Carbon dioxide is more favorably adsorbed compared to carbon monoxide. The capture capacity of 6.5 mmol/g was achieved for activated carbon (Xtrusorb A754) at 303 K with 1 bar which is higher equated to other class of activated carbons. The thermodynamic study on energy efficiency of vacuum-pressure swing adsorption (VPSA) has been accomplished using four different types of adsorbents e.g. zeolite 5A, activated carbon, zeolite 13X, metal-organic framework (MOFs) and silica gels and [45]. The MOF (Mg-MOF-74) performed very well with maximal adsorption capacity of 9.1 mmol/g at 298 K with 1.5 bar pressure followed by Zeolite 5A with a loading of 5.4 mmol/g under similar operating conditions of temperature and pressure. Using 5-step VPSA cycles, the energy consumption was reported in the range 2.0 - 4.5 MJ/kg having second law efficiencies of 4% and 7%.

The two-stage (PSA/VSA) process was suggested to yield high purity H₂ from steam methane reforming gas and to adsorb CO₂ from the tail gas [46]. A PSA process was designed to get 99.99% H₂ with additional 85% recovery from the steam methane reforming gas using adsorbents 5A zeolite and activated carbon. However, silica gel investigated to recover carbon dioxide from tail gas and 95% purity level with a recovery of greater than 90 % was achieved. The capacity of adsorption equivalent to 3.4 mmol/g was determined for SG (silica gel) at 298 K and 6.5 bars and reduced to 2.9 mmol/g at a lower pressure equivalent to 5 bar at the same temperature. The carbon dioxide capture study from dry gas CO₂/CH₄ mixture for biogas upgrading to biomethane was performed upto a total pressure of 6 bar [47]. Commercial adsorbent such as zeolite, silica gel and activated carbon were applied in addition to the prepared zeolite for adsorption study. At a pressure of 2 bars, an adsorption loading of 0.40 mmol/g was attained and

increased to 1.1 at a pressure of 6 bars with a significantly reduced level of CH₄ recovery and CO₂ purity.

An extensive review on CO₂ capture by post-combustion utilizing metal organic framework (MOFs) has been conducted and chemistry link of MOFs to economics for CO₂ capture by adsorption has been attempted [48-49]. The MOFs are evidencing to be excellent materials for CO₂ capture owing to their microporous structure. Also, chemical, thermal, mechanical and hydrothermal stabilities of MOFs together with adsorption mechanism for CO₂ adsorption were reviewed. The research advancement in MOFs for CO₂ capture and separations that are directly associated with CO₂ capture have been described and reviewed in detail. The porous magnesium oxide was utilized for investigating the CO₂ adsorption kinetics under various conditions [50]. The porous magnesium oxide was produced through the calcination of basic magnesium carbonate. The adsorption behavior of porous MgO was very well predicted by Pseudo-second order model. The Table 2.1 summarized the reported adsorption capacity of various commercial adsorbents for CO₂ capture by adsorption.

Table 2.1 Adsorption capacities for CO₂ capture reported using commercial adsorbents

Adsorbent	Temperature (K)	Pressure (bar)	Adsorption capacity (mmol/g)	References
Activated carbon Norit R2030CO ₂	298	1	2.46	[14]
Activated carbon Norit R2030CO ₂	298	3	3.98	[14]
Activated carbon RB2	273	3	10.7	[28]
Activated carbon RB2	298	3	10.4	[28]
Activated carbon 1050	293	10	8.4	[29]
Activated carbon 1050	293	15	10.5	[29]
Activated carbon DARCO FGD	298	1	0.55	[30]
Activated carbon	298	0.2	0.43	[31]

DARCO FGD				
Zeolite NaX	303	1	4.2	[32]
Zeolite 5A	273	10	4.5	[33]
Zeolite 13X	313	3.7	4.7	[34]
Zeolite 13X	273	10	6.1	[35]
Zeolite 13X	308	5	6	[36]
Zeolite 13 X	273	1	5.4	[37]
Zeolite 5A	273	1	4.4	[37]
MOF (A100)	273	1	5.0	[37]
Zeolite 13X	293	10	5.6	[38]
Silica gel	293	10	4.8	[41]
Activated carbon (NC60)	298	8	10.5	[43]
Zeolite 5A	298	8	4.1	[43]
Activated carbon (A754)	303	10	6.5	[44]
Silica gel	303	10	3.2	[44]
Zeolite 13X	303	10	6.1	[44]
Zeolite 5A	303	19	4.1	[44]
MOF (Mg-MOF-74)	298	1.5	9.1	[45]
Zeolite 5A	298	1.5	5.5	[45]
Silica gel	298	1.5	1.4	[45]
Silica gel	298	6.5	3.4	[46]
Silica gel	298	6	1.1	[47]
MgO	323	0.15	1.8	[50]

2.7 ADSORPTION STUDY USING MODIFIED COMMERCIAL ADSORBENT

An isotherms of CO₂, CH₄ and N₂ adsorption on H β and Na β zeolites were examined volumetrically at temperatures of 273 K and 303 K [51]. Na β zeolite

was synthesized using convectional ion exchange method. The outcomes proved that all the isotherms were of Brunauer type-I and very well fitted by model of Langmuir-Freundlich. The selectivities of CO₂ with respect to CH₄ and CO₂ with respect to N₂ increased after sodium exchange. It was also observed that adsorption of CO₂ on β zeolites is highly heterogeneous while adsorption of CH₄ is homogeneous. A strategy to utilize amine containing CO₂ adsorbents has been suggested under the condition of extraordinary stability [52]. The key data with reference to deactivation and regeneration of amine-modified CO₂ adsorbents have been provided. CO₂ adsorption and kinetics on amine-functionalized mesoporous silica was investigated with temperature in the range of 298 K to 323 K [53]. It was also found that model predicted response curves were in close agreement with the obtained data. It was also recommended that CFD can also be used to explain the CO₂ adsorption using amine-containing adsorbents. The kinetics of the carbon dioxide capture utilizing amine-functionalized material was effectively defined by Avrami's kinetic model. The CO₂ capacity of 2.0 mmol/g was also achieved at a 298 K with a pressure of 1 bar.

A series of primary, secondary, and tertiary monoamine – grafted mesoporous MCM-41 were examined for CO₂ adsorption [54]. The primary amine exhibited maximal adsorption capacity followed by adsorbent based on secondary amine. It was also shown that primary amine experienced significant reduction in CO₂ adsorption capacity whereas other type of amines (secondary and tertiary) were observed as stable upto a temperature of 473 K. The CO₂ and CH₄ adsorption study on molecular sieves i.e. silicoaluminophosphate-34 zeotype and T-type zeolite was also performed [55]. The molecular sieve type adsorbents were synthesized by hydrothermal method. The adsorption system performance was measured in terms of CO₂ uptake and adsorption affinity at varied temperatures of 288 K, 298 K and 308 K. The maximal adsorption capacity of molecular sieve SAPO-34 equal to 3.2 mmol/g was obtained at a temperature of 288 K with 20 bars pressure. The isotherm data of CO₂ adsorption was fitted with Sips model

and Langmuir for CH₄ adsorption and good correlation was found among the model prediction and experimental data.

An adsorption study of CO₂ capture by adsorption on immobilized polyethylenimine (PEI) using silica (mesoporous) was experimented in fluid bed [56]. The dynamic ingredient in the adsorbent is PEI which is a composite polymer of aziridine and 1,2-ethanediamine. The breakthrough response was examined with varies flow rates, temperature and feed concentrations. The kinetics was very well explained by pseudo kinetic model (first order). The highest loading of 2.8 mmol/g was determined at 1 bar and 373 K temperature at a feed rate of 30 L/min with inlet CO₂ flow of 5 L/min.

Carbon molecular sieve (CMS) modified by potassium carbonate for CO₂/CH₄ separation by adsorption was utilized [57]. The CMS surface has –OH group that provides extensive support for the chemical activation. Various metal precursors of K, loading amount of K₂CO₃, and calcination temperature were investigated for CO₂ and CH₄ separations by adsorption. The adsorption capacity of CO₂ enhanced to 1.72 mmol/g equated to a lower capacity of 1.15 mmol/g for untreated molecular sieve. Also, the separation factor improved from 1.9 to 2.75. The K₂CO₃ treatment was very effective in producing metal oxide KO₂ and K₂O which may well improve the CO₂ capturing.

The carbon adsorbent was synthesized by MCM-41 template, high hydrogen content, melamine-formaldehyde resin applying technique known as nanocasting for dynamic CO₂ separation [58]. The base material was first carbonized and afterward activated physically by CO₂ at various temperatures. The adsorption capacity of 0.64 mmol/g reported in case of adsorbent prepared at 973 K with feed concentration consisting of 12.5% CO₂ with balance N₂. Also, it was found that modified adsorbent exhibited good regenerability, stability and better selectivity. The fractional order very well explained adsorption kinetics.

The energy required for regeneration determined from isosteric heat of adsorption and sensible heat found to be equal to 2.51 MJ per kg CO₂. CO₂ adsorbents-

modified SBA-15 materials were utilized as CO₂ adsorbent for enhancing the CH₄/CO₂ separation [59]. The adsorption/regeneration properties of SBA-15 modified by MDEA, DIPA and TEA have been equated. The increased separation efficiency was realized for SBA-15 modified by triethanolamine. The highest capacity of 1.6 mmol/g was evaluated at a temperature of 298 K for the SBA-15 modified with TEA. The zeolites were prepared from flyash to capture CO₂ for biogas upgrading to biomethane [47]. The best synthesized zeolite provides CH₄ and CO₂ recoveries of 85.4% and 97.6% at 2 bar with purities level of 97.3 vol.% and 94.9 vol.%, respectively. The CO₂ adsorption capacity of 0.324 mmol/g was determined at a pressure of 6 bars from a CO₂/N₂ mixture.

The utilization of functionalized silica materials with amines for CO₂ separation was investigated for determining the adsorbent viability [60]. CO₂ adsorbent was produced by imbedding diethylenetriamine (DT) or impregnation of polyethyleneimine (PEI) on SBA-15. The adsorption capacity of 1.9 mmol/g at 1 bar was achieved for silica-derived adsorbent developed by method of grafting whereas capacity of 1.7 mmol/g was evaluated for other adsorbent developed by impregnation technique. In both cases, the operating conditions such as 1.5 h and 363 K were identified to separate the CO₂ completely.

The CO₂ capture by adsorption using poly [VBTMA][Arg], a type of ionic liquid was carried out at 298 K upto a highest pressure of 10 bar [61]. The capture capacity improved from 3.23 mmol/g to 7.91 mmol/g with the pressure ranging from 1 to 10 bars with 298 K. The Freundlich, Langmuir, Dubinin Raduschkevich and Temkin isotherms tested to observe the interaction between adsorbate and adsorbent. It was established that Freundlich model and pseudo-first order model explained the kinetic data very well at 298 K.

An adsorbent functionalized with amine for CO₂ capture was synthesized by loading pentaethylenehexamine (PEHA) into KIT-6 mesoporous silica's pores applying wet impregnation method [62]. It was revealed that pore volume, pore size and surface area of the developed adsorbent reduced after loading PEGA into to KIT-6. The utmost CO₂ adsorption capacity of 3.2 mmol/g realized at 343 K.

The adsorption/desorption kinetics were investigated by three models. The adsorption was dominated by intra-particle diffusion whereas; an adsorption rate is limited by the intra-particle diffusion process. The adsorption capacity reported in literature for various modified adsorbents depicted in Table 2.2.

Table 2.2 Adsorption capacity for CO₂ capture reported using modified adsorbents

Adsorbent	Temperature (K)	Pressure (bar)	Adsorption capacity q (mmol/g)	Reference
Zeolite (H β)	273	1	2.8	[51]
Zeolite (Na β)	273	13	3.6	[51]
TRI-PE-MCM-41 (amine functionalized)	298	1	2.0	[53]
3MCM-41 (pMONO)	198	1	2.5	[54]
Molecular sieve (SAPO-34)	288	20	4.3	[55]
Molecular sieve T-type	288	20	3.2	[55]
Mesoporous silica (AX)	373	1	2.8	[56]
Molecular sieve (treated)	298	1	1.72	[57]
MCM-41 (MFZ-700)	303	1	0.64	[58]
SBA-15 (TEA-modified)	298	5	1.6	[59]
SBA-15 (amine functionalized)	318	1	1.9	[60]
Poly [VBTMA][Arg]-ionic liquid	298	10	7.91	[61]
Silica (amine functionalized)	343	0.1	3.2	[62]

2.8 ADSORPTION USING MODIFIED AND BIOMASS DERIVED ACTIVATED CARBON

A commercial activated carbon DTO was modified by activation with KOH, K₂CO₃ and ZnCl₂ at 313 K and pressure upto 40 bar [63]. The results obtained

exhibited enhanced surface characteristics for AC modified with KOH and highest capacity adsorption of 14.44 mmol/g was reported for DTO/KOH. The results were fitted with Langmuir, Freundlich, Sips and Toth equations to examine the isotherm model. The Sips model was identified as best model to describe the adsorption of CO₂. The activated char was developed by passing water through reactor while carrying out the pyrolysis of coal at 923 °C and afterward treated with hydrochloric acid [64]. The obtained char was impregnated with Tetraethylenepentamine to develop adsorbent to CO₂ capture. An adsorption capacity of 3.38 mmol/g was achieved with 10 wt. % TEPA-modified coal activated char at 333 K. The breakthrough curve obtained experimentally for modified adsorbent was very well described by Avrami-Erofeyev model. The impregnation of local coal samples was carried out to produce activated carbons with NaOH, KOH and ZnCl₂ at various temperatures for CO₂ capture by adsorption study [65]. The high surface area of 2,599 m²/g was obtained for the samples prepared with KOH at a temperature of 1073 K with KOH: Coal ratio equal to 4:1. Also, concluded that adsorption capacities were significantly influenced by surface area and micropore volume. The maximum capacity of 9.09 mmol/g was achieved for adsorbent prepared with KOH.

Pitch-based AC from coal tar pitch blended with naphthalene was heated in the atmosphere of N₂ [66]. The blended pitch was then pulverized and pitch activated spheres were synthesized using emulsion method. The highest adsorption capacity of 1.92 mmol/kg for CO₂ was tabulated at 303 K and 200 kPa. Also, a mathematical model was applied to simulate and predict the breakthrough profiles. Biomass based on grass cutting, horse manure and organic waste was chemically and physically activated for CO₂ separation [67]. The physically activated carbon exhibited increased capacity of 1.45 mmol/g at a reduced pressure of 0.1 bar and 273 K. It was proposed that ultra-micropore volume is of utmost importance for CO₂ adsorption.

A mixture of rapeseed oil cake/walnut shell was subjected to pyrolysis process and afterwards, the fraction (solid) was treated at high temperature with CO₂ (65%) balance N₂ to produce activated carbon [68]. The heat treatment with ammonium (NH₃) and impregnation with aqueous monoethanolamine (MEA) were applied to alter the surface characteristics for enhanced CO₂ adsorption. The NH₃ was established to be more decisive than MEA under similar operating parameters. The fast pyrolysis of white wood using three different methods of CO₂ activation, KOH activation and steam activation was performed for CO₂ adsorption applying a fixed bed at 1 atm [69]. The highest CO₂ capacity was determined equal to 1.8 mmol/g owing to high surface area and microporous structure under optimum conditions of CO₂ concentration and temperature for KOH activated adsorbent. The CO₂ capacity for carbon activated with CO₂ and KOH stayed stable even after nearly 50 cycles at a low regeneration temperature of 433 K. The fly ash, bottom ash and the pellets produced from wheat bran combustion were characterized and utilized for CO₂ separation at various temperatures [70]. The pelletized bottom ash exhibited a capacity of 0.07 mmol/g at 298 K followed by capacity based on adsorption equal to 0.06 mmol/g for non-pelletized adsorbent.

The controlled carbonization of wheat flour was carried out to produce microporous carbon compartments (MCCs) for CO₂ separation [71]. The chemical activation with KOH was performed at a temperature of 700 °C with varying mass in the ratio of 1:5. The maximal CO₂ uptake of 5.70 mmol/g at 273 K and 3.48 mmol/g at 298 K were determined for an adsorbent activated with a C/KOH in 3:1 ratio. The pseudo-second order kinetic model explained data very well equated to the pseudo-first order model. Various porous carbon materials were obtained from biomass waste with varied morphological and structural properties [72] and explored as a prospective adsorbent for CO₂ separation in post-combustion condition. An adsorption capacity of 1.3 mmol/g reported from Alcell lignin-biomass. However, an adsorption capacity of the carbon fibre was

totally recovered very fast during desorption under the similar conditions of temperature and pressure.

The chemical activation technique was applied to synthesize activated carbon doped with NH_3 as activating agent and nitrogen source [73]. The nitrogen doped activated carbons showed micropores with increased surface having high N_2 content and CO_2/N_2 selectivity of nearly 82 were evaluated. It was also concluded that activated carbon doped with N_2 can be easily re-used after regeneration under mild operative conditions. The increased adsorption capacity of 4.5 mmol/g was realized at 1 bar and 273 K.

Black locust based biomass was chemically activated with KOH and heat treated with NH_3 for enhancing CO_2 adsorption [74]. The produced adsorbent exhibited a surface area and micropore volume of 2511 m^2/g and 1.16 cm^3/g , respectively. The CO_2 uptakes of 7.19 mmol/g and 5.05 mmol/g were achieved under 1 bar at temperatures of 273 K and 298 K, respectively. It was also substantiated through the thermodynamic parameter that physical and chemical adsorption co-exists in the AC-KOH-N adsorbent. The pomegranate peels and other biomass were chemically activated by KOH with 1:1 ratio of biomass: KOH for CO_2 capture [75]. It was found that precursors had strong effect on the textural properties and CO_2 separation. The carbon based adsorbent developed from pomegranate peels exhibited maximal CO_2 selectivity and uptake. The highest adsorption capacity of 6.0 mmol/g was obtained for pomegranate peels – derived carbon at 273 K and 1 bar.

The production of N-enriched carbon-adsorbent from *Procambarus clarkii* shells was carried for an improved CO_2 adsorption with an activating agent ($\text{K}_2\text{C}_2\text{O}_4 \cdot \text{H}_2\text{O}$) [76]. The produced activated carbon showed adsorption performance of 6.48 mmol/g at 273 K and 4.51 mmol/g at a temperature of 298 K under a fixed pressure of 1 bar. Also, the selectivity of CO_2/H_2 equal to 52 was obtained with CO_2 adsorption heat amount to 33 kJ/mol. Activated carbons were synthesized by activation with H_3PO_4 and also, by physical activation using olive stones for CO_2 adsorption [77]. The chemical activated carbon showed higher

microspore volume and surface area leading to an increased CO₂ loading. The availability of more O₂-groups on water vapor – activated carbon increased adsorption of CO₂. A composite adsorbent prepared by 50% wt. carbon black and 50% wt. magnetite utilized for CO₂ adsorption-desorption study under post-combustion conditions [78]. Three different kinetic models had been adopted to determine an adsorption mechanism and best fit was described by Avrami's kinetic model. It was also proposed that CO₂ adsorption occurs through diffusion based process.

The CO₂ adsorption study was conducted using pine-apple derived porous carbon-adsorbent prepared by hydrothermal carbonation and thermal activation [79]. The adsorbent activated by K₂C₂O₄ at 973 K possess reasonably high surface area amount to 1076 m²/g and pore volume of 0.92 cm³/g. Adsorption capacities of 5.32 mmol/g at 273 K and 4.25 mmol/g at 298 K with a pressure of 1 bar were reported. The selectivity of CO₂ with reference to CH₄ ranged from 18.24 to 38.42 with equitable isosteric heat.

The spent coffee grounds were used to prepare microporous carbon through solid-state K₂CO₃ activation to CO₂ capture by adsorption [80]. The activation was performed at three different temperatures of 873 K, 973 K and 1073 K for 1 or 5 h duration. The enhanced surface area and specific volume of 2337 m²/g and 1.15 cm³/g determined for prepared adsorbent, respectively. The CO₂ loading of 4.54 mmol/g was reported at 298 K and 1 bar for activated carbon synthesized at 973 K for 5 h. The produced activated carbon showed good cyclical stability and selectivity of carbon dioxide over N₂. It was mentioned that narrow microporosity and nitrogen content is critical for CO₂ capture at reduced pressure.

A yellow tuff was examined for CO₂ capture in fixed bed reactor with focus on process thermodynamics and kinetics [81]. It was also found that thermodynamic and kinetics of CO₂ separation in low pressure range can be adequately explained by Freundlich's isotherm model and pseudo-first order model, respectively. The maximal adsorption uptake of 0.71 mmol/g was achieved at a temperature of 298

K with 0.25 bar pressure (gauge). It was also established thermodynamically that CO₂ adsorption on Yellow tuff is spontaneous and physical in nature.

An activated carbon was produced from corncob derived hydro-char by hydrothermal carbonization applying chemical activation with ZnCl₂, H₃PO₄ and KOH with an impregnation ratio of 1:3 at a temperature of 873 K [82]. The capacity of adsorption equal to 4.5 mmol/g was acquired for KOH activated carbon at a pressure of 1 bar. It was suggested that an adsorption of CO₂ on the produced carbon-based adsorbent is spontaneous and exothermic.

Chemically activated carbon with KOH using walnut shells, peanut shells and hazelnut shells were produced for CO₂ separation [83]. The KOH/biomass in the ratio of 1:1 was fixed and mix was carbonized using furnace with temperature ranging from 873 to 1173 K. It was found that surface area of developed adsorbent increases with increased temperature. The highest adsorption capacity of 5.5 mmol/g was realized for peanut based activated carbon developed at 273 K. The CO₂/CH₄ adsorption equilibrium on cherry-based activated carbon was examined at different feed concentrations [84]. The activated carbons were synthesized using single step activation with steam or CO₂ as activating agent. The surface area of 1045 m²/g was obtained for CO₂ activated adsorbent. The maximum CO₂ uptake of 1.98 mmol/g was determined at 303 K and 1 atmosphere. The generated experimental data was very well described by Avrami's kinetic model over varied range of feed concentrations. It was also recommended that mass transfer occurs by diffusion-centered process consists of intra-particle and film diffusion.

The activated carbon was synthesized from biomass based Palm shells using chemical activation with cupric nitrate at various concentrations [85]. These precursors were carbonized in the atmosphere of CO₂ at 1073 K to produce different grades of adsorbents. The developed carbon based-adsorbent showed surface areas between 473 and 1361 m²/g with micropore volume ranging from 0.18 cm³/g to 0.51 cm³/g. The maximal adsorption capacity of 4.93 mmol/g was obtained for synthesized activated carbons at 1 bar with a temperature of 273 K.

The minimal adsorption capacity of 2.34 mmol/g was reached under the same conditions of pressure and temperature. The CO₂ adsorption kinetics for activated carbon prepared with metallic salt of copper is very well described by interparticle diffusion.

The Batch and dynamic adsorption study on activated carbon prepared by activation with ZnCl₂ and also, by physical activation of olive stone was conducted [86]. The maximal CO₂ uptake of 4.81 mmol/g was attained at 1 bar and 273 K temperature. It was also observed that capacity increased monotonically with CO₂ pressure. It was also revealed from textural characterizations that micropore/ultrapore volume increases monotonically with activation time. The date pits – derived activated carbon was synthesized by physical activation with CO₂ and response surface methodology (RSM) was applied to optimize the capture process [87]. The optimum conditions were identified as 1244 K activation temperature, activation time equal to 56 min with a CO₂ flow of 5.1 cm³/min. The surface area and the optimum yield determined equal to 667 m²/g and 14.8 %, respectively. The experimental surface area (710 m²/g) of the sample was nearly equal to that determined by optimization technique. The date seeds were used as suitable biomass material for the synthesis of activated carbon [88]. The activation with phosphoric acid (H₃PO₄) known as chemical activation was carried out for the production of adsorbent. The optimization study was conducted applying RSM technique assuming a Box-Behnken design. The optimized conditions were identified as impregnation ratio (IR) of 3:1 and activation time equal to 71.4 min with a temperature of 773 K for obtained carbon and predicted a capacity of 445.7 mg/g for methylene blue (MB) adsorption. The maximal adsorption capacity of 345 mg/g for methylene blue (MB) was determined through Freundlich adsorption isotherm model confirming the suitability of prepared carbon for macrolayer compounds adsorption.

The methylene blue removal adsorption capacity was examined using the adsorbent synthesized from date pits through chemical activation with 30 wt. % KOH [89]. The surface area of 870 m²/g was obtained for developed activated

carbon with micropore volume of $0.24 \text{ cm}^3/\text{g}$. The adsorption capacity was improved from 80.3 mg/g to 123.1 mg/g for activated carbon produced with chemical activation. The adsorption rate was observed to follow pseudo-second order kinetics with good correlation and equilibrium was very well correlated by Langmuir isotherm equation. Two-grades of activated carbons were produced from date pits – one developed using CO_2 as activating agent and other type obtained by activation with steam under same experimental conditions [90]. After that, additional O_2 -surface groups were introduced by oxidation with nitric acid. The findings suggest that CO_2 and steam activation produced microporous activated carbons with an increased amount of CO evolving groups on the raising the burn-off. In addition to this, oxidation with HNO_3 augmented the amount of CO and CO_2 evolved through the breakdown of surface O_2 -groups.

The influence of activation method on the structure of pores of produced activated carbons derived from date pits for water treatment had been examined [91]. The activated carbons were produced by physical and chemical activation with ZnCl_2 , KOH and H_3PO_4 to investigate the influence of variable on adsorption performance. The mesoporosity exhibited by the adsorbents developed by chemical activation with KOH and H_3PO_4 . It was concluded that adsorption capacity of developed activated carbon relies on the porosity, nature of the compounds and surface area. It was observed that adsorption of potassium hydrogen phthalate and triton on activated carbon is relatively good equated to potassium dichromate. The phenol removal from aqueous solution utilizing activated carbon produced from date pits was examined in a batch system [92]. A statistical method known as Goodness of fit was applied to determine the best fit. It was found that best isotherm to explain the adsorption of phenol on produced activated carbon was Freundlich with a maximal capacity of 33.53 mg/g at a temperature of 298 K in case of models based on 2-parameters.

The date pits were utilized as an inexpensive adsorbent for the removal of heavy metals (HMs) from dilute solution [93]. The adsorption of heavy metals using raw

date pits and thermally activated burnt date pits were explored for adsorption study and findings showed that burnt date pit is more effective and completely adsorb Cu(II). Also, fractional factorial design was applied to develop experimental pattern and it was screened out that adsorbent dose and pH influenced the adsorption performance in positive way. The activated carbon from date pits were chemically prepared with H_3PO_4 for lead removal by single step activation technique [94]. The surface area of $316.9 \text{ m}^2/\text{g}$ was estimated for produced carbon. The influence of dose, contact time, temperature, pH and initial concentration on the removal of lead using developed activated carbon was investigated. The highest adsorption capacity equal to 101.35 mg/g was attained at pH equal to 6 with a contact time of 30 min at 303 K. The adsorption of lead was instantaneous and exothermic as confirmed by thermodynamic study.

A composite of polymer-activated carbon was synthesized by grafting polyglucosamine polymer on the surface of activated carbon [95] and the biomass-derived adsorbent was developed by calcination and oxidation of date pits. Under optimum conditions of pH, composite dose and contact time, the maximal capacity of 35.0 mg/g of adsorption was achieved. The results based on kinetic and thermodynamics confirmed that adsorption is a chemisorption, exothermic and spontaneous. The carbon based adsorbent was developed by activation with KOH and $ZnCl_2$ from biomass based date pits for removal of organic nitrogen amino acid [96]. The batch experimental data were collected to determine an adsorption performance of porous activated carbon. The data were very well and adequately explained by pseudo-first order model and highest adsorption capacity of 178.57 mg/g of I-tyrosine was calculated for date-pits based activated carbon developed by KOH. The adsorption process was very well explained by Langmuir and R-P models.

The chemically activated carbon synthesized from date pit with phosphoric acid for the separation of green dye from synthetic wastewater [97]. A batch absorber was designed which rely on the Freundlich isotherm that was best fitted isotherm model. The process kinetics was very well fitted by pseudo-second order model

and intra-particle diffusion was identified as rate controlling stage. The produced activated carbon exhibited a surface area of 311.38 m²/g. The adsorption capacity of 77.8 mg/g was reported for brilliant green dye. The thermodynamic study showed that adsorption on produced activated carbon was physiosorptive ($\Delta G = -5.9$ kJ/mol) and spontaneous at reduced temperature. An activated carbon by chemical activation with ZnCl₂ was developed from a composite of date pits and olive stones for adsorptive desulfurization of dibenzothiophene (DBT) [98]. The highest % elimination of DBT reached to 92.86% under optimized conditions of 0.30 g AC at 40 °C with 60 min of contact time. The data of adsorption process were satisfactorily explained by Freundlich isotherm and obtained data followed pseudo-second order kinetic model.

The date stone biomass from date products industry was utilized for producing chemically activated carbon with phosphoric acid for malachite green dye removal [99]. A batch of natural date stone was treated with 30% of o-phosphoric acid with an impregnation ratio of 2:1. The chemically treated activated carbon exhibited a surface area of 909 m²/g with malachite green capacity of 64.7 mg/g. The reduced capacity of 31.5 mg/g was acquired for an adsorbent based on natural date stone. The date seeds – derived activated carbons were produced by physical activation for CO₂ capture [100]. The impact of the activation time and pyrolysis temperature on the yield and CO₂ uptake was investigated. The optimum conditions were found to be as pyrolysis temperature equal to 1073 K followed by activation at 1173 K.

The date stone derived activated carbons were prepared using physical activation in the temperature range of 873-1173 K [101]. The physically activated carbon based adsorbent with higher pore characteristics exhibited good adsorption performance and capacity of adsorption equal to 3.21 mmol/g was achieved at 293 K and reduced to 2.98 mmol/g with increased temperature at 298 K. The maximal heat of adsorption was determined at 298 K owing to high loading at reduced temperature.

The date sheets were utilized to synthesize porous activated carbon by chemical activation using KOH and it was observed that pore size ranges from micropores to mesopores [102]. The high surface area of 3337 m²/g was exhibited and primarily achieved from ultra-micropores ranging from 0.7 to 0.9 nm. The highest adsorption capacity of 6.4 mmol/g was acquired at 273 K and 1 bar with good selectivity and enhanced to 22 mmol/g at 298 K with an elevated pressure of 40 bars. It was also explained that pore size is the main cause for enhanced CO₂ capture. The performance of carbon - based adsorbent obtained from date sheets for CO₂ capture in swing adsorption was examined by combined simulation and experimental data [103]. The predicted process parameters were determined and complemented with swing adsorption. It was also realized that presence of pre-adsorbed water does not considerably influence the adsorption performance. An adsorption capacity of modified and biomass-derived activated carbon have been summarized and depicted in Table 2.3.

The novelty of the current work is to study dynamic adsorption and analyze the different adsorption performance parameters using date pits derived-activated carbon and other grade of adsorbents namely molecular sieve, silica gel and commercial activated carbon Norit RB-2 in continuous fixed bed column. The various bed characteristics parameters i.e. mass transfer zone length (L_{MTZ}), capacity utilization factor (f), column efficiency (η) and usable bed height (h) will be determined and analyzed in depth.

Table 2.3 Adsorption capacity for CO₂ capture reported using modified and biomass-derived activated carbon

Adsorbent	Temperature (K)	Pressure (bar)	Adsorption capacity q (mmol/g)	Reference
Activated carbon (Chemically modified)	313	40	14.4	[63]
Activated char-amine	333	1	3.38	[64]

modified				
Activated carbon-Chemical activation	273	1	9.09	[65]
Pitched-based AC-emulsion method	303	2	1.92	[66]
AC: Biomass- physical and chemical activation	273	0.1	1.45	[67]
AC-rapeseed oil cake/walnut shell	298	1	1.58	[68]
AC-white wood	298	1	1.80	[69]
AC-wheat bran	298	1	0.07	[70]
AC-Wheat flour	273	1	3.48	[71]
AC-Biomass waste	298	1	1.31	[72]
AC-Corncob	273	1	4.52	[73]
AC-Black locust	273	1	7.19	[74]
AC-Pomegranate peels	273	1	6.03	[75]
AC-Clarkii shells	273	1	6.48	[76]
AC-Olive stones	303	30	4.60	[77]
AC-Carbon black	291	1	0.57	[78]
AC-Pineapple waste	273	1	5.32	[79]
AC-Coffee	298	1	4.54	[80]
AC-Yellow tuff	298	0.25	0.71	[81]
AC-Corn cob	288	1	4.51	[82]
AC- Hazelnut, walnut & peanut	273	1	5.5	[83]
AC-Cherry stone	303	1	1.98	[84]
AC-Palm shell	273	1	4.93	[85]
AC-Olive stone	273	1	4.81	[86]
AC-Date seeds	293	1	3.21	[101]
AC-Date seeds	298	2	2.94	[101]
AC-Date sheets	273	1	6.40	[102]

CHAPTER 3 RESEARCH METHODOLOGY

3.1 MATERIALS

The commercially available porous activated carbon (Norit-RB2) with average diameter of 1.83 mm was purchased from Sigma-Aldrich. The Norit RB-2 was used as such without any further treatment for experimental investigation. Also, the commercially available molecular sieve (MS-3Å) with average diameter of 1.60 mm was purchased & procured from Sigma-Aldrich (Germany). Silica gel type-III (SG) with average size of 2 mm was also procured from Sigma-Aldrich. The date stones based biomass were purchased from the regional market of Abha city Kingdom of Saudi Arabia. These collected date pits biomass was rinsed with water to get rid of dust particles. The sample was dried overnight at 383 K (110°C) using oven. The multifunctional grinder (LC: 36250) was utilized for size reduction purpose. The milled date stone particles were then passed through 4 mm screen (BS-series) and thereafter, particle size equivalent to -1.7 mm + 1.0 mm with an average diameter of 1.35 mm is used for an further processing. The screened date pits particles (DS) are stored in air-proof containers for further use to produce activated carbon.

3.2 EXPERIMENTAL UNIT

Setup (Model: UOP-15, Armfield U.K.) used for the experimental work is shown in Fig. 3.1(a)-(d). The 25 cm is the operative length of column and adsorption column was filled with each adsorbent upto a height of 25 cm for collecting the data for each adsorbent.

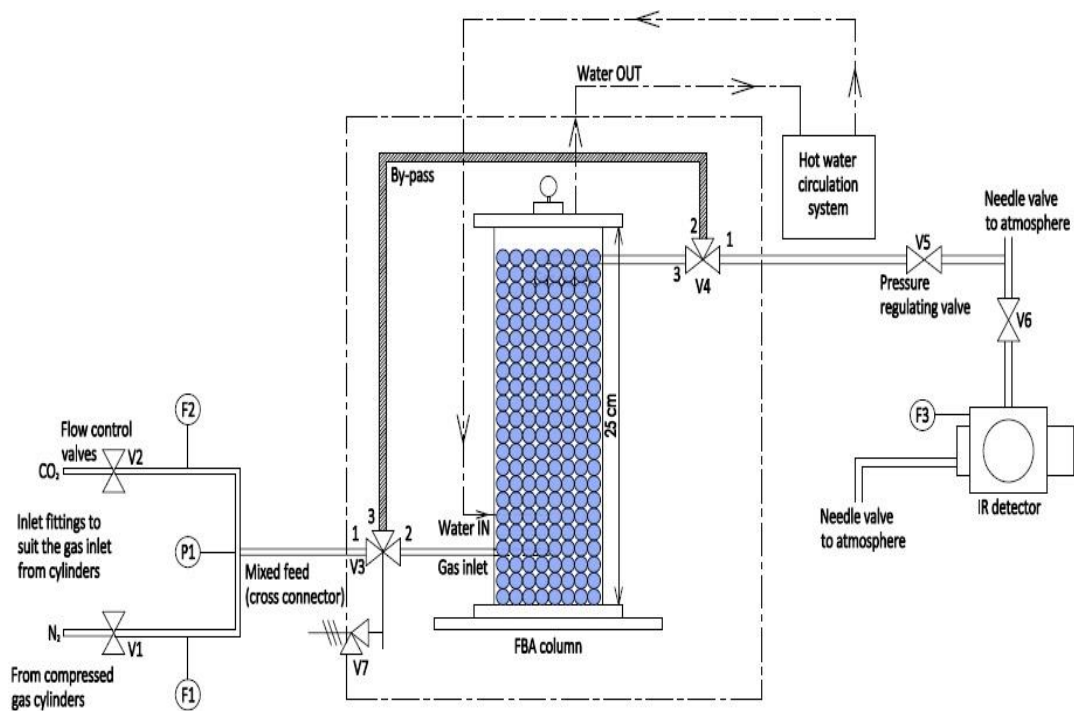


Fig. 3.1(a) Sketch of Continuous fixed bed adsorption column

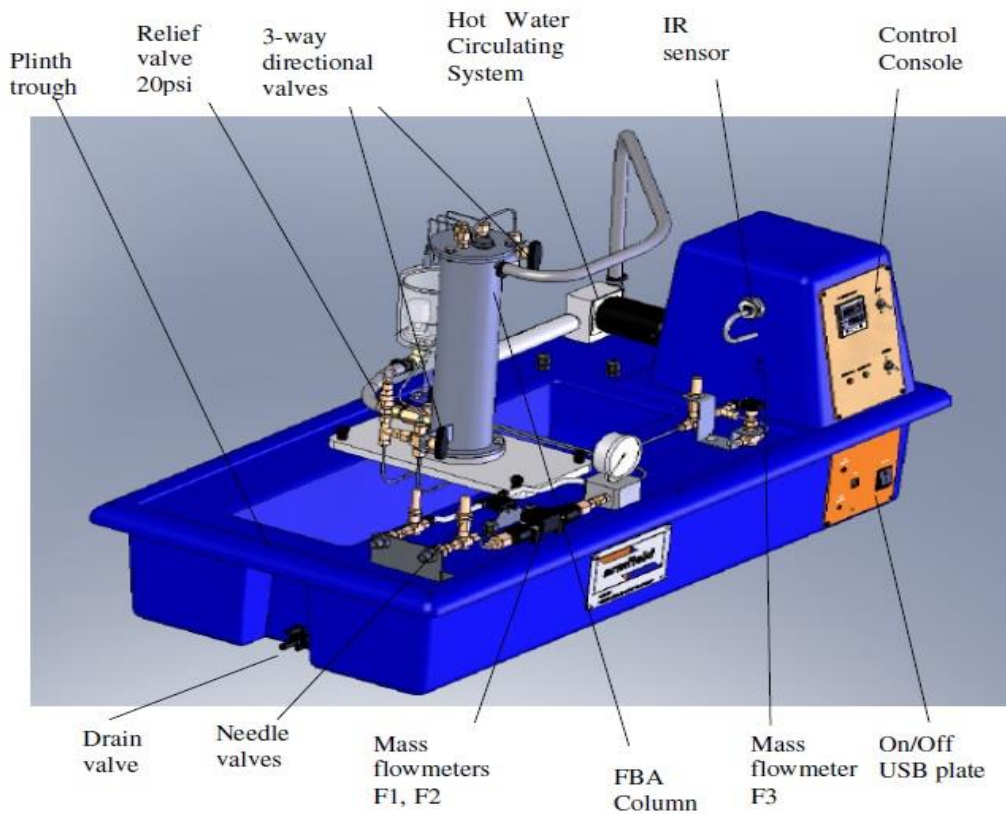


Fig. 3.1(b) Setup 3-D layout of continuous fixed bed unit

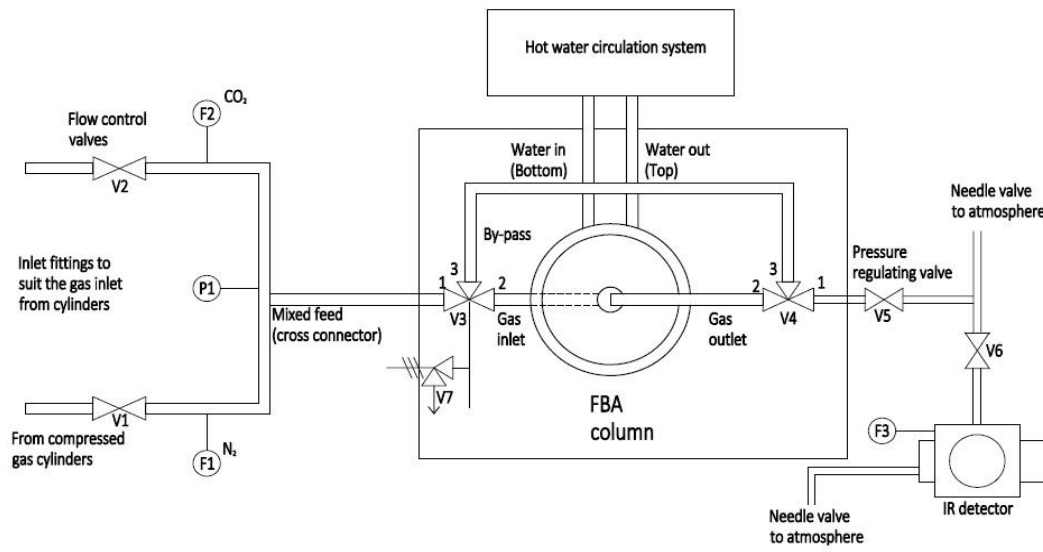


Fig. 3.1(c) Top view of continuous fixed bed unit

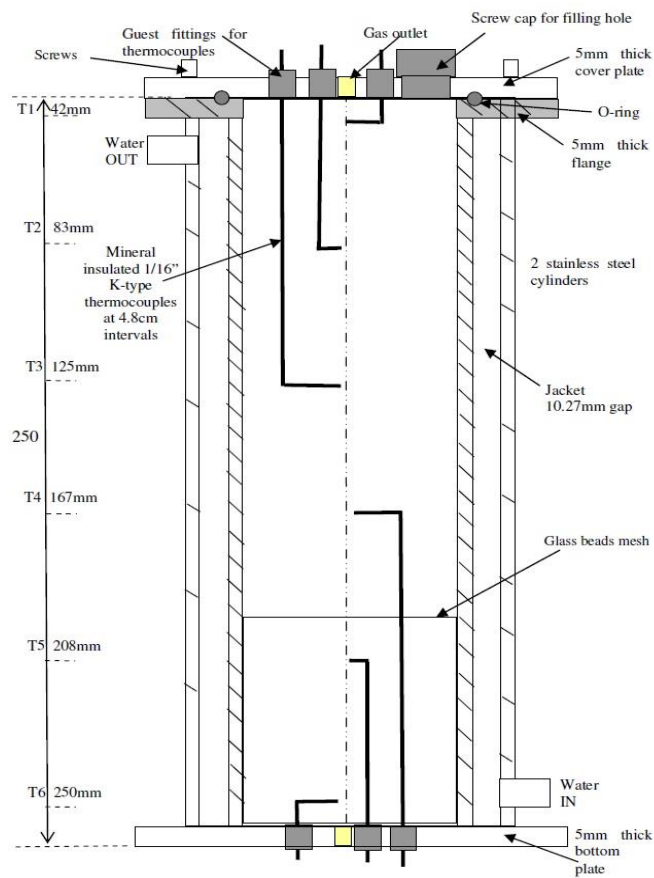


Fig. 3.1(d) Thermocouple positions in continuous fixed bed adsorption column

The flow rates of both the gasses are measured and adjusted by flow controllers. The flow rate of carrier gas N_2 was measured by flow controller F1. The flow rate of adsorbate gas (CO_2) was measured by flow controller F2. The flow to IR sensor is measured by flow controller F3. All the flows are measured in terms of slpm stands for standard liter per min. It signifies that all mass flow controllers have been calibrated under standard conditions of temperature and pressure. The feed made of CO_2/N_2 mixture passes into the column from bottom side. The treated gas leaves the column from top side of the column. The necessary flow to IR sensor for estimating the CO_2 concentration in outgoing gas from column is measured by third flow controller F3. Six thermocouples (T1 to T6) placed inside the adsorption column provides information about the temperature variation during adsorption-desorption process. The other sensor T7 measures the water circulator temperature and always remains equal to the set point temperature. It is ensured that all temperatures shown by sensors T1 –T6 reached temperature equal to the set point temperature as indicated by sensor T7 and considered as bed or column temperature.

3.3 PROCEDURE

The mixture of CO_2/N_2 with determined operating values of feed rate, temperature and adsorbate compositions is allowed to enter the fixed column as per the configuration shown in Fig.3.1a from bottom side. Both the gases are considered dry and purity level of both the gases equal to 99.999% is ensured. The mixture of N_2 with CO_2 is used in the current study although many adsorption studies focused only on pure CO_2 adsorption. By doing so, the effect of $CO_2\%$ (vol.%) in the mixture can be examined on adsorption performance. Also, N_2 serves as a carrier gas for CO_2 . An IR sensor provided for measuring the CO_2 concentration in column outlet works well with maximum concentration of 5% (vol.%) in the feed mixture. The IR sensor works accurately upto 5% inlet CO_2 concentration in the feed or flow to IR sensor. Infra-red (IR) sensor measures and record the adsorbate CO_2 concentration at adsorbent bed outlet. The bed outlet adsorbate

data is recorded at desired regular interval of times of 30 s and time interval can be changed as per the requirement. The required water circulator temperature may be changed as needed using proportional integral derivative (PID) controller provide with control console of adsorption unit.

After the completion of adsorption process, CO₂ desorption from bed was carried out by constantly flowing the N₂ for sufficiently longer duration. The thorough desorption of adsorbent bed is confirmed by measuring the column outlet CO₂ concentration (C) and C = 0 % was measured upto 3 places after the decimal point before starting next set of experiment under different sets of operating conditions. The accuracy (uncertainty) of F1, F2, and F3 was calculated in addition to that for thermocouple. An accuracy analysis for all the sensors (mass flow and temperature) is presented in Table 3.1. The accuracy of temperature sensor is determined equal to ± 0.15 K. An uncertainty related to IR sensor for mass flow controller F3 calculated equivalent to ± 0.01 L/min whereas precision of ± 0.04 L/min and ± 0.02 L/min relate to mass controllers F1 and F2, respectively.

Table 3.1 Sensitivity of the sensors used for measurements

Variable (x)	Sensor type	Uncertainty (δx)
N ₂ flow rate (L/min)	F1	± 0.04
CO ₂ flow rate (L/min)	F2	± 0.02
IR flow rate (L/min)	F3	± 0.01
Temperature (K)	Thermocouple type-K	± 0.15

3.4 ADSORPTION ISOTHERMS, KINETICS AND MODELING

3.4.1 ADSORPTION ISOTHERMS

The adsorption equilibrium is very well explains by an adsorption isotherms. It is graphical illustration of relation between equilibrium adsorption capacity and the adsorbate partial pressure at equilibrium under constant condition of breakthrough

curve. The Langmuir model [81] is the simplest theoretical model and it describes monolayer adsorption onto homogeneous surfaces:

$$q_e = q_L \frac{K_L P^*}{1 + K_L P^*} \quad (3.1)$$

where q_e (mmol/g) is the amount of CO₂ adsorbed per unit mass of sorbent at equilibrium, q_L (mmol/g) is the represents maximum monolayer adsorption capacity of adsorbent, while K_L represents Langmuir adsorption constant. Another significant parameter is the dimensionless term knows as separation factor or equilibrium parameter (R_L) which is described by the equation [81]:

$$R_L = \frac{1}{1 + K_F P^*} \quad (3.2)$$

The value of R_L describes the shape of breakthrough curve.

One of the mostly used isotherm model is the Freundlich model [81]. The main assumption is that adsorption energy differs exponentially with vacant adsorption sites and described mathematically as:

$$q_e = K_F P^{1/n} \quad (3.3)$$

where K_F is the Freundlich isotherm constant and n corresponds to heterogeneity factor. The ratio $1/n$ describes Freundlich intensity parameter. The ratio $1/n$ is termed as Freundlich intensity parameter.

The experimental data corresponding to adsorption isotherms is also fitted by the Langmuir-Freundlich's equation (Sips model) and defined mathematically as:

$$q_e = q_L \frac{(bP^*)^{1/n}}{1 + (bP^*)^{1/n}} \quad (3.4)$$

where, q_L , b and n are Langmuir-Freundlich's model parameters. Considering that Van't Hoff equation is valid, and then the parameter b can be calculated using the following equation:

$$b = b_0 e^{-\frac{\Delta H}{RT}} \quad (3.5)$$

where, $-\Delta H$ = heat of adsorption, and b_0 is pre exponential factor.

The superiority of the adsorption isotherms to the experimental data can be measured by calculating the coefficient of correlation, R^2 which varies between 0 and 1.

The adsorption isotherm can also be described by Toth model [44] and it is mathematically represented as:

$$\frac{q_e}{q_L} = \frac{\beta P^*}{1 + ((\beta P^*)^t)^{1/t}} \quad (3.6)$$

Where, β is the parameter of Toth model.

3.4.2 ADSORPTION KINETICS

The estimation of kinetic parameters of the adsorption process is usually complex. Mostly applied approach deals with fitting the experimental adsorption data to various available kinetic models and, after that selecting the one characterized by best fitting. The pseudo-first order and pseudo-second order are the most widely used among the existing kinetic models for adsorption/desorption [81]. The major characteristic of these apparent models is that all adsorptions steps inclusive of mass transfer resistances are coupled together.

The key postulation of the pseudo-first order kinetic model is that adsorption rate varies directly with number of free active sites on the surface of adsorbent and the pseudo-first order kinetic model [81] in the differential form can be explained as:

$$\frac{dq_t}{dt} = k_f (q_e - q_t) \quad (3.8)$$

Where q_t (mmol/g) signifies quantity of CO_2 adsorbed per unit mass of adsorbent at time t , and k_f is the rate constant for first-order adsorption. Using the boundary conditions $q_t = 0$ at $t = 0$ and $q = q_e$ at $t = \infty$, the equation (3.8) can be written as:

$$q_t = q_e [1 - \exp(-k_f t)] \quad (3.9)$$

A reversible type of adsorbent/adsorbate interaction result can be properly explained by above model as the case of adsorption of CO₂ on physical adsorbent e.g. molecular sieve, silica gel and activated carbon.

According to the pseudo-second order kinetics model [81], the adsorption rate varies directly with the square of the number of active sites on the surface of the adsorbent and it is expressed as:

$$\frac{dq_t}{dt} = k_s(q_e - q_t)^2 \quad (3.10)$$

Where, k_s is the constant of second order, utilizing the boundary conditions $q_t = 0$ at $t = 0$ and $q = q_e$ at $t = \infty$, the equation (3.10) can be expressed as:

$$q_t = \frac{q_e^2 k_s t}{1 + q_e k_s t} \quad (3.11)$$

The above model assumes that in addition to weak physical interaction, the adsorption is also related to chemical adsorbent/adsorbate interaction and hence most appropriate to describe as chemisorption. The quality of the data to fit kinetic model is characterized by determining coefficient of determination R^2 and its value near to 1 implies the closeness of data to particular kinetic model.

Another kinetic model known as Elovich model [97] is normally described as:

$$q_t = (1/(\beta \ln \alpha \beta)) + (1/(\beta \ln t)) \quad (3.12)$$

where, α is the initial adsorption rate and β signifies the extent of surface coverage and activation energy for chemisorption.

Another kinetic model [97] is known as intra-particle diffusion model refers to the theory proposed by Weber and Morris relying on the following equation:

$$q_t = K_{pi} t^{0.5} + C \quad (3.13)$$

where, K_{pi} is the intra particle diffusion rate constant, and constant C (mmol/g) signifies boundary layer thickness.

Another kinetic model [53] that takes into consideration the CO₂ uptake by chemical and physical adsorption is explained by the equations (3.14)

$$\frac{dq_t}{dt} = k_A^n t^{n-1} (q_e - q_t) \quad (3.14)$$

Kinetic constant defined above is independent of initial adsorbate concentration.

3.4.3 MATHEMATICAL MODEL

Predictions of the breakthrough curves mainly rely on the mathematical model to represent the adsorption phenomenon. The adsorption column or bed goes through a mass transfer resistance, axial dispersion, and solid diffusion resistance. The following estimates are applied in order to develop mathematical model: i. the column assumed to be under isothermal conditions with one -component adsorption, ii. No reaction occurs or mass transfer without chemical reaction, iii. The gas-phase follows ideal behaviour, iv. radial temperature, velocity gradient, and concentration are considered to be insignificant, and v. The bed dynamics described by the LDF (linear driving force) model [104]. Utilizing above approximations, the following one-dimensional equation describes the mass balance with axial dispersion:

$$-D_{ax} \frac{\partial^2 C}{\partial z^2} + u \frac{\partial C}{\partial z} + \frac{\partial C}{\partial t} + \frac{(1-\varepsilon)}{\varepsilon} \rho_p \frac{\partial q}{\partial t} = 0 \quad (3.15)$$

Where C stands for adsorbate concentration, z is axial coordinate, t signifies adsorption time, D_{ax}: an axial dispersion coefficient, ρ_p is adsorbent density, ε characterizes bed void fraction, q stands for the adsorption capacity, and u is the gas velocity through the packed bed. It is approximated that equilibrium can be sufficiently explained by the Freundlich isotherm. The isotherms adequately agreed with the Freundlich model (eqn. (3.3)) and using K_F = α, P* = P, 1/n = β, the equation (3.3) reduces to

$$q = \alpha P^\beta \quad (3.16)$$

where α and β depict the Freundlich model's parameters. The initial and boundary conditions can be appropriately written as follows:

$$C = C_0, \quad \text{for } z = 0 \text{ and } t > 0 \quad (3.17)$$

$$\frac{\partial C}{\partial z} = 0 \quad \text{for } z = L \text{ and } t > 0 \quad (3.18)$$

Where, C_0 : initial CO₂ concentration. Assuming perfectly plug flow and thus, the axial dispersion can be ignored and Eqn. (3.15) reduces to the following form:

$$u \frac{\partial C}{\partial z} + \frac{\partial C}{\partial t} + \frac{(1-\varepsilon)}{\varepsilon} \rho_p \frac{\partial q}{\partial t} = 0 \quad (3.19)$$

3.5 PHYSICAL ACTIVATION

A tubular furnace consists of three different zones from MTI corporation (OTF-1200 X) is utilized for developing carbon based adsorbent from date pits by activation technique. The physical activation technique was used for activation purpose. The furnace consists of 3-zones that can be used to control three dissimilar temperatures at the same time period.

3.6 ADSORBENT CHARACTERIZATIONS

The synthesized activated carbons (AC-DS) and other class of commercial adsorbents were characterized using NovaWin: Quantachrome analyzer for BET surface properties. The thermal stability of the raw date stone (DS) and produced activated carbon (AC-DS) was analyzed using Thermogravimetric analyzer (Model: TG209 FI Libra). The components of activated carbon AC-DS were also examined by X-Ray diffraction XRD (Model: PANalytical). The morphology of investigated adsorbents has been analyzed by Scanning Electron Microscope (Quanta 250-FEI). The Raman spectra is obtained using Raman microscope (Model: DRX FT, Thermofisher Scientific).

CHAPTER 4 RESULTS AND DISCUSSION

4.1 ADSORPTION STUDY USING COMMERCIAL ACTIVATED CARBON NORIT-RB2

The commercially available porous Norit RB-2 activated carbon in extruded form (cylindrical form) with average diameter of 1.83 mm was procured from Sigma-Aldrich. It is used in the same form as obtained. The apparent density of the activated carbon was 0.82 g/cm^3 and the interparticle porosity was estimated equal to 0.627. The average length of the carbon-based adsorbent is 3.86 mm with an adsorbent's specific volume equivalent to $10.13 \text{ mm}^3/\text{g}$. The commercial activated carbon Norit-RB2 utilized for the adsorption study is depicted in Fig. 4.1.



Fig. 4.1 Commercial activated carbon Norit RB-2

4.1.1 CHARACTERIZATION OF NORIT-RB2

The NovaWin (Quantachrome) surface analyzer is used to characterize commercial activated carbon (AC-Norit) for surface properties at outgas

temperature of 573 K. The N₂ is supplied for analysis purpose with analysis period of 88.3 min. The surface characterization data for AC-Norit is depicted in Table 4.1. The surface area (single point) of 834.04 m²/g is exhibited for commercial activated carbon AC-Norit. The volume of pore equal to 0.44 cm³/g was exhibited for AC-Norit and the pore radius of commercial activated carbon is tabulated equal to 21.78 Å. Essentially, the adsorbents are vastly porous type of adsorbents. The sorption occurs typically either at fixed sites on the pore walls or within the particles. The external surface area is determined by applying t-plot method and observed equal to 124.95 m²/g. The external surface area is substantially smaller than Langmuir and BET surface areas as presented in Table 4.1. The internal surface area of the carbon-based adsorbent is larger than the external area due to the fact that pores are extremely small. The experimental N₂ isotherm and pore size distribution curve by Barnett-Joyner-Halenda (BJH) method for carbon-based adsorbent are presented in Fig. 4.2(a) – (b) using N₂ gas (99.999% pure). The Fig. 4.2(a) explains the N₂ isotherm obtained upto a relative pressure (P/P₀) of 0.99 for AC-Norit whereas Fig. 4.2(b) explains the pore size distribution. The observed pores are in nm scale. The BJH method is the suitable method to measure the mesopores which lies in 2 nm to 50 nm range. The commercial AC-Norit has mesopores with pores ranging from 3 nm to 19 nm.

Table 4.1 BET Surface characterization results for commercial activated carbon AC-Norit

Surface characteristics	AC-Norit
Single point surface (m ² /g)	834.04
BET surface area (m ² /g)	816.31
Langmuir surface area (m ² /g)	1213.34
Pore volume (cm ³ /g)	0.44
Pore size (Å)	21.78

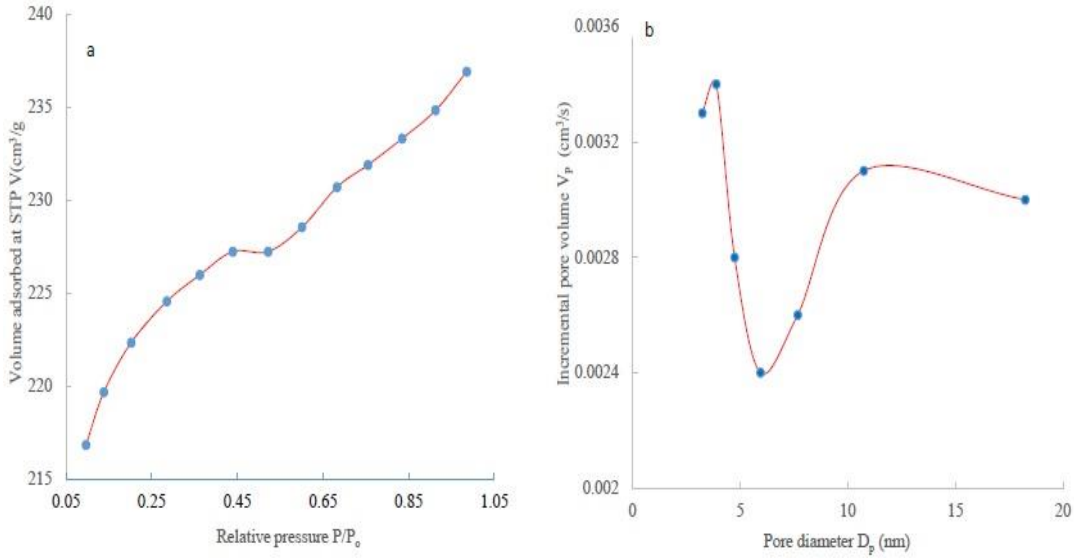


Fig. 4.2 N₂-adsorption isotherm and pore size distribution curve: (a) Experimental N₂ adsorption isotherm for AC-Norit, (b) BJH pore size distribution for AC-Norit

The surface morphology of AC-Norit is investigated by Quanta 250-FEI Scanning electron microscope (SEM). The structural images in Fig. 4.3 (a) – (b) for AC-Norit are produced at different magnification levels. The several pores can be clearly anticipated in the structure and the pores approximately dispersed completely on the structure, as presented in Fig. 4.3 (a) at 2500 x and Fig. 4.3(b) at 20,000 x.

The SEM images for AC-Norit have a high degree of roughness and an irregular surface shape, resulting in a large number of irregular cylindrical cracks or cavities. This further suggests that activation can promote the development of biochar (BC) pores. Tiny particles of irregular shapes may help increase the surface area, promoting CO₂ adsorption on adsorbent surface. The SEM structures with high density pores are exclusively effective for CO₂ separation by adsorption.

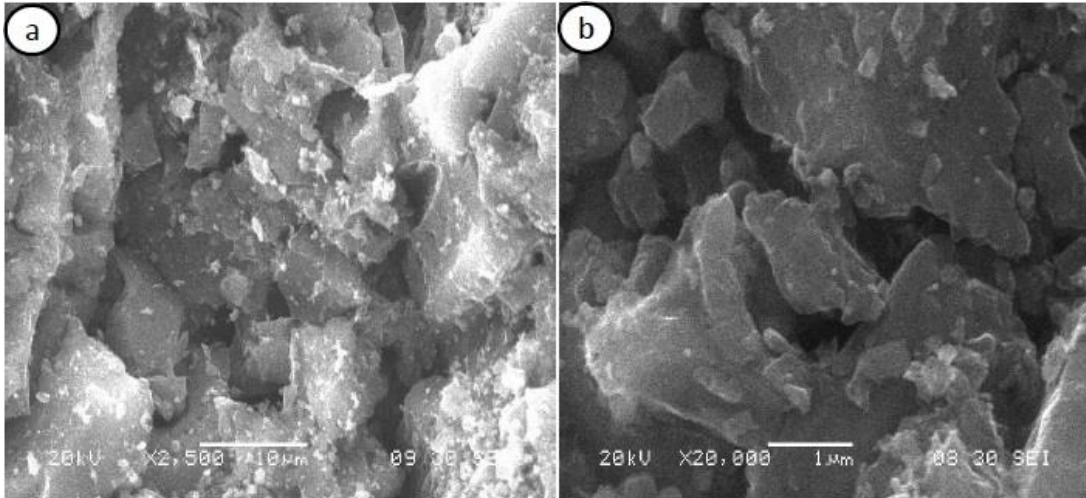


Fig. 4.3 SEM images of AC-Norit: (a) 2500 x magnification and (b) 20,000 x magnification

4.1.2 BREAKTHROUGH PROFILES

The temperature effect on adsorption response for commercial activated carbon AC-Norit obtained is depicted in Fig. 4.4. The data were collected at 4 L/min feed flow and initial CO₂ concentration is fixed at 5% (vol. %). It is recommended to perform the experiments at a total flow rate of feed mixture (CO₂/N₂) in range of 0-5 L/min for good results. The operating pressure of the continuous fixed bed adsorption unit is fixed at 1.25 bars. The breakthrough period relies on bed temperature at which the adsorption takes place.

Usually, the time it takes to reach 5% of the maximal feed concentration (in current study, it is 5%) is known as breakthrough time, whereas saturated period $t = t_s$ corresponds to $C/C_o = 95\%$ using breakthrough curve. Stoichiometric time or period (t_{st}) corresponds total bed capacity at $C/C_o = 1$. Thereafter, it is essential to regenerate an adsorbent for increased adsorption capacity. At a fixed bed temperature equivalent to 298 K, the breakthrough time of 767 s has been achieved corresponding to a saturation period of 897 s. The breakthrough time reduces to 705 s on increasing the temperature at 308 K. The time corresponding to $C/C_o = 5\%$ reduces to 610 s with increased temperature at 318 K for AC-Norit type adsorbent. Also, the saturation and breakthrough time spans of 600 s and 523

s have been determined at 328 K temperature. The lengthy breakthrough or exhaustion spans are envisioned essential for the better CO₂ uptake by carbon-based adsorbent. Over-all, the prolonged breakthrough/saturation periods at reduced temperatures attribute to an improved CO₂ loading and very much is agreement with the literature [81,106].

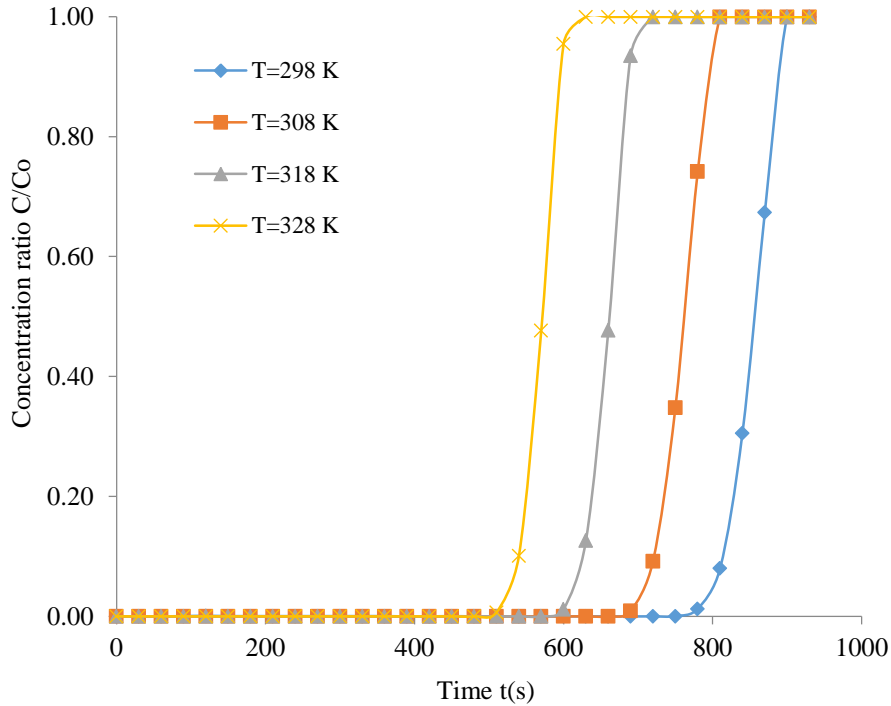


Fig. 4.4 Temperature dependent breakthrough profiles for AC-Norit at $F= 4$ L/min, $C_0=5\%$

Consistently, steepness of adsorption profiles defines utilization of CO₂ bed capacity under breakthrough conditions. The utilization of required CO₂ loading corresponding to breakthrough state is always favored for profitable CO₂ adsorption by capture. The steepness of breakthrough profiles produced under different operating conditions is characterized by narrowness of mass transfer zone. The variations in molecular weight of gaseous compounds lead to the occurrence of adsorption on the surface of adsorbent. Also, some molecules held more firmly than others on the adsorbent surface due to the polarity of gaseous

molecules. In various instances, the adsorbate (CO_2) is held firmly and adequately to permit comprehensive adsorption of CO_2 from gaseous feed with very small or no sorption of non-absorbable gas component (N_2). Undeniably, sharpness of all the adsorption breakthrough profiles signifies and confirms alike utilization of capture capacity under the breakthrough condition. Mostly and largely, adsorption occurs over a narrow mass transfer zone in which the adsorbate concentration varies speedily.

The feed flow dependence on adsorption response curves obtained for AC-Norit is depicted Fig. 4.5. The various feed flows ranging from 2 - 5 L/min have been examined under absolute pressure of 1.25 bars at 298 K temperature. The minimal gaseous flow of 2 L/min contributes to a breakthrough time of 1830 s. The breakthrough period is perceived to decrease to 1390 s with an increased feed flow to 3 L/min.

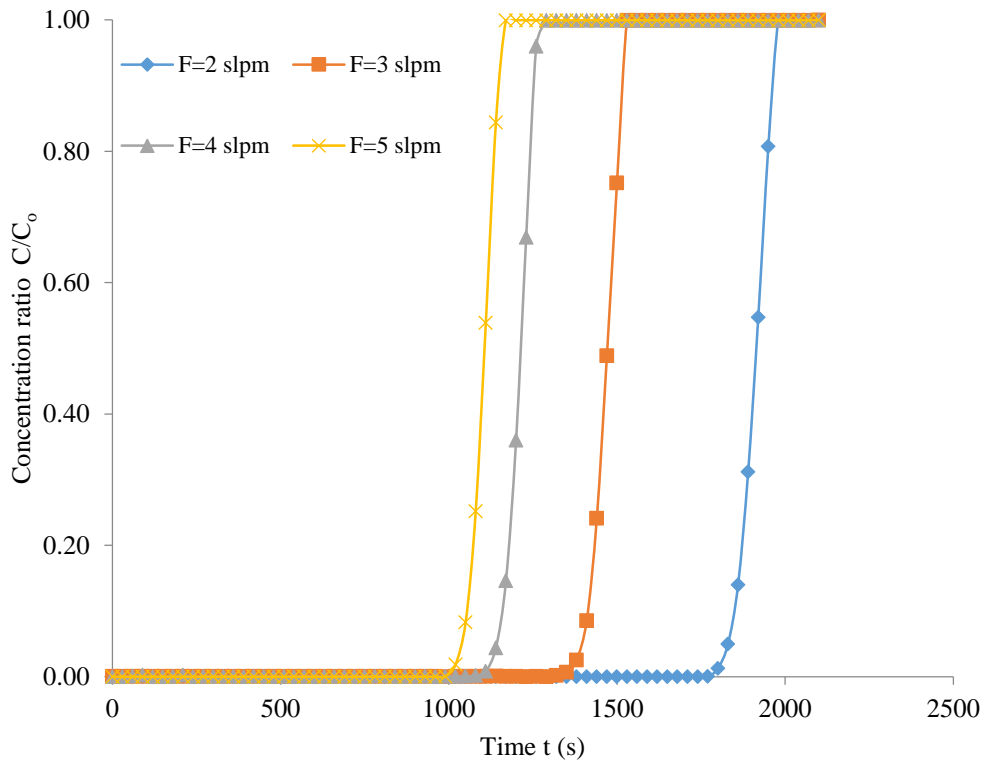


Fig. 4.5 Flow rate dependent breakthrough profiles for AC-Norit at $T=298$ K, $C_0=5\%$

The increased feed rate corresponding to 4 L/min leads to decreased exhaustion and breakthrough spans of 1259 s and 1143 s at 298 K temperature and $C_o = 5\%$, respectively. The breakthrough time equivalent to 1035 s has been tabulated at highest examined feed flow of 5 L/min with $T=298$ K. Hence, the exhaustion/or breakthrough periods decrease suggestively on increasing the feed rate and is in agreement with the literature [56, 62]. Similarly, the mass transfer zones described for adsorption response profiles are to a certain extent narrow, demonstrating an improved utilization of bed capacity. The S-shape curve steepness is specifically important and much beneficial for the cost-effective CO_2 capture using adsorption. The adsorbate concentration raises rapidly equivalent to the ending of breakthrough curve at the situation the adsorbent is warranted as unproductive and this condition occurs when the breakthrough point is reached. The initial CO_2 concentration dependence on adsorption profiles at 4 L/min feed flow and 298 K has been depicted (Fig. 4.6) for commercial adsorbent.

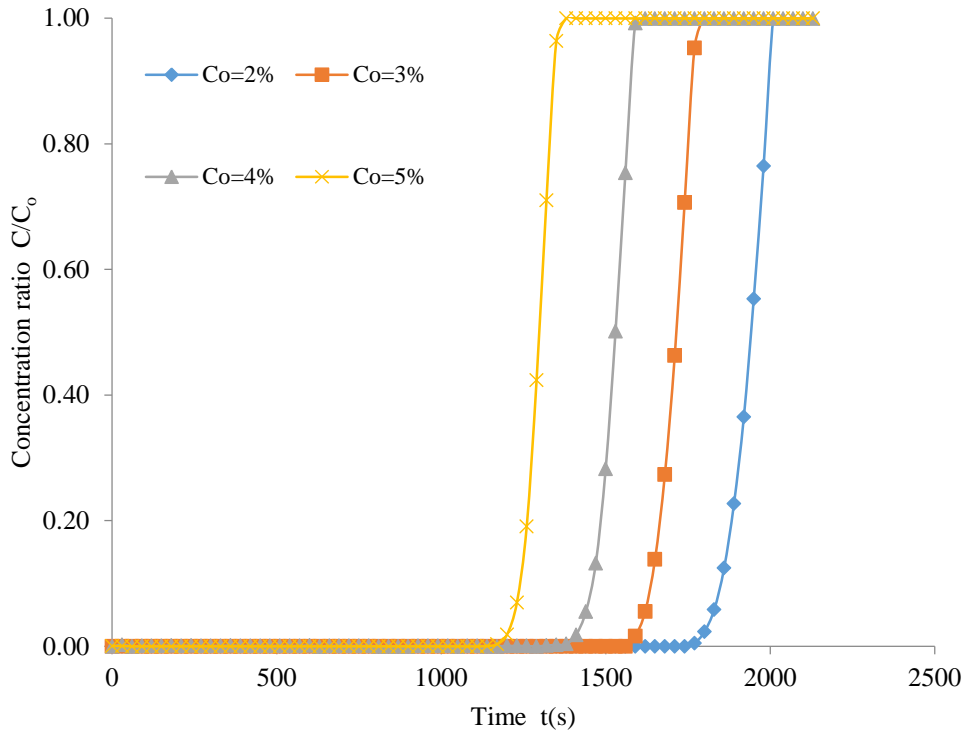


Fig. 4.6 CO_2 concentration dependent breakthrough profiles for AC-Norit at $F= 4$ L/min, $T= 298$ K

The different initial adsorbate amount in the range of 2 - 5% are fixed with a system 1.25 bars pressure absolute. The concentration $C_o = 2\%$ in feed mixture at 298 K contributes to a breakthrough period of 2004 s at 4 L/min feed flow rate. The exhaustion period is observed to reduce to 1770 s with an increased level of initial CO_2 gas in feed at 3%. The breakthrough period further reduces to 1403 s with an increased C_o to 4% with 298 K and 4 L/min. The exhaustion period further lessens to 1349 s on raising the CO_2 level at 5% under the constant condition of feed flow. The prolonged breakthrough and exhaustion periods are always needed for increased CO_2 uptake. The breakthrough span is proportional to the CO_2 uptake and also varies reciprocally with feed concentration [62].

4.1.3 ADSORPTION CAPACITY AND COLUMN EFFICIENCY

The CO_2 loading is assessed by applying material balance. Utilizing an adsorption breakthrough profiles, the stoichiometric period (t_{st}) equivalent to the total capacity is generally calculated as [56]:

$$t_{st} = \int_0^{\infty} \left(1 - \frac{C}{C_o}\right) dt \quad (4.1)$$

Knowing stoichiometric period t_{st} , the CO_2 capacity q of the bed may be evaluated [53] as:

$$q = \frac{F t_{st} C_o}{m_a} \quad (4.2)$$

Where, m_{ad} : adsorbent mass, F : feed flow rate, C : adsorbate (CO_2) concentration at time t , C_o : initial CO_2 concentration in the feed. The above equation is multiplied by CO_2 density and divided by adsorbate molecular weight to determine the adsorption capacity in terms of mmol/g. Upto the breakthrough time t_b , the time equal to the usable capacity can be calculated as:

$$t_u = \int_0^{t_b} \left(1 - \frac{C}{C_o}\right) dt \quad (4.3)$$

The column capacity until the breakthrough point can be determined as:

$$q_u = \frac{F t_u C_o}{m_a} \quad (4.4)$$

The efficiency based on column capacity is determined as:

$$\eta = \frac{q_u}{q} = \frac{\int_0^{t_b} \left(1 - \frac{c}{C_o}\right) dt}{\int_0^{\infty} \left(1 - \frac{c}{C_o}\right) dt} \quad (4.5)$$

The usable bed length upto the breakthrough point Eq. (4.6):

$$L_b = \frac{t_u}{t_{st}} L \quad (4.6)$$

L: total column height

The adsorption effectiveness determined for AC-Norit at various temperatures has been summarized and shown in Table 4.2. The CO₂ uptake varies substantively with temperature for AC-Norit and varies negatively with temperatures. The maximal CO₂ uptake (q) equal to 0.613 mmol/g for AC-Norit at 298 K with 4 L/min is achieved. The minimal adsorbent capacity of 0.377 mmol/g was obtained at an elevated temperature of 328 K. Every CO₂ adsorption based capture system forecasts a lessening in the CO₂ uptake with an increased in temperature. The fraction of total column capacity efficiently used is 87.8% for AC-Norit at an increased temperature of 318 K. It is observed that column efficiency varies marginally with temperature. The total column length (L) for the adsorption experimental study is 25 cm. The bed length used upto the breakthrough point is 21.41 cm at 298 K for carbon based adsorbent. The maximal usable bed height equal to 21.95 cm is determined at increased temperature of 318 K. The bed is effectively used upto the usable bed height and afterwards, the bed is regenerated for further adsorption study. Technologically, the cycle period and feed flow decides the size of adsorber. Applying a bed length of less than or equal to 12 cm is infrequently recommended to decrease an adsorber height and drop in pressure. However, empty bed requires more regeneration energy and does not provide inclusive separation.

Table 4.2 The temperature dependent adsorption performance for AC-Norit (F= 4 L/min, C₀=5%)

T (K)	q (mmol/g)	η (%)	L _b (cm)
298	0.613	85.6	21.41
308	0.519	87.7	21.59
318	0.446	87.8	21.95
328	0.377	87.2	21.79

An adsorption capacity, column efficiency and usable bed height for commercial adsorbent (AC-Norit) studied at different feed flows have been summarized and presented in **Table 4.3**. The CO₂ uptake differs positively and substantially as a function of feed flows for carbon based adsorbent. The utmost CO₂ loading of 0.997 mmol/g for AC-Norit at 298 K with 5 L/min was achieved. The minimal studied feed flow of 2 L/min attributes to a capacity of adsorption and capture capacity nearly equal to 0.628 mmol/g was realized for AC-Norit at 298 K with C₀= 5%. It is clearly observed that adsorption capacity increases with increased feed flow rates. The adsorption performance of commercial activated carbon is reasonably good under different conditions of feed flows.

The highest fraction of total capacity effectively used is 92.8 % for AC-Norit with a feed flow of 2 L/min under the same condition of temperature and initial adsorbate gas level. In general, it is seen that effective column efficiency decreases marginally with increased feed flow from 2 to 5 L/min. The utilized bed length upto the breakthrough reduces with increased feed flows. Also, the bed length utilized upto the breakthrough point is 23.20 cm at 2 L/min with 298 K for AC-Norit. It can be predicted that effective column efficiency and bed length utilized upto the breakthrough point varies negatively with augmented feed flows. It can be suggested that Norit-RB2 activated carbon performs well and may be suitable for CO₂ separation from CO₂/N₂ feed.

Table 4.3 Feed rates dependence adsorption performance for AC-Norit at $C_0=5\%$, $T=298\text{ K}$

F (L/min)	q (mmol/g)	η (%)	L_b (cm)
2	0.628	92.8	23.20
3	0.783	91.2	22.82
4	0.878	90.8	22.69
5	0.997	89.2	22.29

Initial CO_2 concentration dependent adsorption performance for AC-Norit investigated has been outlined in Table 4.4 under constant conditions of temperature and feed flows. The CO_2 loading differs largely and positively with initial concentration of CO_2 in feed. The maximal CO_2 uptakes of 0.941 mmol/g has been obtained for AC-Norit at 5% adsorbate concentration. The adsorbate capacity is proportionate with the initial adsorbate gas concentration in feed mixture. The adsorption performance of developed activated carbon is reasonably high at any fixed initial CO_2 gas level in feed.

There is no clear tendency of efficiency change as a function of C_0 under constant conditions of column temperature and feed rate. The reason of such efficiency trend is due to small incremental change in CO_2 concentration (from 2 % to 5% maximal with 1% incremental value). It is due to the fact IR sensor used for measuring the CO_2 concentration in the bed outlet works well upto CO_2 concentration of 5%. Therefore, it is also suggested to fix the adsorbate amount ranging from 0 - 5 % for the precise and correct measurements. The maximal fraction of total capacity successfully used is 91.0 % at the 2 or 3 % CO_2 level with 4 L/min for AC-Norit. The maximal bed length of 22.75 cm is utilized for commercial activated carbon for bed length of 25 cm. The commercial activated carbon performs reasonably well in view of adsorption capacity, column efficiency and usable bed length as a function of initial carbon dioxide concentration.

Table 4.4 CO₂ concentration dependence adsorption performance at F= 4 L/min, T=298 K

C _o (vol.%)	q (mmol/g)	η (%)	L _b (cm)
2	0.550	91.0	22.74
3	0.737	91.0	22.75
4	0.884	88.6	22.14
5	0.941	90.3	22.57

4.1.4 MASS TRANSFER ZONE AND CAPACITY UTILIZATION FACTOR

An adsorbate gas volume (C) in solid phase and fluid phase vary as a function of time and location. Initially, CO₂ molecule movement happens typically in the locality of bed input and feed comes in contact with fresh porous adsorbent. The CO₂ concentration in the feed mixture decreases drastically with position effectually to zero before the end point of column is reached as long as porous adsorbent has no CO₂ at t = 0 as adsorption starts. The column portion, where CO₂ is really gets adsorbed on the adsorbent or the column portion where CO₂ concentration differs mostly is usually known as zone of mass transfer (L_{MTZ}) [56]. The confines are generally presumed as C/C_o = 5 to 95% (vol.%). A lean MTZ symbolizes the efficient utilization of the chosen adsorbent leading to minimization of the cost of regeneration. MTZ explicitly moves from the inlet to the exit side, indicating that the adsorbent nearby the input achieves the state of saturation by CO₂. Fig. 4.7 exhibits an adsorption breakthrough profiles and subsequently, the movement of mass transfer zone.

The steady adsorption of CO₂ by capture is anticipated for approximating the mass transfer zone [105] through the Equation (4.7):

$$L_{MTZ} = \frac{2L(t_s - t_b)}{t_s + t_b} \quad (4.7)$$

The t_b: breakthrough period, t_s: exhaustion period, L: total column height.

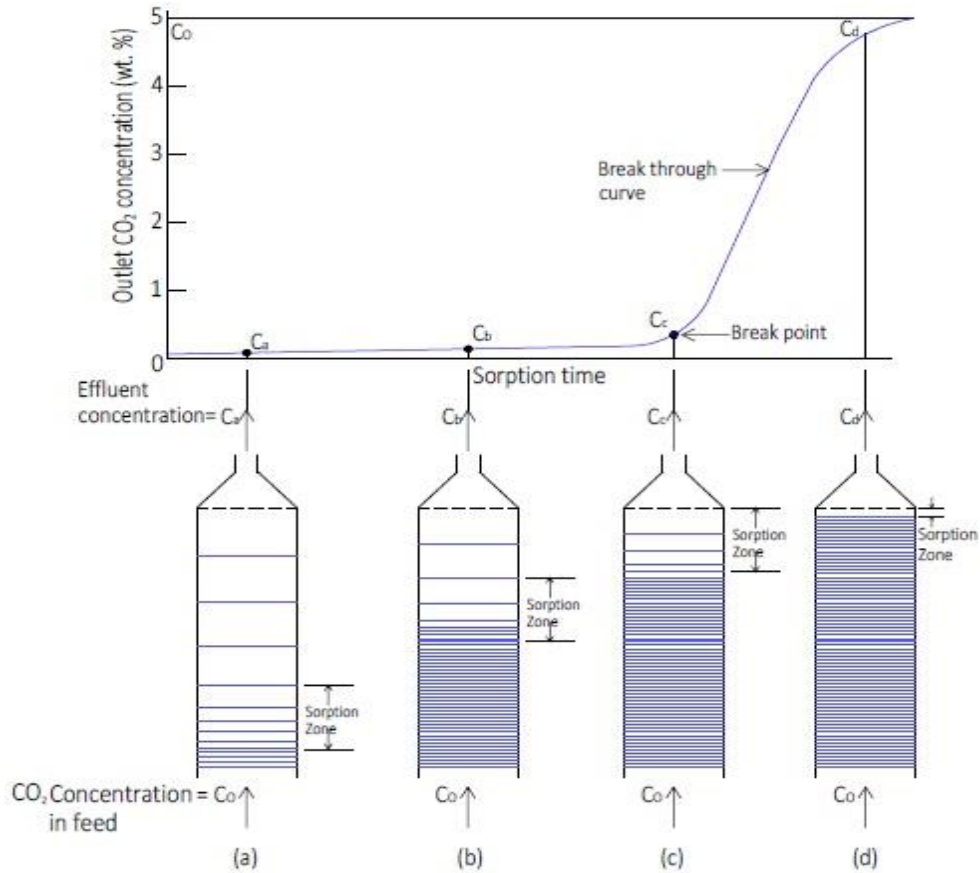


Fig.4.7 Adsorption breakthrough profile and shifting of MTZ

The area above the adsorption breakthrough profiles to the breakthrough period (t_b) signifies the actual amount of CO_2 adsorbed. The adsorption breakthrough profiles are normally steep in case the L_{MTZ} is narrow compared with the column height and breakthrough point confirms the utilization of the nearly most of the capacity. An adsorption profile very much extended in the situation in case L_{MTZ} is nearly equal to column height. The mass transfer zone is described by insignificant width and no resistance to mass transfer. Under such state, the adsorption breakthrough curve conceivably remains a vertical line between $C/C_o = 0$ and 1.0 when examined adsorbent become saturated completely. The porous adsorbent is wholly saturated between the column inlet and the start of the L_{MTZ} under the breakthrough condition.

The adsorbent under the MTZ goes from approximately saturated to almost no adsorbate, and for a rough average the porous adsorbent possibly assumed to be nearly 50% saturated. For the supposed adsorption breakthrough profiles as uniform, the capacity utilization factor (f) is obtained as given below:

$$f = 1 - \frac{0.5 L_{MTZ}}{L} \quad (4.8)$$

Parameters of the CO₂ adsorption by capture, i.e. saturation time, breakthrough time, L_{MTZ} and f have been estimated for AC-Norit and depicted in Table 4.5. The saturation and breakthrough periods diminish with increased temperature.

Table 4.5 Summary of characteristic parameters for CO₂ capture of AC-Norit activated carbon

T(K)	F (L/min)	C _o (vol.%)	t _b (s)	t _s (s)	L _{MTZ} (cm)	f
298	4	5	767	897	3.88	0.922
308	4	5	705	804	3.28	0.934
318	4	5	610	695	3.26	0.935
328	4	5	523	600	3.43	0.931
298	2	5	1830	1972	1.87	0.963
298	3	5	1390	1523	2.28	0.954
298	5	5	1035	1161	2.87	0.432
298	4	2	1823	2004	2.36	0.953
298	4	3	1613	1770	2.32	0.954
298	4	4	1403	1584	3.03	0.939

The capacity utilization factor varies slightly with increased temperature. Smaller mass transfer zone yields to an improved utilization factor. The shortest L_{MTZ} equal to 3.26 cm yields to a good utilization factor of 0.935 at a temperature of 318 K with F= 4 L/min and C_o= 5%. The breakthrough and saturation periods lessen with increased feed flow ranging from 2 to 5 L/min. The different feed

rates contribute substantially to L_{MTZ} and f as apparent from the findings. The L_{MTZ} of 1.87 cm was determined at lowermost feed flow of 2 L/min resulting to an increased utilization factor of 0.963 with 298 K and $C_o = 5\%$. The reduced utilization factor of 0.432 was estimated at maximal selected feed flow of 5 L/min under constant operating conditions of initial CO_2 concentration and temperature. The breakthrough time also depends on the initial CO_2 concentration in feed. The utilization factors assessed at various C_o do differ markedly under constant temperatures and feed flows. Largely, the under different constant operating conditions, smaller L_{MTZ} suggests good utilization factor. The minimal L_{MTZ} equivalent 1.87 cm for 25 cm total bed length means the utilization of good column capacity under breakthrough condition. The maximal $f = 0.963$ was forecast at lowest temperature of 298 K with $F = 2$ L/min and $C_o = 5\%$. The high utilization factor is always measured and assumed essential for cost-effective separation of CO_2 from feed gas mixture.

4.1.5 TEMPERATURE PROFILES AND REPEATABILITY MEASUREMENT

Fig. 4.8 illustrates the profiles of temperature measured by thermocouples T1 to T6 positioned along the longitudinal position in the column for adsorption-desorption phenomenon with $F = 4$ L/min and $C_o = 5\%$. Temperature of hot-water circulator was preset at 298 K using PID controller for observing the temperature variations during the adsorption-desorption cycle. The temperature sensors (T1-T6) are sited at different axial locations inside the column. T6 and T1 relate to temperatures at extreme bottom and top positions, correspondingly. The T5 to T2 denotes in-between temperatures from the bottom to top side. All the temperature sensors are insulated type-K thermocouples with ± 0.15 K accuracy.

The rise in temperature as observed in Fig. 4.8 (also in Figs.4.14, 4.23 and 4.38) above the set value (298 K) during the adsorption period attributed to an exothermic nature of adsorption and associated with the liberation of heat. During initial period, the rise in temperature as shown for temperature sensors T1-T6

signifies the exothermic nature of adsorption. After that, the reduction in temperature below set point of 298 K confirms the endothermic nature of desorption process. The similar nature of profiles was observed for other examined adsorbents also [56]. The thermal deviations during CO₂ adsorption process increased the temperature above the set point indicated by sensor T7. The temperature deviation became smaller as mass transfer zone (MTZ) moves toward the end side of column.

In general, a bed temperature increase of 283 K to 323 K may occur when handling vapors having only 1% adsorbate concentration. The temperature increase is limited by bed heat loss for small diameter bed, but a large adsorber approximately adiabatically. Mass transfer forefront is signified by an increased temperature due to exothermic nature of process and aided by perceived profiles at various axial locations inside the column. Furthermore, with increased concentration of CO₂ in the mixture, the heat evolved during adsorption leads to increase in temperatures at various positions.

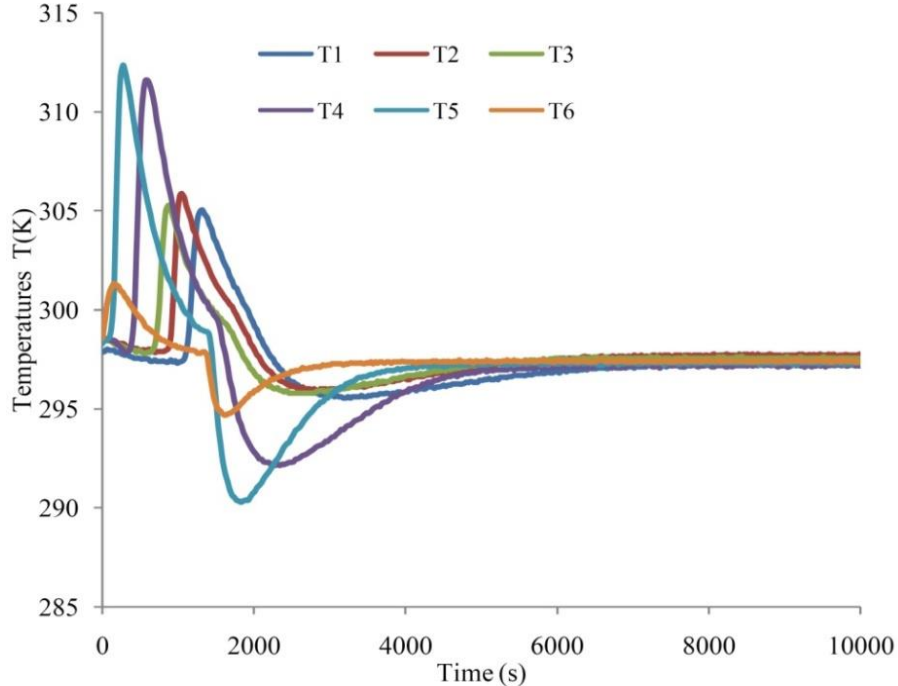


Fig. 4.8 Temperature profiles along axial positions for AC-Norit ($F= 4$ L/min and $C_o = 5\%$)

4.2 ADSORPTION STUDY USING MOLECULAR SIEVE MS-3Å

The commercially available molecular sieve (MS-3Å) in cylindrical shape with average diameter of 1.60 mm was procured from Sigma-Aldrich for experimental study. It is used as such without any further treatment. The molecular sieve used for the investigation has been depicted in Fig. 4.9. The same operating conditions are applied for adsorption using MS 3Å as examined in case of study using Norit-RB2.



Fig. 4.9 Molecular sieve 3Å (MS-3Å)

4.2.1 CHARACTERIZATION OF MOLECULAR SIEVE MS-3Å

The molecular sieve 3Å is characterized using NovaWin (Quantachrome) surface analyzer at outgas temperature of 573 K. The analysis period was 88.3 min and N₂ supplied for carried out an analysis. The surface characterization findings for investigated adsorbent are depicted in Table 4.6. The surface area (single point) of 26.42 m²/g was acquired for molecular sieve. The Langmuir surface area is almost double of either single or multiple point surface area. The 0.02 cm³/g pore volume was obtained for MS 3Å which is much smaller. The pore radius of 8.44 Å was determined for commercial available molecular sieve. Largely, the adsorbents are

vastly porous materials. The adsorption takes place mostly either at definite sites within the particles or on the pore walls of the adsorbent.

Table 4.6 BET Surface characterizations of molecular sieve MS-3Å

Surface characteristics	MS-3Å
Single point surface (m^2/g)	26.42
Multiple point surface area (m^2/g)	26.87
Langmuir surface area (m^2/g)	46.21
DFT Pore volume (cm^3/g)	0.02
DFT Pore radius (Å)	8.44

The surface morphology of MS-3Å was analyzed by the Scanning electron microscope (Model: Quanta 250-FEI, Japan). The structural images have been depicted in Fig. 4.10 (a) - (b) for MS-3Å. The pores can be envisioned and the pores nearly spread above the produced porous structure, as shown in Fig. 4.10 (a) with 2500 x level and Fig. 4.10(b) with 20,000 x magnifications for MS-3Å adsorbent.

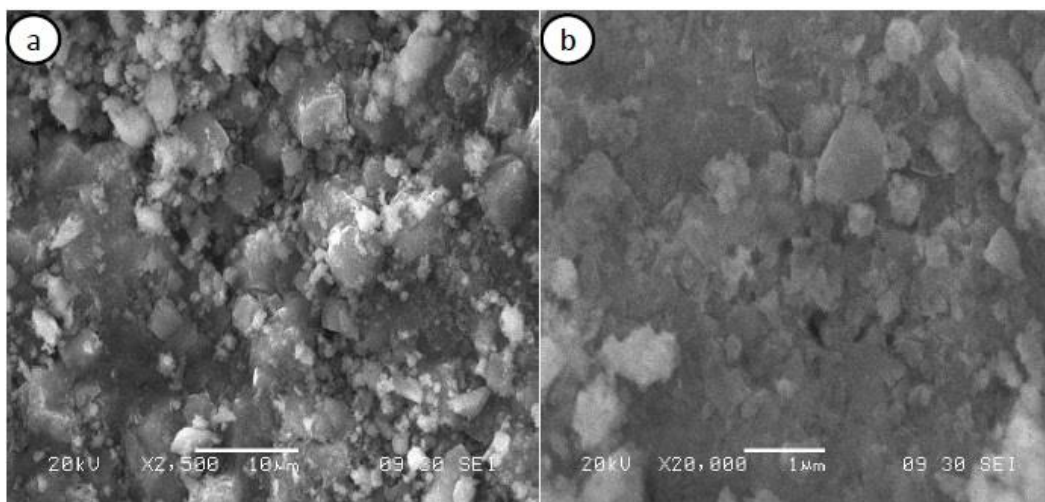


Fig.4.10 SEM characterization of molecular sieve MS-3Å: (a) 2500 x magnification and (b) 20,000 x magnification

SEM images show a sponge-like surface morphology with micro-sized particles of irregular surface shape. There is an accumulation of ash on the adsorbent surface, which may reduce the surface area due to the blockage of pores. The reduced surface area as observed in the SEM micrograph is confirmed through data obtained through BET surface analyzer. The very consistent and high-density pore structures are particularly effective for CO₂ capture by adsorption from feed.

4.2.2 BREAKTHROUGH PROFILES

The different feed flows are measured and regulated by mass flow controllers equipped with control console. The experiments were performed at 4 L/min feed flow with an CO₂ concentration fixed at 5% (vol. %). The operating system pressure was controlled at 1.25 bars absolute.

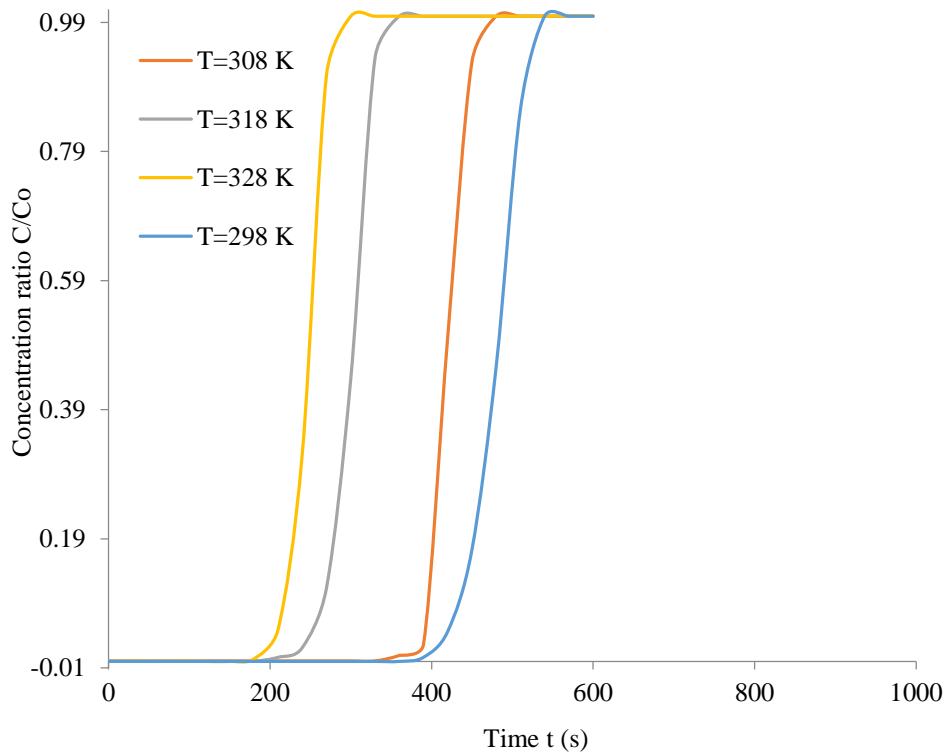


Fig. 4.11 Temperature dependent breakthrough profiles for MS-3Å at F= 4 L/min, C_o=5%

The adsorption breakthrough curves generated at various temperatures i.e. 298 K, 308 K, 318 K and 328 K for MS-3Å have been depicted in Fig. 4.11. The total mass equal to 230 g was used for the study. The breakthrough span of 417 s has been calculated with a saturation period of 513 s at 298 K. The breakthrough period reduced to 388 s with increased temperature at 308 K. The breakthrough period further lessens to 250 s for MS-3Å with an increased temperature at 318 K. The saturation and breakthrough periods of 210 s and 283 s have been determined at 328 K using the breakthrough curves.

It is observed clearly that breakthrough and saturation periods reduce considerably with increased bed temperature. The lengthy breakthrough or saturation periods are always considered essential for an improved CO₂ capture. In general, the prolonged breakthrough time at lower temperatures indorses increased CO₂ loading. The breakthrough period relies significantly on the temperature at which the adsorption takes place. Generally, the time it takes to touch 5% of the maximal concentration at column exit position is known as breakthrough time.

The performance of bed for CO₂ adsorption is thoroughly explained by the steepness of breakthrough profiles as apparent from Fig. 4.11. The utilization of required CO₂ loading corresponding to breakthrough condition is preferred for profitable adsorption of adsorbate CO₂ by capture. The abruptness of adsorption breakthrough profiles attributed to the narrowness of mass transfer zone. A smaller MTZ zone symbolizes the faster capture of CO₂. Also, some molecules apprehended more firmly than others by adsorbent surface due to polarity. In many cases, the adsorbate is detained firmly and sufficiently to permit comprehensive capture of CO₂ from feed with very small/no adsorption of other gas component like N₂. The steepness of adsorption breakthrough curves shown in Fig. 4.11 postulates comparable utilization of CO₂ loading.

Fig. 4.12 depicts the feed flow dependent breakthrough curves for MS-3Å. The feed flows ranging from 2 to 5 L/min are investigated at 1.25 bars with a temperature of 298 K. The 2 L/min flow exhibits a breakthrough period of 650 s.

The breakthrough period is observed to decrease to 460 s with a raised feed flow to 3 L/min. The increased feed rate of 4 L/min contributes to reduced saturation and breakthrough periods of 311 s and 415 s with 298 K and $C_o= 5\%$, respectively. The breakthrough time of 200 s was achieved at maximal examined flow of 5 L/min feed rate with $T= 298\text{K}$. Accordingly, the breakthrough and saturation periods reduce with increased feed flow consisting of one of the component as an adsorbate gas. It can be suggested that increase feed flow rate contributed to early appearance of breakthrough due to that fact that more CO_2 is passed through the column compared to a reduced flow rate and similar trends were also observed in literature [56].

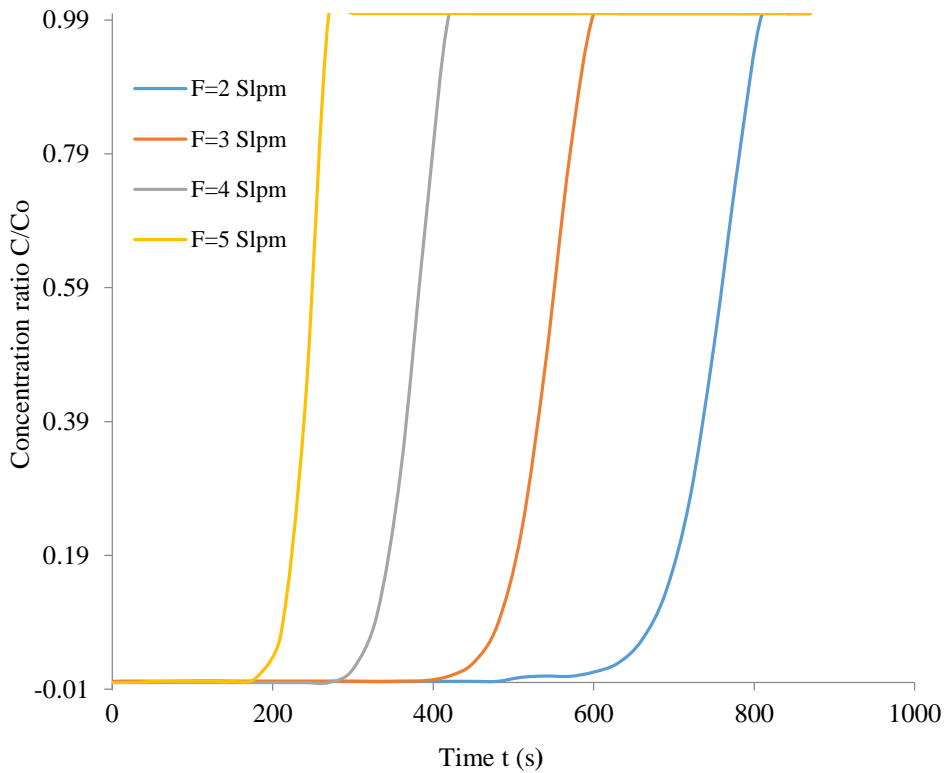


Fig. 4.12 Flow rate dependent breakthrough profiles for MS-3Å at $C_o=5\%$, $T= 298\text{ K}$

It is found that saturation and breakthrough times depend unusually on flow rate of feed. Consistently, improved bed capacity utilization is described by narrow mass transfer zone witnessed for adsorption breakthrough profiles. The vastly steepness of the profiles is beneficial for the economical capture of CO_2 from feed

consists of CO₂ and N₂. The C increases rapidly equivalent to the curve ending under the condition where the adsorbent is reflected as unproductive and this condition arrives when the breakthrough point is achieved.

The reliance of C₀ on the breakthrough profiles for MS-3Å has been depicted in Fig. 4.13 under the same operating conditions of feed flow (F = 4 L/min) and temperature (T = 298 K). The different initial adsorbate concentration ranging from 2 - 5% were controlled with operating 1.25 bars pressure. The adsorbate concentration C₀= 2% in feed at 298 K attributed to a breakthrough period of 420 s at 4 L/min. The exhaustion and breakthrough periods were identified to reduce to 543 s and 413 s with increased level of initial adsorbate gas in feed at 3% level. The breakthrough period further reduced to 360 s with an increased C₀ to 4% with 298 K and 4 L/min. It can be concluded that breakthrough and saturation periods slightly reduces with increased inlet CO₂ concentration and according to the findings [56, 81].

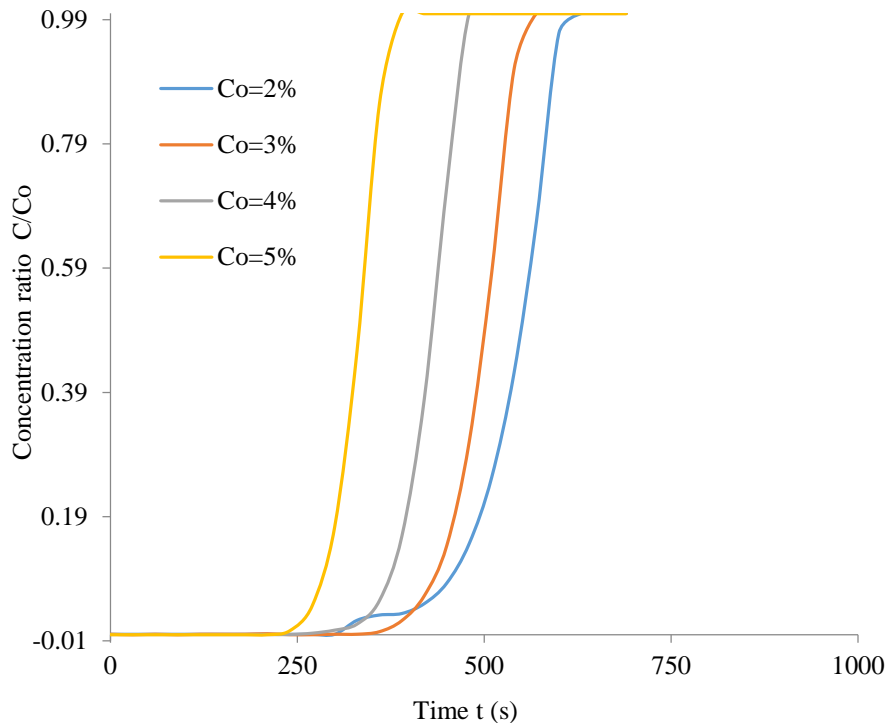


Fig. 4.13 CO₂ concentration dependent breakthrough profiles for MS-3Å (F=4 L/min, T=298 K)

The exhaustion period further diminishes to 380 s on increasing the CO₂ level at 5% under the fixed operating condition of feed flow. The prolonged breakthrough and exhaustion times are always required for increased CO₂ uptake. Utmost 5% adsorbate concentration in the feed forecast the breakthrough time of 1695 s and establishes that the augmented initial CO₂ amount documented to the early appearance of exhaustion/breakthrough periods. The breakthrough span is proportional to the CO₂ loading and varies reciprocally with feed concentration.

4.2.3 ADSORPTION CAPACITY AND COLUMN EFFICIENCY

The adsorption performance with reference to column efficiency, adsorption capacity and usable bed height calculated for MS-3Å at various temperatures is presented in Table 4.7. The CO₂ loading varies noticeably with temperature for examined adsorbent and changes negatively with bed temperatures. The maximal CO₂ capacity of 0.314 mmol/g is obtained for MS-3Å at 298 K and feed flow of 4 L/min. The adsorption loading reduces to 0.265 mmol/g with an increased temperature at 308 K. The lowest CO₂ loading of 0.153 mmol/g is obtained at highest examined temperature of 328 K.

Most the CO₂ capture system forecasts a decrease in the carbon dioxide capture capacity with an increased temperature. The fraction of total capacity effectively exploited is 0.845 for MS-3Å at 298 K. The effective column length (L) for the adsorption unit is equal to 25 cm. Also, the bed length used upto the breakthrough point is 19.44 cm at 298 K for MS 3Å. The minimal usable bed height of 17.07 cm is determined at maximum examined temperature of 328 K. It is suggested clearly that all adsorption characteristics column capacity, column efficiency and usable bed height reduce with increased bed temperature. Industrially, the essential cycle period and feed flow decides the size of adsorber. In general, applying a bed length of less than or equal to 12 cm is sometimes advised to reduce adsorber height and drop in pressure, however empty column requires more regeneration energy and does not offer comprehensive separation.

Table 4.7 Adsorption characterizations at different temperatures MS-3Å at F= 4 L/min, C_o=5%

T (K)	q (mmol/g)	η (%)	L _b (cm)
298	0.314	84.5	19.44
308	0.265	83.4	19.18
318	0.187	74.6	17.16
328	0.153	74.2	17.07

The feed flow dependent adsorption performance for MS-3Å has been determined and summarized in Table 4.8. The CO₂ uptake changes positively and noticeably with feed flow for examined adsorbent. The lowest examined feed flow of 2 L/min contributed to a minimal capture capacity and CO₂ loading of 0.194 mmol/g was attained for MS-3Å at the 298 K and C_o= 5%. The highest value of adsorption capacity 0.262 mmol/g was achieved at 3 L/min of feed rate with constant concentration of C_o=5%. The maximal fraction of total capacity effectively used is 0.890 for MS-3Å with a feed flow of 2 L/min under the same constant conditions of initial adsorbate concentration and temperature.

At large, it is seen that effective column efficiency decreases slightly with increased feed flows from 2 to 5 L/min. The usable bed height upto the breakthrough reduces with increased feed flows. Also, the column length utilized upto the breakthrough point is 20.47 cm at 2 L/min with 298 K for MS-3Å. The minimum usable bed height of 17.16 cm with column efficiency of 74.6 % is determined for maximum investigated flow rate of 5 L/min. It is clearly observed that column efficiency and usable bed height reduce with increased feed rate. It can be predicted that effective column efficiency and bed length utilized upto the breakthrough point varies negatively with augmented feed flow rates. The unutilized or unusable bed length of the total bed height of MS-3Å is comparatively more.

Table 4.8 Adsorption characteristics at various feed rates for MS-3Å at T=298 K, $C_o=5\%$

F (L/min)	q (mmol/g)	η (%)	L_b (cm)
2	0.235	89.0	20.47
3	0.262	77.6	17.80
4	0.244	74.9	17.23
5	0.194	74.6	17.16

The adsorption performance for MS-3Å using fixed bed continuous column determined as a function of initial adsorbate gas concentrations in the feed has been depicted in Table 4.9. The CO₂ uptake varies largely and positively with initial concentration of adsorbate gas in feed mixture. The minimal and maximal CO₂ loading of 0.181 mmol/g and 0.279 mmol/g achieved for MS-3Å at 2% and 5% CO₂ level, respectively. An increased adsorption capacity of 0.248 mmol is realized at an increased initial CO₂ concentration to 3%. The CO₂ uptake varies proportionally with the initial adsorbate gas level i.e.CO₂. The highest fraction of total capacity which is effectively used stands at 0.760 for MS-3Å at 3 % CO₂ level with 4 L/min.

Table 4.9 Adsorption characteristics at different initial adsorbate concentration for MS-3Å (T=298 K, F= 4 L/min)

C_o (vol.%)	q (mmol/g)	η (%)	L_b (cm)
2	0.181	70.2	16.15
3	0.248	76.0	17.48
4	0.276	75.8	17.43
5	0.279	71.1	16.35

The lowest column efficiency of 70.2% was achieved at examined feed concentration of 2% at a fixed condition of temperature and feed flow. Also, the minimal usable bed height of 16.15 cm was realized of the total bed height of 25

cm. The unutilized bed height is significant that specifies improper utilization of bed capacity. The maximum usable bed height equal to 17.48 cm was tabulated at an initial $C_o = 3\%$. The variations in the usable bed height as function of initial CO_2 level is insignificant and it may be due to the small change in C_o . This is because of operational limitations of the instrument.

4.2.4 MASS TRANSFER ZONE AND CAPACITY UTILIZATION FACTOR

An adsorbate amount in solid phase and fluid phase varies with time and also the location in the column. At earliest, the basically CO_2 movement occurs in the vicinity of the bed input and feed comes in contact with fresh porous sorbent. The CO_2 concentration in the feed reduces drastically with position effectually to zero before the end point of bed is reached on condition that that porous adsorbent has no CO_2 at the start of adsorption. The characteristics parameters of the CO_2 adsorption are evaluated for MS-3Å as shown in Table 4.10.

Table 4.10 Summary of characteristic CO_2 capture parameters of MS-3Å

T(K)	F(L/min)	C_o (vol.%)	t_b (s)	t_s (s)	L_{MTZ} (cm)	f
298	4	5	417	513	4.75	0.897
308	4	5	388	459	3.86	0.916
318	4	5	250	335	6.67	0.855
328	4	5	210	283	6.81	0.852
298	2	5	650	803	4.84	0.895
298	3	5	460	593	2.28	0.950
298	5	5	200	268	6.68	0.855
298	4	2	420	598	8.04	0.825
298	4	3	413	543	6.26	0.864
298	4	4	360	475	5.53	0.880

The breakthrough period decrease with increased column temperature. The capacity factor f differs slightly with bed temperature. Reduced zone of mass transfer leads to an increase in utilization factor. The L_{MTZ} equivalent to 2.28 cm results in good utilization factor of 0.950 at 298 K with $F= 3$ L/min and $C_o = 5\%$. The utilization factor decreases with increased temperature and similar trend of reliance of utilization factor on temperature has been reported in literature [56]. The breakthrough and exhaustion spans decrease with increased feed flow consisting of CO_2 varying from 2 to 5 L/min. The feed rate variations contribute substantially to L_{MTZ} and f as evident from the findings presented in Table. The declined f equal to 0.855 is determined at the maximal feed rate of 5 L/min under constant conditions. The breakthrough period also differs with initial adsorbate volume.

The f estimated at different adsorbate volume do change considerably under constant conditions of temperature and feed flow. Largely, the smaller L_{MTZ} specifies good utilization factor. The L_{MTZ} equivalent to 2.23 cm suggests the reasonable usage of bed capacity. The utmost $f = 0.950$ determined at 298 K and $C_o = 5\%$. An improved utilization factor is constantly considered essential for reasonable adsorption of adsorbate gas.

4.2.5 TEMPERATURE PROFILES AND REPEATABILITY MEASUREMENT FOR MS-3Å

The temperature profiles for temperature recorded by various thermocouples are shown in Fig. 4.14. The two sets data collected for molecular sieve MS-3Å. Temperature of hot-water circulator system was fixed at 308 K using proportional integral derivative (PID) controller. The thermocouples are stationed at various positions inside the column. In over-all, temperature rise of approximately 283 K to 323 K may possibly take places in case of treating vapors with just 1% adsorbate (like CO_2 in present study) component. The temperature increase is constrained by heat loss for small diameter adsorption column; however a large adsorber will function nearly adiabatically. Furthermore, with an increased

adsorbate concentration, the heat generated for the period of the adsorption process results in increased temperatures as certified by observed temperatures at different positions using temperature sensors T1-T6.

Repeatability analysis (Fig. 4.15) is performed for examined adsorbent MS-3Å to investigate the re-applicability of the measurement data obtained under different set of operating conditions. The experimental data were recorded at 4 L/min feed flow, 328 K with $C_o=5\%$. The IR sensor equipped with the unit for gauging the exit CO_2 concentration measures accurately upto 5% maximal CO_2 concentration (vol.%) in the feed mixture consisting of CO_2 and N_2 . The tabulated value of coefficient of correlation $R^2 = 0.994$ established a good correlation between the obtained experimental data. The standard deviation $\sigma = \pm 0.012$ (vol. %) was determined as recorded and measured by IR detector. The σ value describes outstanding conformism between the measured quantities. It was acclaimed that measured repeatability was acceptable to rely upon the data obtained for the CO_2 capture by adsorption.

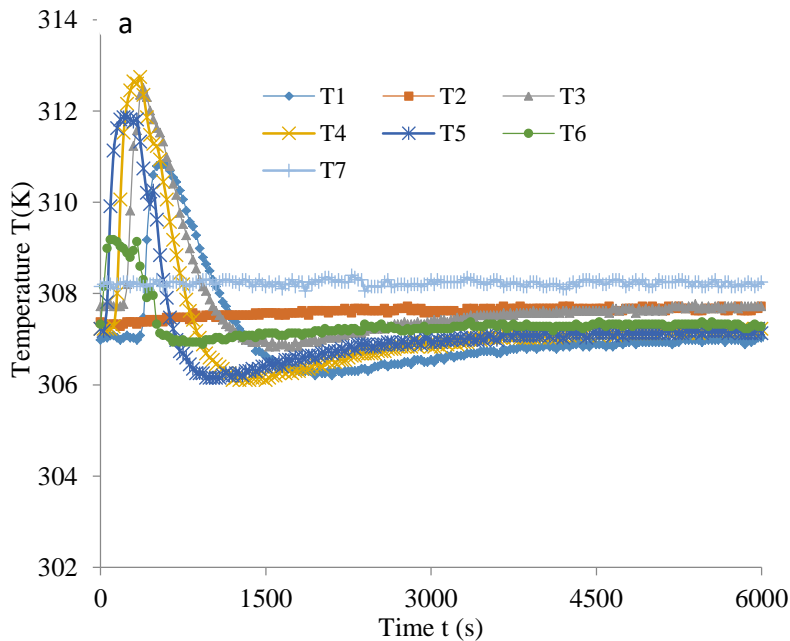


Fig. 4.14 Temperature curves for MS- 3Å at $F= 4$ L/min, $C_o= 5\%$

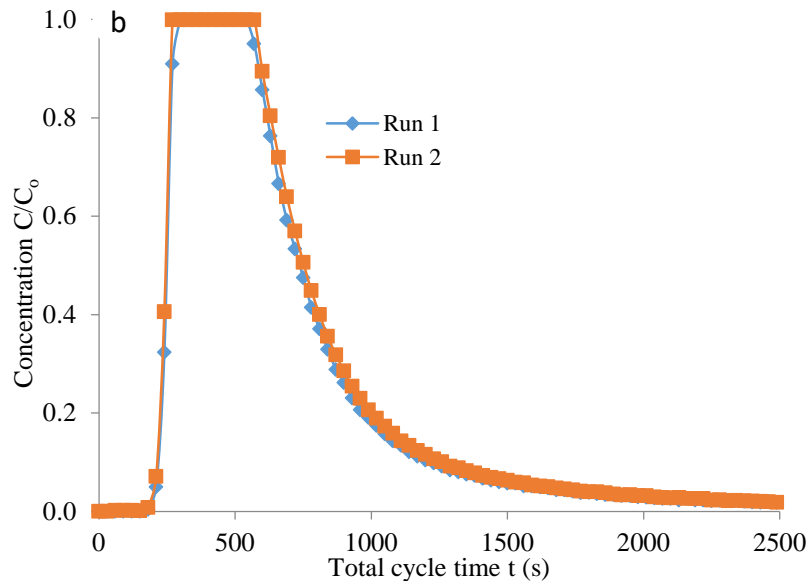


Fig. 4.15 Repeatability measurement for MS-3Å at $F= 4$ L/min, $C_0=5\%$ and $T= 328$ K

4.3 ADSORPTION STUDY USING SILICA GEL TYPE-III

Silica gel type-III (SG) having an average size of 2 mm was purchased from Sigma-Aldrich. It is used as such for experimental investigation of CO_2 capture without any further treatment/operation. The SG was for used comparative analysis with other commercial adsorbents and date pits based activated carbon as depicted in Fig. 4.16.



Fig. 4.16 Silica gel type-III used for adsorption investigation

4.3.1 CHARACTERIZATION OF SILICA GEL TYPE-III

Silica gel type-III was characterized by NovaWin -Quantachrome analyzer for surface properties at 573 K outgases temperature. Earlier to measurement of isotherms, the sample was degassed by the degasser equipped with BET analyzer. After attaining the desired degassing temperature of 523 K, the degas station is chosen with vacuum degas option. The degassing of the adsorbent (sample) is carried out for a period of 150 min. The analysis time span was 88.3 min with N₂ was supplied for analysis. The characterization results for adsorbent SG has been depicted in Table 4.11. The relatively good surface area (single point) equal to 556.4 m²/g is obtained for SG and exhibited a pore volume of 0.06 cm³/g.

The pore volume of the adsorbents has been determined by Barrett –Joyner-Halenda method generally known as BJH method. The tabulated data show that the pore sizes for SG are in nm range. Essentially, the adsorbents are massively porous materials. The sorption occurs mostly either at definite sites within the adsorbent particles or on the pore walls. The experimental N₂ isotherms and pore size distribution (BJH method) have been shown in Fig. 4.17 and Fig. 4.18 using N₂ gas (99.999% pure). The Fig. 4.17 describes the N₂ isotherm obtained upto a pressure (P/P₀) of 0.99 whereas Fig. 4.18 corresponds to pore size distribution with pore size in nm scale.

Table 4.11 BET Surface characterizations of silica gel type-III

Adsorbent characteristics	SG
Single point surface (m ² /g)	556.4
Multipoint surface area (m ² /g)	572.2
Langmuir surface area (m ² /g)	1038.0
Pore volume (cm ³ /g)	0.06
Pore size (Å)	20.45

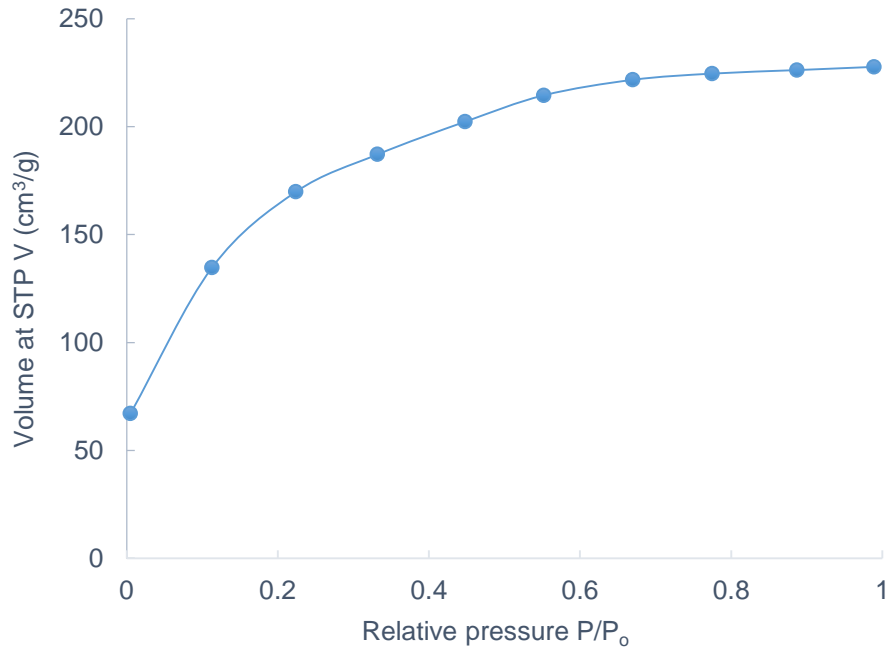


Fig. 4.17 N_2 - adsorption isotherm for silica gel type-III

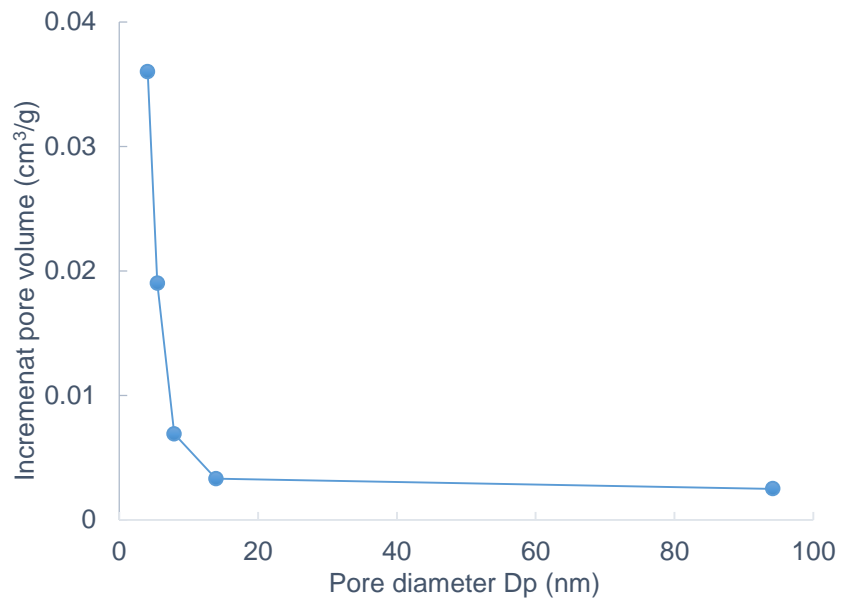


Fig. 4.18 Pore size distribution (BJH method) for Silica gel type-III

The morphology of SG was examined by the SEM (Model: Quanta 250-FEI, Japan). The structural images have been depicted in Fig. 4.19 (a) – (b). Few pores can be envisaged and the observed pores do not practically spread all over the surface, as presented in Fig. 4.19 (a) with 2,500 x level and Fig. 4.19 (b) at 20,000

x magnification for SG. As expected, SEM images do not show any specific morphology but a large cavity of irregular sizes. The SEM images at higher magnification exhibit high roughness. The very irregular and reduced density pore structures are especially in-effective for CO₂ capture from feed gas consisting of N₂ and CO₂.

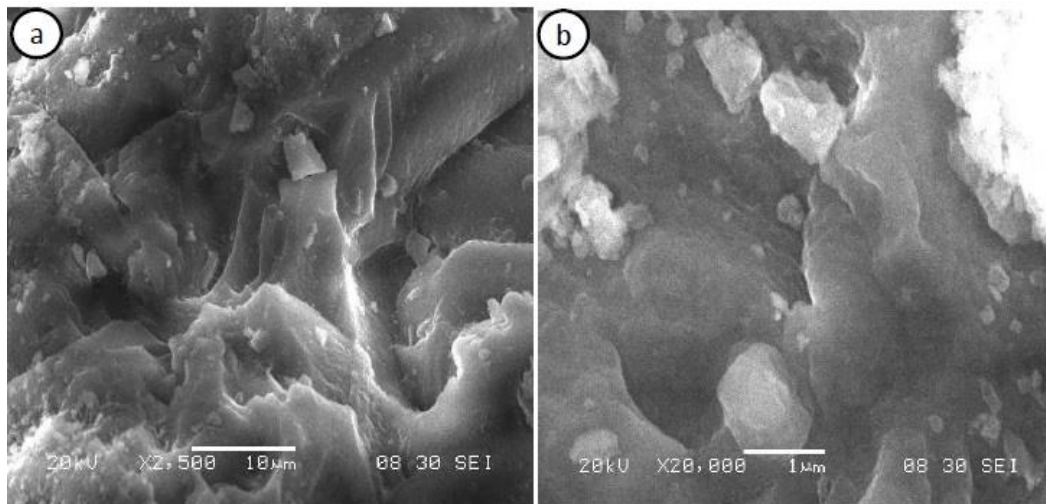


Fig. 4.19 Morphological image of Silica gel type-III: (a) 2500 x magnification and (b) 20,000 x magnification

4.3.2 BREAKTHROUGH PROFILES USING SILICA GEL TYPE-III

The feed flow rates are controlled and measured using mass flow controllers F1 and F2. The mass flow controllers F1 and F2 measure flow rate of N₂ and CO₂, respectively. The feed rate was adjusted at 4 L/min with preset C₀= 5% CO₂ concentration in feed. The system pressure fixed at 1.25 bars (absolute). An adsorbent mass equal to 300 g was used to fill the column upto the effective bed height of 25 cm. The breakthrough profiles corresponding to different temperatures for SG have been shown in Fig. 4.20. The breakthrough period of 224 s has been attained with a saturation period of 358 s at 298 K under constant conditions of flow rate and initial CO₂ level. The breakpoint and exhaustion periods reduces to 183 s and 281 s, respectively with increased temperature at 308 K.

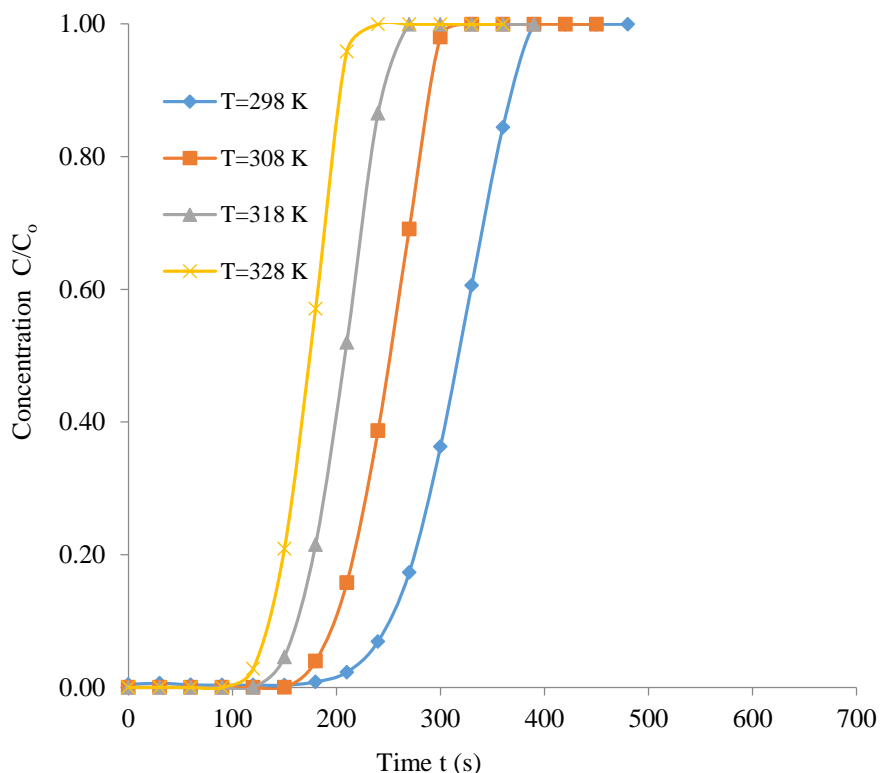


Fig.4.20 Breakthrough profiles for various temperatures at $F= 4$ L/min, $C_o=5\%$ for SG

The breakpoint period reduces to 149 s with saturation period of 245 s using same adsorbent on increasing the temperature to 318 K. The reduced saturation and breakthrough periods of 121 s and 197 s have been tabulated at higher temperature to 328 K. It can be recommended that breakthrough and saturation periods reduced remarkably with increased temperature. The prolonged breakthrough or saturation spans are decisive for the enhanced and better CO_2 uptake. Generally, the extended period (breakthrough or saturation) at decreased temperature advocates enhanced capture capacity of CO_2 .

The utilization of required CO_2 capacity is continuously favored to separate CO_2 cost-effectively. The breakthrough curve steepness infers the degree of thinness of mass transfer zone. Usually, faster adsorption is credited to smaller MTZ. The variations in molecular weight yield to the happening of sorption process. Furthermore, several molecules detained more inflexibly compare to others on the adsorbent surface due to polarity. In various instances, the adsorbate is detained

resolutely and sufficiently to allow inclusive capture of CO₂ by adsorption from feed with very small or no adsorption of non-adsorbate gas molecule.

The dependence of feed flow on breakthrough profiles for SG is shown in Fig. 4.21. The effect of volumetric flow rates in the range from 2 - 5 L/min examined at 298 K and 1.25 bars system pressure. It is noticed that flow rate of 2 L/min attributed to a breakthrough period of 447 s that is significantly lower than the period reported for AC-Norit at the same feed rate. The saturation and breakthrough periods are seen to reduce to 489 s and 330 s with an increased feed flow to 3 L/min. The increased feed rate to 4 L/min attributed to decreased saturation and breakthrough spans of 381 s and 228 s with 298 K and C₀= 5%, respectively. The breakthrough time of 204 s was achieved at highest feed rate of 5 L/min and T= 298 K. It can be acclaimed that saturation (also breakthrough) period reduced with augmented flow rate of gaseous feed mixture.

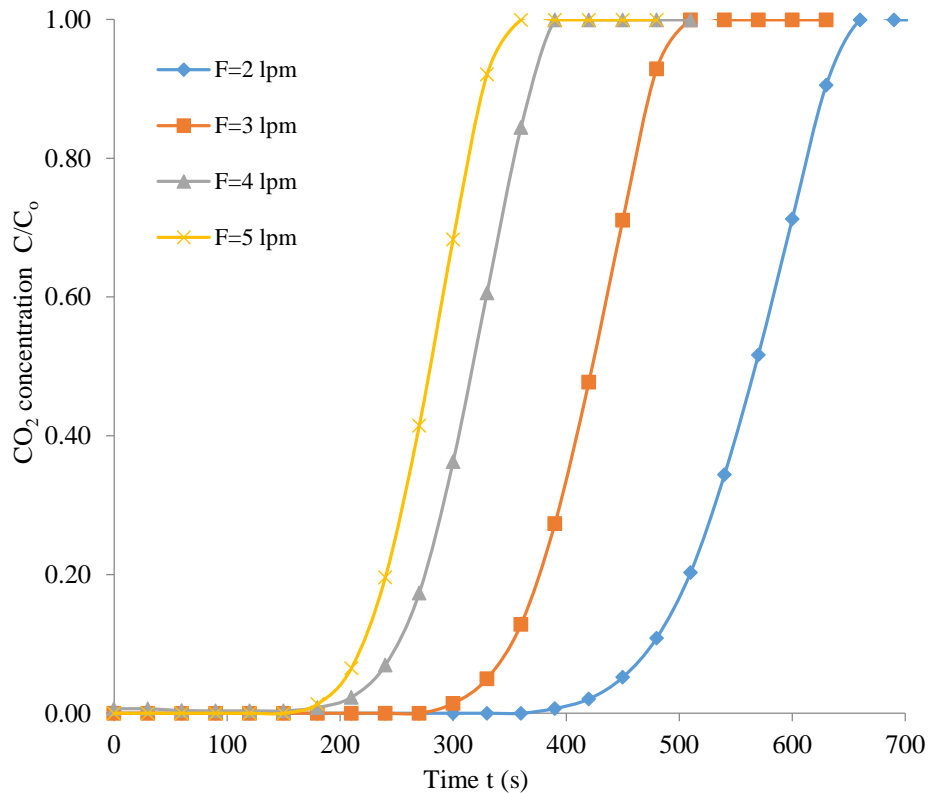


Fig. 4.21 Breakthrough profiles at various feed flow for SG at T= 298 K, C₀=5%

The breakthrough profiles obtained for Silica gel are less steep representing the decreased adsorption performance. Moreover, the mass transfer zones visualized for breakthrough profiles are equally wide, signifying a reduced utilization of CO₂ capture capacity. The sharpness of the response curve is advantageous for the inexpensive capture of CO₂ from feed. The bed outlet concentration C raises quickly equivalent to the curve ending at the condition that an adsorbent is presumed as unproductive and this occurs when the breakthrough point is reached.

The dependence of initial feed concentration C_0 on the breakthrough profiles is explained in Fig. 4.22 for Silica gel at 4 L/min and 298 K. The different CO₂ levels in feed mixture have been fixed with system pressure adjusted at 1.25 bars.

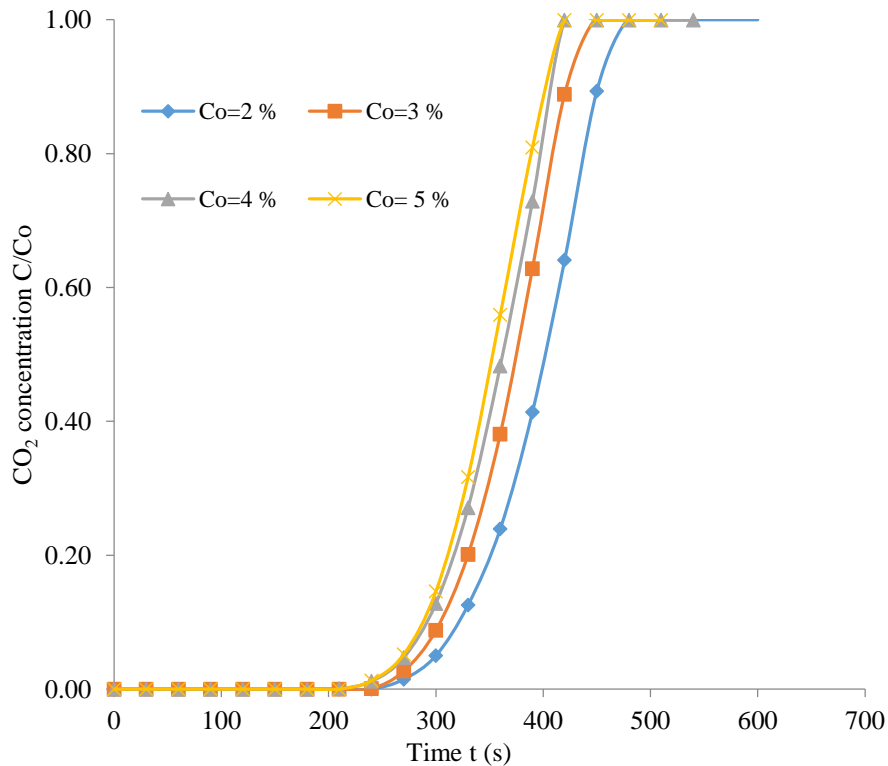


Fig. 4.22 Breakthrough profiles at various CO₂ level for SG at $F=4$ L/min, $T=298$ K

The carbon dioxide concentration $C_0 = 2\%$ in feed fed to the column at 298 K credited to breakthrough and saturation time spans of 300 s and 466 s with flow rate of 4 L/min. The breakthrough and exhaustion spans were observed to

diminish to 278 s and 416 s with augmented initial adsorbate gas concentration in feed at $C_o=3\%$ level. The breakthrough period was further reduced to 270 s with an augmented C_o to 4% with 298 K and 4 L/min. The exhaustion period further lessens to 392 s on raising the CO_2 level at 5%. The findings recommend that breakthrough span decreases on increasing the feed rates. The prolonged breakthrough and saturation periods are always essential for increased CO_2 uptake.

The CO_2 concentration of 4% in feed mixture has projected early onset of saturation period equal to 1976 s. It is clearly noticed that saturation and breakthrough spans are relatively shorter as determined for SG adsorbent. The breakthrough period varies proportionally to the CO_2 loading/capture capacity and differ reciprocally with feed concentration.

4.3.3 ADSORPTION CAPACITY AND COLUMN EFFICIENCY FOR SILICA GEL TYPE-III

The CO_2 capture capacity for SG calculated at investigated temperatures has been depicted in Table 4.12. The CO_2 uptake in terms of mmol/g differs considerably with temperature for chosen adsorbents and changes negatively with bed temperatures. The highest CO_2 uptake (q) of 0.169 mmol/g was attained for SG at temperature of 298 K with 4 L/min.

Table 4.12 The dependence of temperature on CO_2 capacity, column efficiency and usable bed height for SG at $C_o=5\%$, $F= 4$ L/min

T (K)	q (mmol/g)	η (%)	L_b (cm)
298	0.169	62.6	15.02
308	0.124	65.1	15.62
318	0.095	60.6	14.54
328	0.092	61.6	14.78

The minimal CO₂ loading of 0.092 mmol/g was exhibited by SG at maximal examined temperature of 328 K. All the CO₂ capture systems forecasts a reduction in the CO₂ uptake with an increased bed temperature. The fraction of total capacity effectively used is 0.63 for SG at a temperature of 298 K. Meaningfully, highly efficiency adsorbent specifies its feasibility for cost-effective CO₂ capture by adsorption. The column efficiency varies slightly with augmented temperature for selected adsorbents. The efficiency obtained for Silica gel is not very high under different varied operating conditions as presented in Table 4.12.

An adsorption performance for SG tabulated at different feed flows has been shown in Table 4.13. The CO₂ uptake differs positively and considerably with feed rate for examined SG adsorbents. The minimal investigated feed flow of 2 L/min added to a least capacity of adsorption and CO₂ uptake of 0.146 mmol/g was achieved for SG at the 298 K and C₀= 5%.

Table 4.13 The dependence of flow rate on CO₂ capacity, column efficiency and usable bed height for SG at T=298 K, C₀ = 5%

F (L/min)	q (mmol/g)	η (%)	L _b (cm)
2	0.146	72.6	17.43
3	0.168	67.5	16.20
4	0.171	59.8	14.35
5	0.196	59.8	14.35

The efficiency based on column capacity obtained at different flow rates has also been depicted in Table 4.13 for SG. The maximal fraction of total capacity effectually used is 0.73 with a feed flow of 2 L/min for Silica gel under the similar operating conditions of temperature and initial adsorbate concentration. The average value of column efficiency, η is found to be equal to 0.65. In overall, it is perceived that effective column efficiency reduces slightly with augmented feed flow from 2 to 5 L/min under examined range of feed flow rates. Suggestively, comparatively lower efficiency of SG-III commands its unsuitability

for economical CO₂ adsorption from feed gas mixture. It can be suggested that effective column efficiency differs negatively with increased feed rates.

The adsorption performance for SG evaluated as a function of initial adsorbate gas concentrations in feed mixture has been outlined in Table 4.14. The CO₂ uptake varies largely and positively with initial concentration level in feed. The lowest and highest CO₂ capacity of 0.084 mmol/g and 0.184 mmol/g were achieved for SG at 2% and 5% CO₂ level, respectively. Also, an adsorption capacity of 0.148 mmol/g is obtained at a concentration of 4 % CO₂ under constant conditions of temperature and feed rate. The column efficiency based on column capacity varies positively with CO₂ % except at the 4% CO₂ concentration.

Table 4.14 The dependence of initial CO₂ level on capacity, column efficiency and usable bed height for SG at T=298 K, F= 4 L/min

C _o (vol.%)	q (mmol/g)	η (%)	L _b (cm)
2	0.084	64.4	15.46
3	0.119	66.8	16.03
4	0.148	64.8	15.55
5	0.184	68.9	16.54

The minimal column efficiency of 64.4% was determined at minimal CO₂ concentration of 2%. On the other hand, the highest column efficiency of 68.9% was tabulated by adjusting the initial CO₂ concentration equal to 5% in feed mixture. The usable bed height is relatively less ranging from 15.46 cm to 16.54 cm for maximum bed height of 25 cm. The usable bed height of 15.55 cm has been determined on fixing the C_o = 4%. The bed height should be less for more for efficient and economical adsorption. The average value of usable bed height is 15.90 cm for total bed height of 25 cm and which is relatively less.

4.3.4 MASS TRANSFER ZONE AND CAPACITY UTILIZATION FACTOR FOR SILICA GEL TYPE-III

The adsorbate gas amount in fluid phase and solid phase vary with time and the location inside the adsorption column. At initial, basically CO₂ movement takes place in the neighborhood of the bed input and feed comes in contact with fresh investigated sorbent. The bed characteristic for CO₂ adsorption, i.e. L_{MTZ} and f have been evaluated for SG and shown in Table 4.15. The breakthrough and saturation periods vary reciprocally with temperature, feed flows and CO₂ concentration. The width of mass transfer zone and utilization factor varies marginally with raised up temperature.

Table 4.15 Characteristic parameters of CO₂ adsorption for Silica gel type-III

T (K)	F (L/min)	C _o (vol.%)	t _b (s)	t _s (s)	L _{MTZ} (cm)	f
298	4	5	224	358	11.05	0.770
308	4	5	183	281	11.14	0.789
318	4	5	149	245	11.78	0.755
328	4	5	121	197	11.42	0.762
298	2	5	447	643	7.61	0.842
298	3	5	330	489	9.32	0.806
298	5	5	204	341	12.07	0.875
298	4	2	300	466	10.40	0.783
298	4	3	278	416	9.57	0.801
298	4	5	270	392	8.94	0.814

Reduced L_{MTZ} yields to an improved utilization factor. The shortest L_{MTZ} equivalent to 7.61 cm with utilization factor of 0.840 was tabulated at 298 K with F= 2 L/min and C_o= 5% for SG. The highest value of 11.78 cm of utilization factor was determined at 318 K, F= 4 L/min with C_o =5%. It is perceived clearly that L_{MTZ} rises with augmented flow rates yielding to reduced utilization factor. The SG type adsorbent showed maximal f = 0.875 at 298 K and F= 5 L/min with

$C_o=5\%$ with an average value of 0.800. The feed rates variations contribute considerably to L_{MTZ} and f as evident from the findings. The utilization factor (f) measured at various C_o do differ particularly under fixed operating conditions of temperature and feed flow. Generally, smaller L_{MTZ} signifies increased capacity utilization factor. Usually, the under different operating conditions, reduced L_{MTZ} imply good utilization factor.

4.3.5 TEMPERATURE PROFILES AND REPEATABILITY MEASUREMENT FOR SILICA GEL

Fig. 4.23 demonstrates the profiles of temperature measured by different sensors positioned at various distances in the fixed column. The data were collected for same SG type adsorbent. Temperature of hot-water circulator was fixed at 308 K by PID controller equipped with control console. Temperature sensors from T1 - T6 are located at different axial positions. Temperatures sensor type-K thermocouple has ± 0.15 K accuracy.

In general, temperature rise of magnitude $\Delta T= 283$ K to 323 K (10 - 50 °C) may possibly ensue on treating vapors with just 1% adsorbate gas component. The temperature rise is limited by heat loss for bed of small diameter; however a big adsorber will function nearly adiabatically. Mass transfer front is specified by increased temperature due to exothermic nature and supported by observed temperature vs. adsorption-desorption time profiles. Additionally, with higher concentration of adsorbate, the heat released during the adsorption result in increased temperatures. The measurement of repeatability for Silica gel is shown in Fig. 4.24. The data points of two runs were used to gauge repeatability. The data were measured at a 4 L/min and 308 K temperature with initial adsorbate concentration adjusted at 5%. The strong correlation between the data sets was revealed by $R^2 =0.99$. The mean error (σ) determined as $\pm 0.01 C/C_o$ in terms of dimensionless concentration. The measured value of σ defines exceptional conformity. It was suggested that repeatability was agreeable to reliance upon the adsorption data.

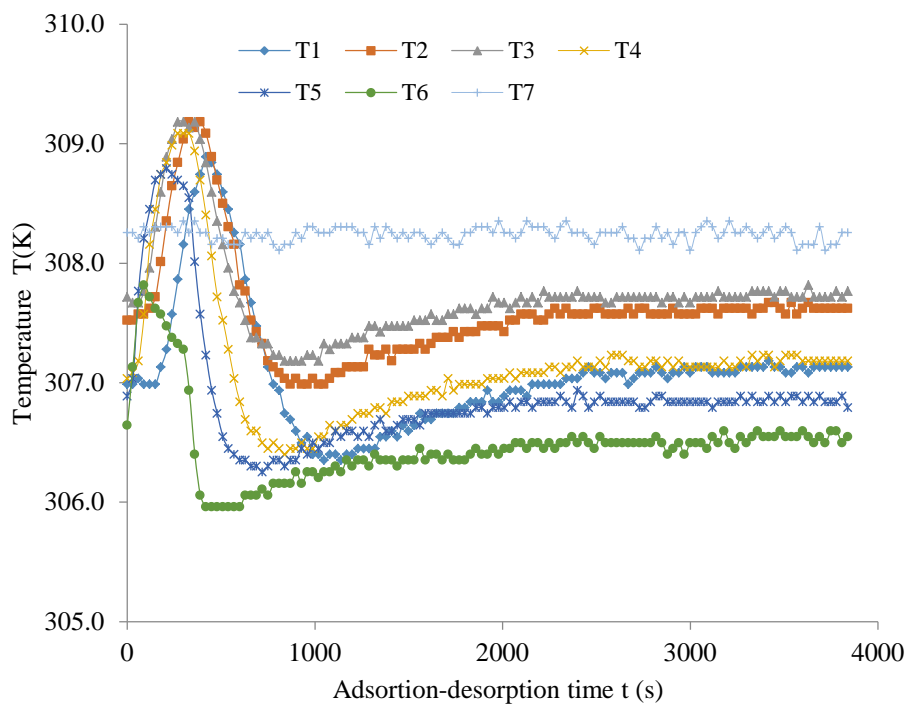


Fig. 4.23 Temperature contours for SG at $F= 4$ L/min, $C_o= 5\%$

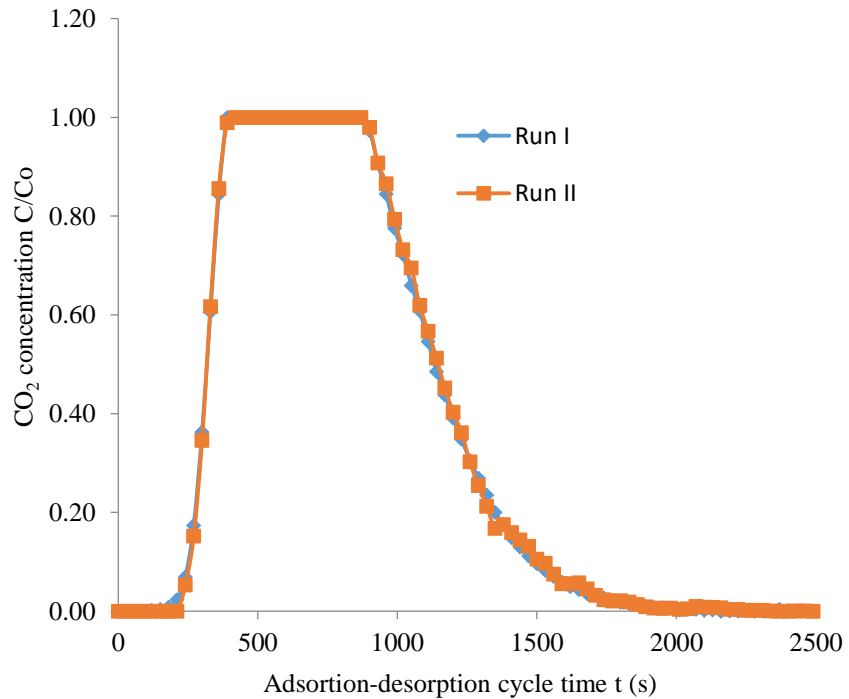


Fig. 4.24 Repeatability assessment utilizing SG at $F= 4$ L/min, $C_o=5\%$ and $T=308$

K

4.4 ADSORPTION STUDY USING ACTIVATED CARBON FROM DATE PITS

The date pits based biomass was purchased from the regional market of Abha City, Saudi Arabia. The Abha City is situated in the Asir Province of Saudi Arabia. This collected biomass was rinsed with distilled H₂O, a number of times to get rid of dust particles. After that, the sample was dried overnight at 150°C using oven. The size reduction of date pits was carried out by Ultrafine-Grinder (Model DLC-36250, Shine Best, Shenzhen, China). The milled biomass particles of different sizes were then passed through 4 mm screen (BS-series). The screened and undersize Date pits particles are stored in air-proof bottles for further activation purposes. The date trees and cleaned raw date pits are shown in Fig. 4.25 and Fig. 4.26, respectively.



Fig. 4.25 Date tree with dates



Fig. 4.26 Rinsed and cleaned date pits before size reduction

4.4.1 SYNTHESIS OF DATE PITS - DERIVED ACTIVATED CARBON

An activated carbon was synthesized using tubular furnace (MTI Corporation: OTF-1200 X) from date pits by physical activation. The tubular furnace consists of three different heating zones that can be utilized to fix three dissimilar temperatures at the same time span. Same or different biomass materials may be activated at the same time for activation purpose. A known sieved date pits weight was placed inside the tube of tubular furnace and subsequently, the temperature was raised at desired 283 K with a heating rate of 10°C/min with N₂ flow maintained equal to 150 ml/min to achieve the required temperature 873 K.

The N₂ flow has been constantly maintained for an additional 2 h for carbonization purpose. After that, the N₂ flow was stopped and CO₂ flow permits continually for 2 h at 873 K to develop desired porous carbon (AC-DS). The produced porous activated carbons from milled date pits are shown in Fig. 4.27. There is substantial reduction in adsorbent size after the activation from date pits

biomass. The produced activated carbon named as AC-DS with average size of 1.35 mm was selected for the experimental investigation.

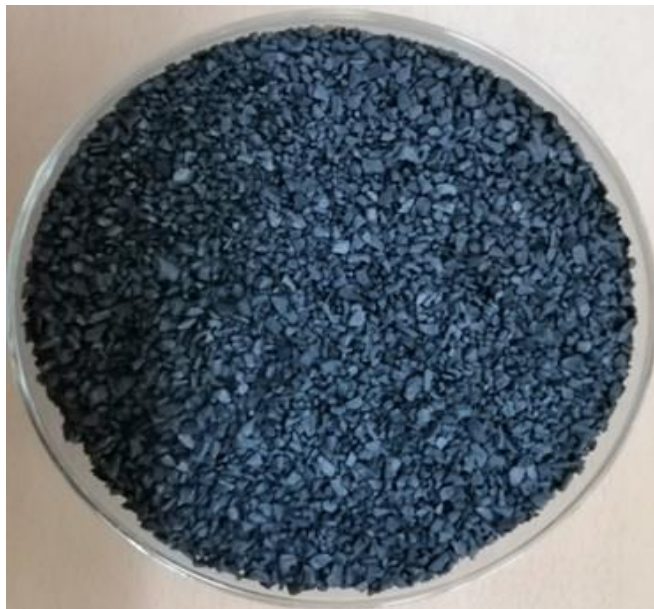


Fig. 4.27 An activated carbon produced from date pits

4.4.2 CHARACTERIZATIONS OF SYNTHESIZED ACTIVATED CARBON

Synthesized activated carbons (AC-DS) were characterized using NovaWin (Quantachrome) analyzer for surface properties with an outgas temperature of 573 K. Prior to determination of isotherms, the adsorbent samples were degassed by the degasser equipped with BET analyzer. After attaining the desired degassing temperature (523 K) through heating mental, the degas station is chosen with vacuum degas option. The degassing of the chosen adsorbent sample is conducted for the duration of 150 min. The analysis was carried out for a period of 88.3 min and N₂ was utilized for analysis purpose. The surface characterizations result for AC-DS are shown in Table 4.16. The high surface area (single point) equivalent to 848.27 m²/g was obtained for synthesized activated carbon AC-DS which is higher than other commercial examined adsorbents (AC-Norit). Significantly, surface areas smaller/ larger than 847.27 m²/g for AC-DS have been reported in literature for date pits- derived activated carbon. The surface area in the range 627-3337 m²/g obtained for date pits derived activated carbon using physical and

activation techniques has been very well reported [88, 89, 90, 91, 96,99, 101, 102 and 103] and these biomass adsorbents have been utilized for a variety of applications.

The BET multipoint surface area obtained for AC-Ds is also larger than that determined for other investigated adsorbents. The pore volumes equal to 0.45 cm³/g was obtained for AC-DS which is much larger than that obtained for SG (0.06 cm³/g). The pore volume of developed adsorbent based on biomass has been determined by Barrett –Joyner-Halenda method also termed as BJH. The pore radius of activated carbon is considerably larger equated to that of molecular sieve (MS-3Å). It is shown by tabulated data that the pores of produced AC-DS are in nm range. Also, BET analysis ratifies that the pore sizes are in nm range. Essentially, the adsorbents are very porous materials. The adsorption occurs mostly either at certain sites within the particles or on the pore walls of the adsorbent.

Table 4.16 BET surface characterization of date-pits derived activated carbon AC- DS

Surface characteristics	AC-DS
Single point surface area (m ² /g)	848.27
BET surface area (m ² /g)	821.69
Langmuir surface area (m ²)	956.87
Pore volume - BJH method (cm ³ /g)	0.41
Pore volume - DH method (cm ³ /g)	0.45
Pore radius –BJH method (Å)	22.68

The experimental N₂ isotherms and pore size distribution (BJH method) have been depicted in Fig. 4.28 (a) – (b) using N₂ gas of 99.999% purity, respectively. The Fig. 4.28(a) presents the N₂ isotherm developed for adsorption upto a pressure (P/P_o) of 0.99 for AC-DS whereas Fig. 4.28(b) represents pore size

distribution with pore size in nm scale. P_0 signifies total pressure selected during BET analysis.

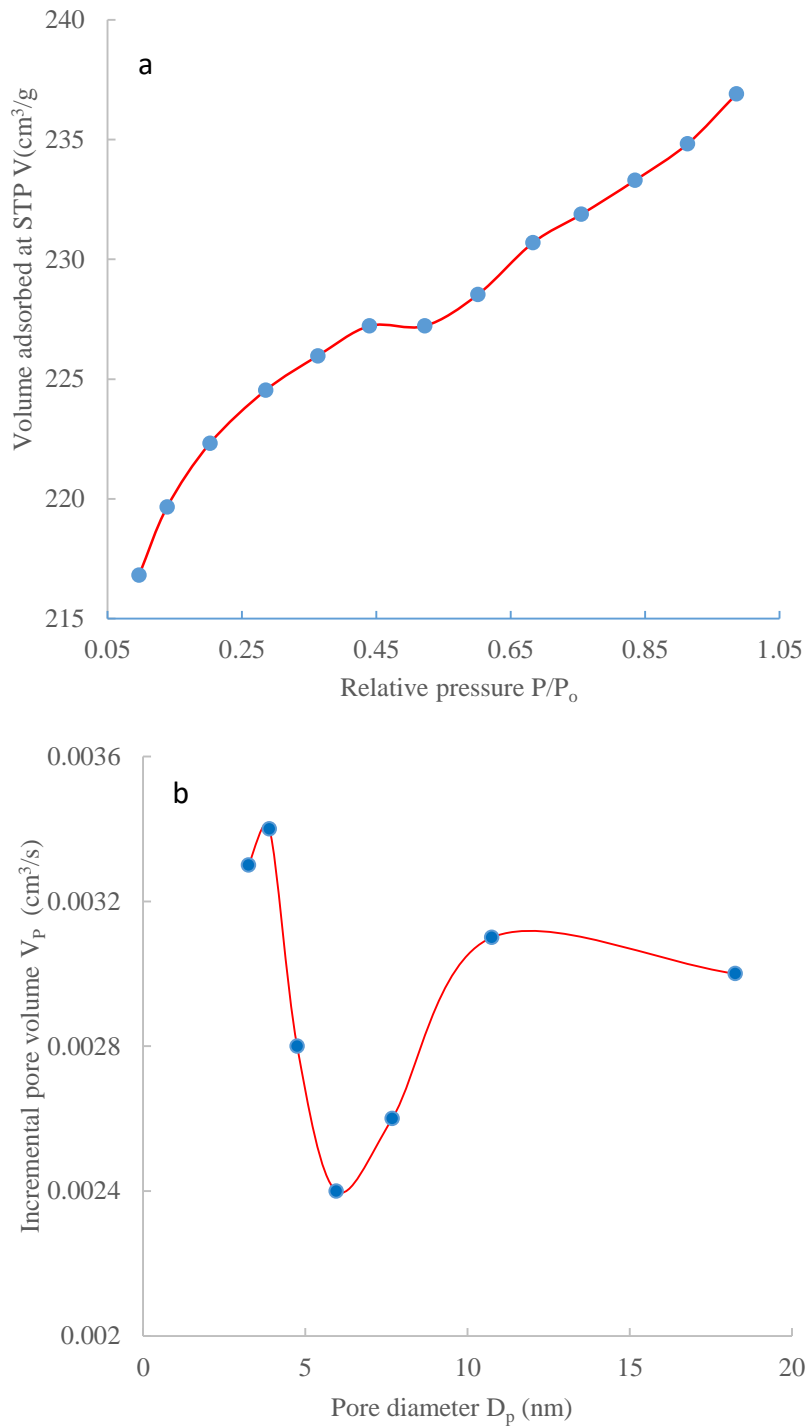


Fig. 4.28 N_2 - adsorption isotherm and PSD (a) Experimental adsorption isotherm for AC-DS, and (b) BJH pore size distribution for AC-DS

The surface morphology of developed activated carbon AC-DS was examined by the Scanning electron microscope (Model: Quanta 250-FEI, Japan). The structural image has been represented in Fig. 4.29 (a) –(b) for AC-DS. Owing to resolution limitations of SEM model, it is problematic to envision the pores on the surface of date pits - derived activated carbon. Many pores can be envisaged and the perceived pores are almost spread all over the surface, as depicted in Fig. 4.29 (a) with 2,500 x level and Fig. 4.29b with 20,000 x magnification level. SEM images exhibit a slit-like surface morphology, adding to a large surface area per unit weight of an adsorbent. The sample looks denser and agglomerates at higher magnification with large cavities. A clean surface for adsorbent promotes a large surface area. The high density and very regular pore structures are particularly effective for CO₂ separation by adsorption.

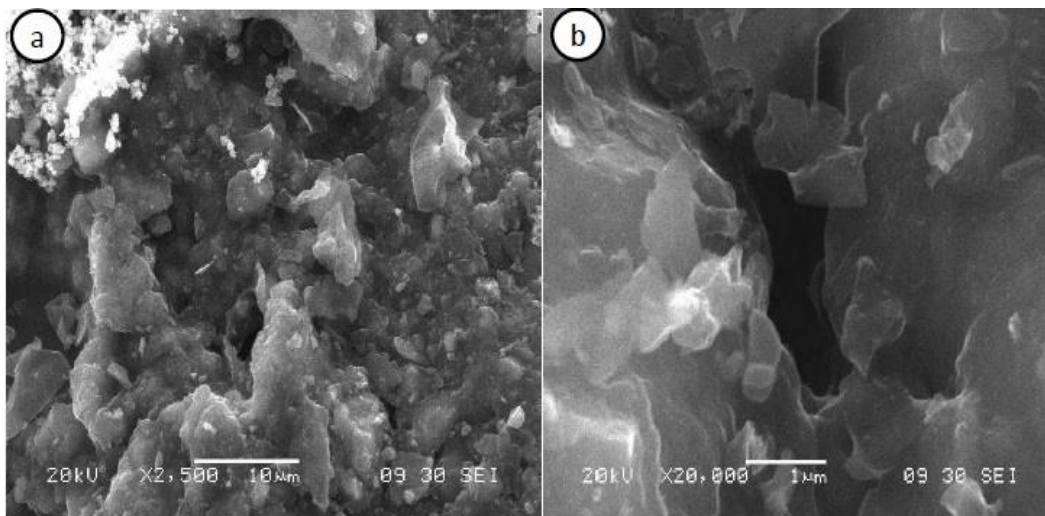


Fig. 4.29 (a) – (b) Morphological images of produced activated carbon AC-DS: (a) 2500 x magnification and (b) 20,000 x magnification

The thermogravimetric instruments-TGA (TG-209 FI Libra) is used to examine the behavior of date pits and developed carbon based adsorbent as shown in Fig. 4.30 (a) – (b). A sample mass (DS) of 18.4 mg was used and temperature increased to 900 °C (1173 K) at reasonable rate. The temperature was increased at a rate of 20 °C (293 K)/min to attain desired temperature of 900 °C (1173 K). Flow rate of N₂ purge gas was controlled at 20 ml/min. The reliance of weight

loss on temperature was measured by proximate analysis. The derivative weight change was described by ostensive loss of weight. A 5.11% change in weight is observed for a temperature less than 250 °C (523 K). The dependency of TG (%) on temperature for porous AC-DS has been observed as shown in Fig. 4.30 (b). A sample mass of 37.4 mg was heated upto 800 °C (1073 K) temperature with 20 °C (293 K)/min heating rate. The N₂ flow was controlled at 20 ml/min with protective gas rate fixed at 10 ml/min.

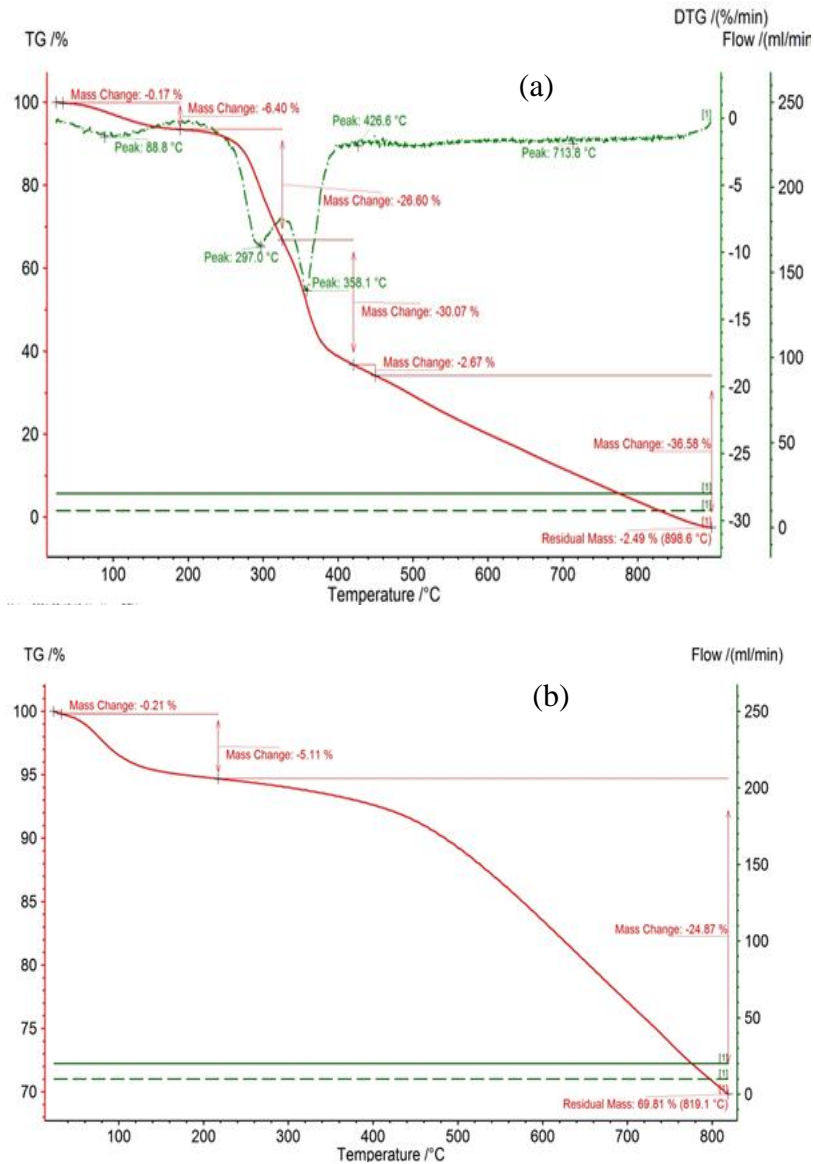


Fig. 4.30 Thermogravimetric analysis of (a) Date pits biomass, and (b) porous AC-DS

The synthesized activated carbon (AC-DS) was examined using X-ray diffraction (XRD) (Model- X'Pert Pro) for molecular structure of the sample. The scan range $2\theta = 0-100^\circ$ was selected to analyze X-ray patterns as presented in Fig. 4.31. The visualized unstructured form of biomass-derived adsorbent is credited to the existence of broad peaks. This is the desired characteristics of developed carbon-adsorbent for CO_2 capture. The peaks of diffraction at $2\theta = 23.96^\circ$ and 45.34° are imagined from porous material which are related to the peaks of amorphous carbon. Nearly the same diffraction peaks for developed activated carbon-based adsorbents also observed as reported in the literature [80].

The broad (002) peak ($2\theta = 15-30^\circ$) can be credited to unstructured nature of synthesized activated carbon adsorbent. The broad and weak (101) diffraction peak ($2\theta = 40-50^\circ$) are because of *a* axis of structure attributed to graphite. The nonexistence of sharp peaks indicates that the carbon structure is mostly amorphous which is advantageous for well-defined adsorbent.

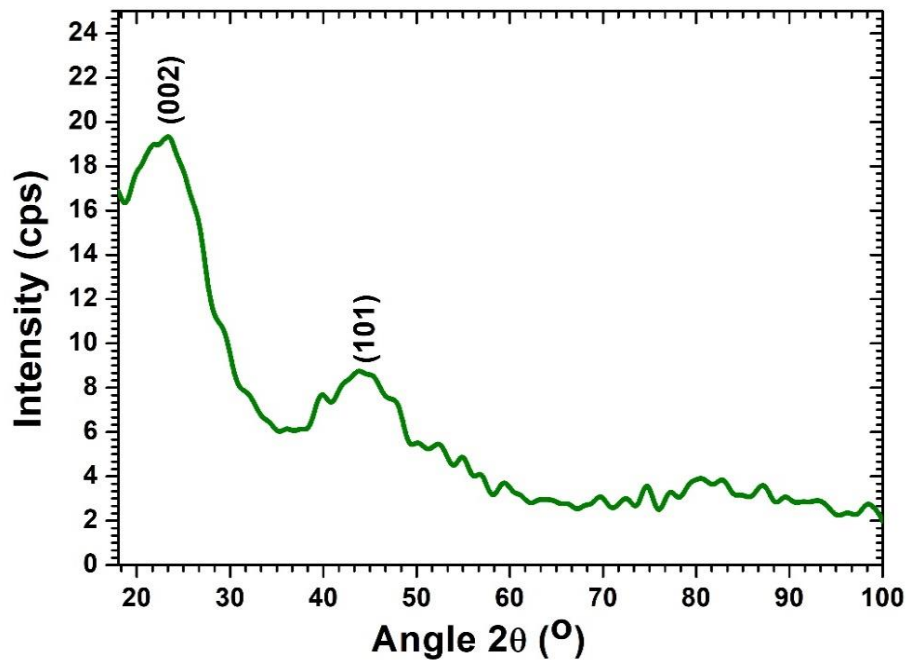


Fig. 4.31 XRD of date pits derived porous activated carbon AC-DS

The Raman spectra depicted in Fig. 4.32 was examined by a Raman Microscope (DXR FT-Thermofisher Scientific, Berlin Germany) equipped with excitation source of wavelength 532 nm with a laser power of 8 mW. The spectrum range of 0 – 3500 cm^{-1} was chosen for adsorbent scanning. The most intense bands were detected between 0 and 3500 cm^{-1} . The D and G bands were observed at 1341.82 cm^{-1} and 1590.07 cm^{-1} , respectively. The ratio of the D to G bands' intensity i.e., I_D/I_G postulates the level of the defects that occur in the produced adsorbent and the ratio was established to be equivalent to 0.799. A smaller I_D/I_G ratio confirms less carbon comprising defects ensuing the formation of O_2 -containing groups at the carbon surface.

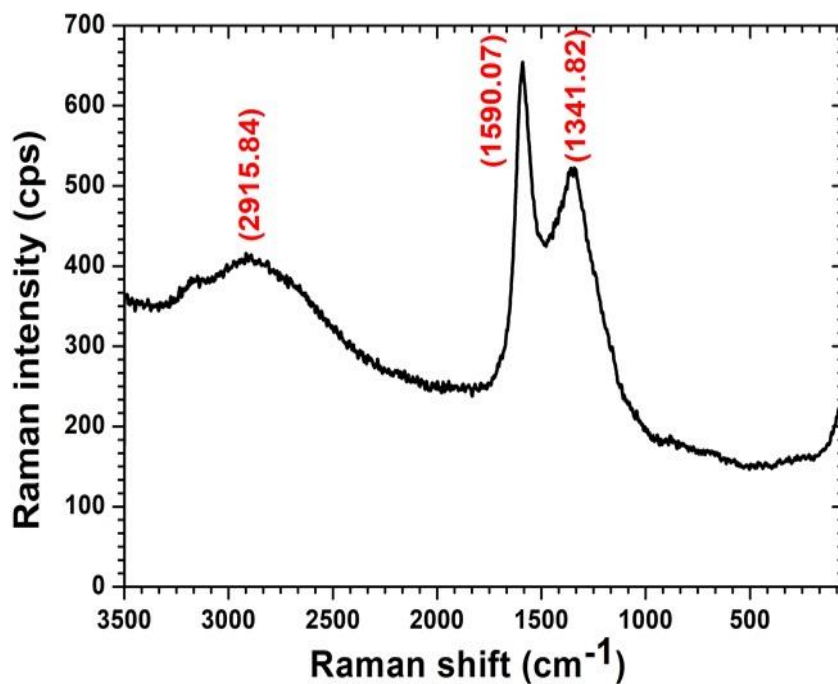


Fig. 4.32 Raman spectra for the produced activated carbon AC-DS in the spectrum range 0 – 3500 cm^{-1}

4.4.3 BREAKTHROUGH PROFILES USING DATE PITS DERIVED ACTIVATED CARBON

The equipped mass controllers equipped with control console are used to control and measure the feed flow. The data were obtained at 4 L/min feed flow with a CO_2 concentration fixed at 5% (vol. %) to examine the effect of temperature. The

operating pressure of fixed bed adsorption unit was adjusted at 1.25 bars. The prolonged breakthrough or saturation spans are constantly well-thought-out necessary for an improved CO₂ capture. At large, the longer breakthrough time at decreased temperatures endorses improved CO₂ adsorption capacity.

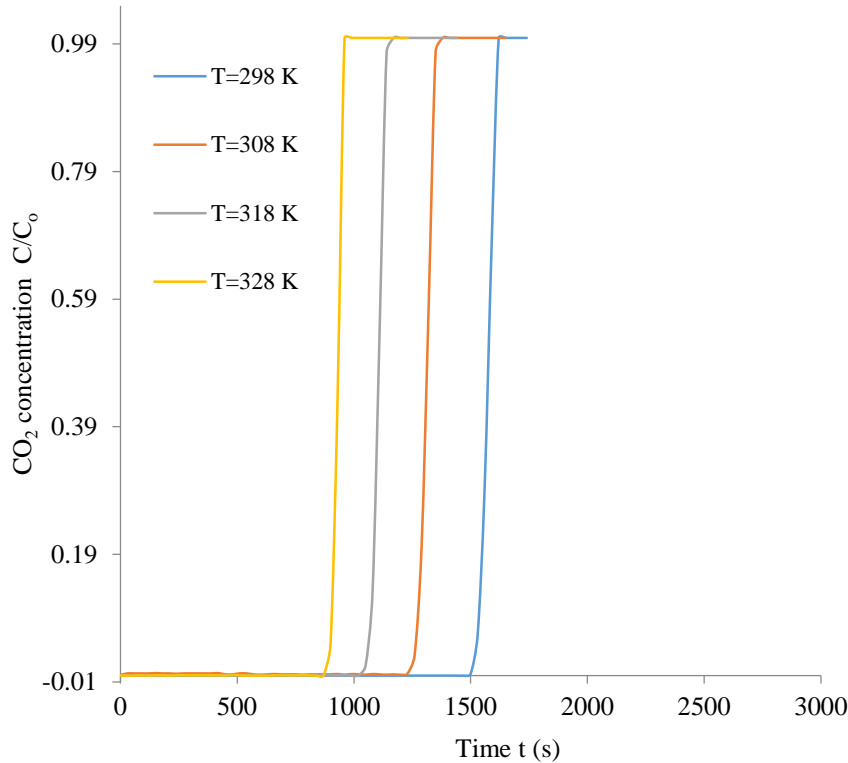


Fig. 4.33 Breakthrough profiles at various temperatures for activated carbon AC-DS at $F= 4 \text{ L/min}$, $C_o=5\%$

The breakthrough curves for AC-DS (Mass, $m_{ad} - 150 \text{ g}$) produced under examined temperature have been shown in Fig. 4.33. The breakthrough period considerably banks on the temperature at which the adsorption phenomenon occurs. Generally, the time it takes to attain 5% of the highest concentration (5% in the present case) in the feed is called breakthrough time. The longer saturation and breakthrough periods correspond to reduced temperature at 298 K. The prolonged breakthrough period of 1524 s was attained at 298 K temperature. The breakthrough period reduced to 1265 s with increased temperature at 308 K. The condition of breakthrough and saturation appears early analogous to 1059 s and

1138 s at 318 K. The uppermost examined 328 K credited to reduced breakthrough period of 900 s. Longer exhaustion/ or breakthrough time spans have been observed for AC-DS comparative to other investigated commercial adsorbents. The breakthrough profiles obtained for AC-DS are reasonably steeper compared to that obtained for Molecular sieve, AC-Norit and Silica gel and it signifies better utilization of bed capacity and reduced length of mass transfer zone for produced adsorbent.

An improved performance of adsorbent for CO₂ adsorption is exhaustively recognized by the steepness of breakthrough profile as apparent from Fig. 4.33. The exploitation of necessary CO₂ loading corresponding to breakthrough condition is preferred for cost-effective adsorption of carbon dioxide from feed. The abruptness of adsorption profiles credited to the thinness of mass transfer zone length (L_{MTZ}). A lesser MTZ zone describes quicker uptake of CO₂. The deviations in molecular weight of feed mixture gas molecules yield to the occurrence of adsorption phenomenon. In various occasions, the adsorbate is held resolutely and sufficiently to allow inclusive capture of CO₂ from feed mixture with very small or no adsorption of non-absorbable gas which is N₂ in present study. Indeed, steepness of adsorption breakthrough profiles shown in Fig. 4.33 identifies comparable utilization of CO₂ loading.

Fig. 4.34 depicts the dependence of feed flow on breakthrough response profiles for produced activated carbon from date pits. The feed flows in the range of 2 to 5 L/min have been chosen at 1.25 bars with 298 K bed temperature. The feed flow reliance on adsorption response profiles obtained for AC-DS are depicted in Fig. 4.34. The exhaustion and breakthrough times rely significantly on flow rate of feed gas mixture. The prolonged breakpoint and saturation periods of 2603 s and 2769 s are witnessed at flow of 2 L/min. The period equivalent to $C/C_0 = 0.05$ observed to decrease from 2603 s to 1833 s on increasing flow from 2 - 3 L/min at 298 K temperature. Additional, the breakthrough period reduced to 1564 s with augmented 4 L/min flow rate. The lowest breakthrough period of 1401 s was achieved for activated carbon at 5 L/min feed flow. It was comprehended clearly

that the longer breakthrough and exhaustion periods are obtained for activated carbon compared with other investigated adsorbents at any preset feed rate.

The adsorption breakthrough profiles produced under different feed rate for activated carbon are much steep as shown in Fig. 4.34. Similarly, enhanced bed capacity utilization is described by narrow mass transfer zone perceived for adsorption breakthrough profiles. The sharpness of the breakthrough contours is beneficial for the reasonable separation of CO₂ by adsorption from feed mixture. The concentration C increases at the adsorption column exit rapidly equivalent to the curves ending at the condition where the adsorbent is considered as unproductive and this occurs when the breakthrough point is achieved.

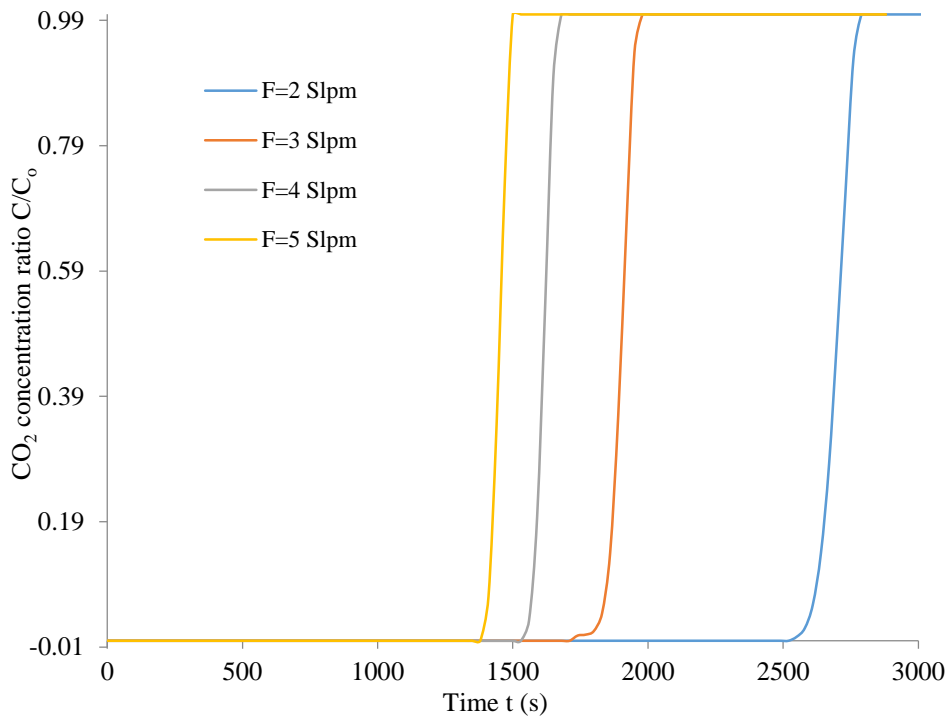


Fig. 4.34 Breakthrough profiles at different feed flow rates for AC-DS at T= 298 K, C₀=5%

The dependence of column exit concentration C on the breakthrough profiles for produced adsorbent AC-DS has been depicted in Fig. 4.35 under the same operating conditions of feed flow F = 4 L/min and temperature, T = 298 K. The various initial adsorbate concentrations in the range of 2 to 5% were controlled

with system pressure of 1.25 bars absolute. The prolonged breakthrough and saturation periods are always needed for increased CO₂ uptake/adsorption capacity. The breakthrough period is apparent to diminish with increased carbon dioxide concentration in feed. The minimal CO₂ concentration of 2% adds to exhaustion time equal to 2422 s. The breakthrough period reduced to 1884 s on raising the carbon dioxide concentration amount equal to 3% (vol.%). The 4% adsorbate concentration has showed early appearance of saturation period of 1976 s. Maximal 5% CO₂ concentration in the feed contribute to a breakthrough time of 1695 s and indicates that the increased initial CO₂ amount indicates an early appearance of exhaustion/breakthrough time spans. It was obviously observed that exhaustion and breakthrough periods are longer for date pits-derived activated carbon compared to that determined for other type of investigated adsorbents. The breakthrough period is comparative to the CO₂ loading and varies also inversely with feed concentration.

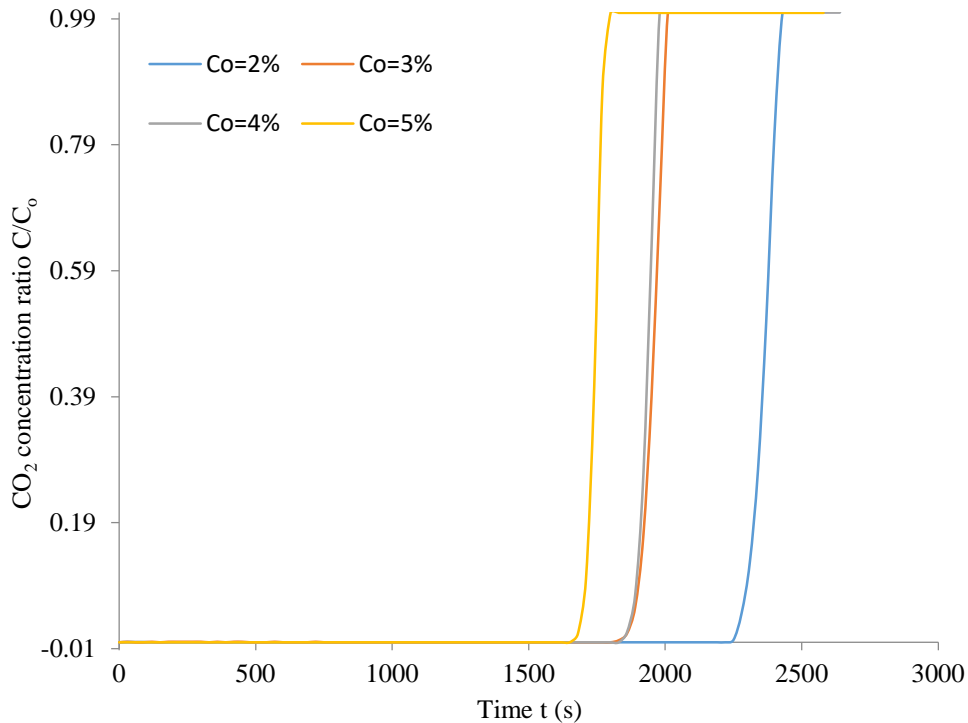


Fig. 4.35 Breakthrough profiles at different CO₂ level for AC-DS at F= 4 L/min, T= 298 K

4.4.4 ADSORPTION CAPACITY AND COLUMN EFFICIENCY FOR PRODUCED ACTIVATED CARBON AC-DS

The adsorption capacity, efficiency, and usable bed height for synthesized activated carbon AC-DS tabulated at various temperatures have been shown in Table 4.17. The CO₂ uptake differs considerably with temperature for produced activated carbons and varies negatively with temperatures. The maximal CO₂ loading (q) of 1.44 mmol/g was achieved for AC-DS compared to a lower value of 0.613 mmol/g for commercial AC-Norit at 298 K and 4 L/min flow rate. An adsorption loading 0.75 mmol/g is obtained for AC-DS under maximal investigated temperature of 328 K. Each CO₂ capture system based on adsorption depicts a decrease of the capture capacity with an augmented temperature.

Table 4.17 Adsorption characterizations for AC-DS at different temperatures with F = 4 L/min and C₀=5%

T(K)	q (mmol/g)	η (%)	L _b (cm)
298	1.436	94.4	23.59
308	1.150	93.8	23.46
318	0.942	93.1	23.26
328	0.752	93.9	23.49

The prepared activated carbon contributes to higher effective column efficiency (η) as evident from the Table 4.17. Furthermore, the column efficiency (η) based on column capacity obtained for developed activated carbon is significantly higher and a maximal value 94.4% at 298 K temperature is achieved. Considerably, the higher efficiency of AC-DS specifies its viability for efficient CO₂ capture. The effective column length (L) for the adsorption is 25 cm. It means the column was loaded with adsorbent upto a height of 25 cm. The maximal bed length of 23.59 cm was utilized for AC-DS which is higher than obtained for other investigated adsorbent. Industrially, the essential cycle time and

feed flow are the responsible for sizing of an adsorber. Using a bed length of less than or equivalent to 12 cm is sometimes recommended to decrease pressure drop and adsorber height. Though, empty bed necessities more regeneration energy and does not offer complete separation of CO₂ from other gas. It can be proposed that developed activated carbon performs superbly and appropriate for CO₂ separation from CO₂/N₂ feed mixture.

The adsorption performance with reference to an adsorption capacity, column efficiency and usable bed height for AC-DS tabulated at different feed flows has been depicted in Table 4.18. The CO₂ adsorption capacity differs positively and substantially with feed flow for produced carbons from Date pits based biomass. The highest CO₂ uptake of 1.66 mmol/g was obtained for AC-DS compared to a lesser value of other class of adsorbents under similar operating conditions (298 K and 5 L/min). The minimal examined feed flow of 2 L/min adds to a minimal capture capacity of adsorption and adsorption capacity nearly equal to 0.63 mmol/g was realized for AC-Norit at a temperature of 298 K and C₀= 5%. The adsorption performance of synthesized activated carbon is rationally higher at any constant feed flow rate. The developed activated carbon attributes to higher effective column efficiency as apparent from the Table 4.18. Correspondingly, the efficiency computed for synthesized carbon based adsorbent is noticeably greater with a highest value of 94.0% at 2 L/min with C₀= 5% and 298 K.

The utmost fraction of total capacity effectively utilized is 92.8 % for AC-Norit with a feed flow of 5 L/min under the similar conditions of temperature and initial adsorbate concentration. In over-all, it is realized that effective column efficiency decreases slightly with raised feed flow from 2 to 5 L/min. Suggestively, higher efficiency of AC-DS orders its appropriateness for economical CO₂ capture by adsorption. The usable bed length upto the breakthrough decreases with increased feed flows for AC-DS. The bed length of 23.50 cm is utilized in case of AC-DS higher than determined for any other examined grade of adsorbents. It can be projected that column efficiency and bed height utilized upto the breakthrough condition differs negatively with increased feed flows. The unutilized bed length

of other investigated adsorbents is more in comparison to AC-DS. It can be proposed that developed activated carbon does very well and appropriate for CO₂ separation from CO₂/N₂ feed gaseous mixture.

Table 4.18 Feed rates dependence on adsorption performance for AC-DS at C_o=5%, T=298 K

F (L/min)	q (mmol/g)	η (%)	L _b (cm)
2	1.234	94.0	23.50
3	1.308	94.0	23.49
4	1.487	93.9	23.48
5	1.661	93.8	23.44

An adsorption performance with reference to an adsorption capacity, column efficiency and usable bed height for synthesized activated carbon AC-DS determined as a function of C_o have been presented in Table 4.19. The CO₂ adsorption capacity differs mostly and direct proportionately with initial concentration of adsorbate gas (CO₂). The maximal CO₂ loading of 1.59 mmol/g is obtained for AC-DS equated to a lower capacity observed for other class of adsorbents at C_o=5% with 298 K and 4 L/min feed flow. The lowest C_o= 2 % adds to a minimal capacity of adsorption and an adsorption of capacity of 0.86 mmol/g is gauged for biomass-based porous activated carbon. The adsorbate capacity is proportionate with the initial adsorbate gas amount. The adsorption performance of synthesized activated carbon is reasonably higher at any value of initial adsorbate gas in feed mixture.

The prepared activated carbon attributes to higher effective column efficiency as shown in the Table 4.19. Also, the efficiency (η) calculated for synthesized carbon is high and highest η equal to 94.9% obtained at C_o= 4% CO₂ concentration in feed with 4 L/min flow rate and 298 K temperature. There is no clear tendency of efficiency deviation as a function of C_o. The cause of such efficiency variation is due to small change in concentration from 2 % to 5% with 1% incremental value. It is also suggested to use the adsorbate concentration in

the range of 0 - 5 % for the precise values. Especially, an improved efficiency of AC-DS specifies its suitability for efficient CO₂ capture. Also, extended bed length L_b is observed for AC-DS upto the breakthrough equated to the bed height exploited for other class of examined adsorbents for the total bed length of 25 cm. The bed length of 23.72 cm is utilized in case of AC-DS which is relatively higher equated to other type of adsorbents i.e. Molecular sieve, Norit-RB2 and Silica gel.

Surface area of AC-DS (848.27 m²/g) is slightly higher than obtained for AC-Norit (834.04 m²/g), however there is considerable difference in adsorption capacities and other performance parameters. In general, the CO₂ adsorption capacity increases with the increase in the surface area of the adsorbent. This is because when we increase the surface area, there are more adsorbing sites. Therefore, finely divided solids and some porous substances are suitable adsorbents. However, the surface area of the adsorbent is one of the reasons which define the adsorption rates on solid adsorbents; there are several physicochemical properties and the adsorption system parameters that highly influence the rate of adsorption of gases on solid adsorbents, as reported in the published literature. The pore size and its distribution, contaminates on the surface, surface electronic structure, acidic and essential nature of the surface and the gas, and operating conditions like adsorption temperature, flow rate, and diluent are a few parameters that were cited in the literature. The produced activated carbon performs judiciously well in view of adsorption capacity, column efficiency and utilized bed length relying on initial CO₂ volume in feed mixture.

Table 4.19 Adsorbate amount dependence on adsorption performance for AC-DS at F= 4 L/min and T=298 K

Co (vol.%)	q (mmol/g)	η (%)	L _b (cm)
2	0.862	94.1	23.53
3	1.067	94.0	23.49
4	1.405	94.9	23.72
5	1.594	94.8	23.70

The adsorption isotherms as a function of various temperature, feed rate and initial CO₂ concentration have been shown in Fig. 4.36 (a) – (c). The isotherms of adsorption at varied temperatures are shown in Fig. 4.36 (a). The CO₂ capture capacity augments to a great extent with an increased CO₂ partial pressure. The maximal uptake of 1.44 mmol CO₂/g has been determined at 0.25 bars (gauge) with 298 K temperature. Under the breakthrough condition, the CO₂ capacity decreases from 1.44 mmol/g to 0.07 mmol/g with decreased pressure from 0.25 bars to 0.01 bars. The lowest likely CO₂ loading of 0.053 mmol /g at 0.013 bars was determined and the capacity perceived to rise to 1.12 mmol/g at 0.25 bars for isotherm obtained at 308 K.

The CO₂ capture capacity of 1.07 mmol/g was obtained under condition of saturation at 308 K. The CO₂ loading of 0.94 mmol/g was evaluated at 318 K and 0.25 bars. The CO₂ loadings of 0.75 mmol/g and 0.04 mmol/g were determined at 328 K with 0.25 bars and 0.01 bars, respectively. The partial pressure of CO₂ is thought to add surely to augmented CO₂ capacity. Accordingly, it could be recommended from the curves shown in Fig. 4.36 (a), that rising CO₂ pressure will permit that more adsorbate molecules are adsorbed. The isotherms produced at 298 K with feed flow in the range of 2 to 5 L/min have been shown in Fig. 4.36 (b). The CO₂ uptake increases with increased feed flows and the pressure of CO₂ in the feed mixture of CO₂/N₂.

The saturation adsorbate capacity of 1.23 mmol/g was achieved at 0.25 bars (absolute) CO₂ pressure (C₀= 5%) with a feed rate of 2 L/min and an enhanced to 1.31 mmol/g at 3 L/min feed rate. The saturation and breakthrough conditions credited to capacity of 1.23 mmol/g and 0.12 mmol/g, respectively with 3 L/min feed flow and C₀= 5%. The CO₂ uptake was observed to increase to 1.49 mmol/g with 4 L/min at 0.25 bars. The feed rate of 5 L/min led to an increase of CO₂ capacity to 1.66 mmol/g at 0.25 bars. Usually, the CO₂ loading was recognized to enhance enormously and positively with the feed flow. The flows equivalent to 4 L/min and 5 L/min contribute to an adsorption uptakes of 1.17 mmol/g and 1.31 mmol/g with 0.20 CO₂ pressure (partial pressure), respectively. The dependence

of CO₂ uptake is highly apparent with partial pressures of CO₂ equated to gaseous flow rates.

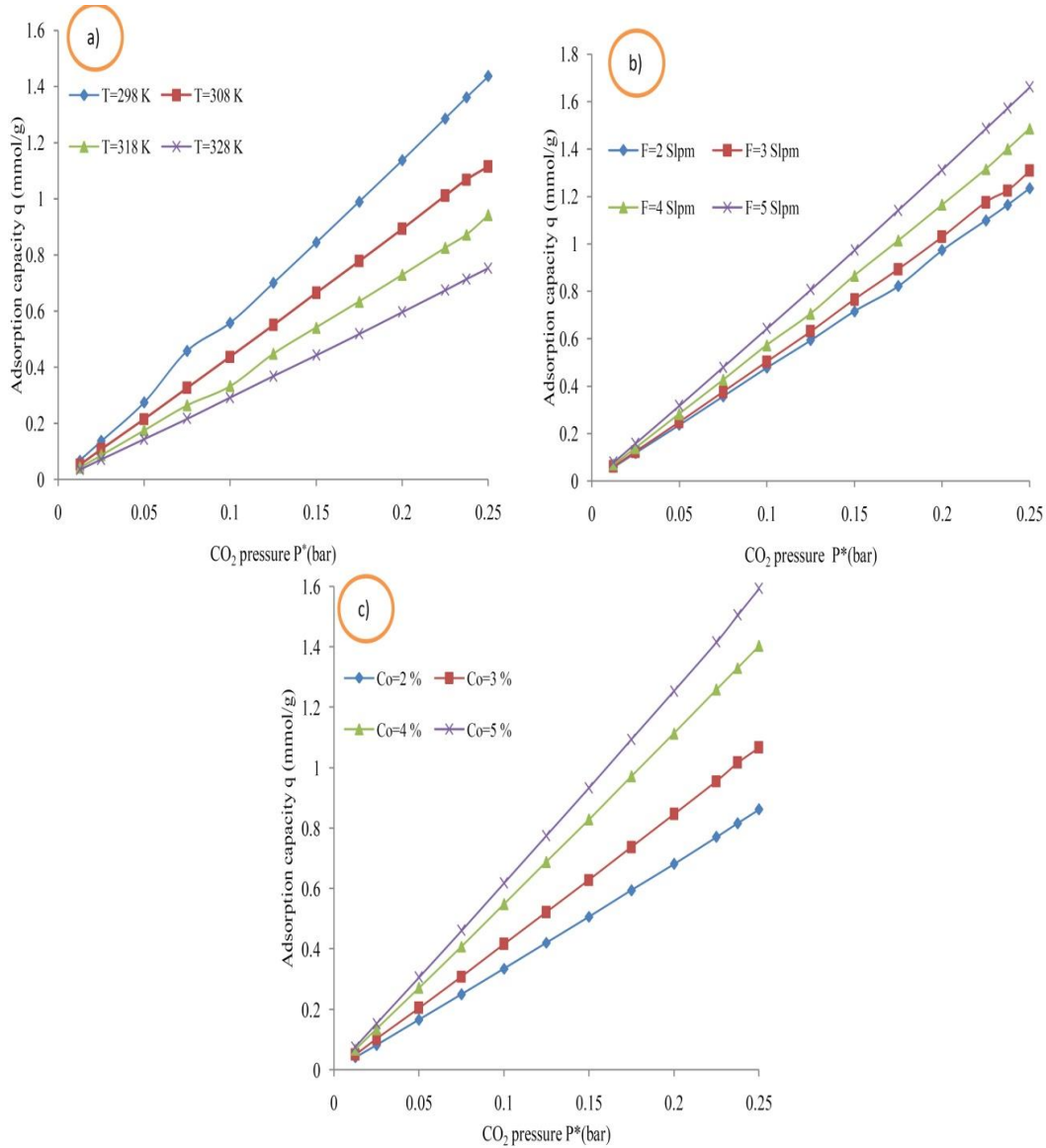


Fig. 4.36 Parametric dependence of CO₂ uptake; (a) at different temperatures with $C_0=5\%$, $F=4$ L/min, (b) at different feed flows with $C_0=5\%$, $T=298$ K and (c) at different initial levels with $T=298$ K, $F=4$ L/min

The dependence of initial CO₂ level on CO₂ capacity has been presented in Fig. 4.36(c) at $T=298$ K and $F=4$ L/min. The capture capacity varies positively with CO₂ concentration and partial pressure. The CO₂ uptake has been observed to

increase from 0.041 mmol/g to 0.816 mmol/g with augmented pressures from 0.013 bars to 0.238 bars at $C_o=2\%$. The maximal CO_2 capacity of 0.862 mmol/g was achieved at 0.25 bars with 2% CO_2 in feed mixture. The $C_o=3\%$ yields to 1.067 mmol/g CO_2 uptake at 0.25 bars gauge pressure of carbon dioxide.

The CO_2 uptake equivalent to 1.02 mmol/g has been determined at 0.25 bars gauge with $C = 95\% C_o$ under the condition of saturation. An adsorption capacity of CO_2 from feed consisting of CO_2 and N_2 has been perceived to increase from 0.07 mmol/g to 1.41 mmol/g with an increased in the CO_2 pressure from 0.013 bars to 0.25 bars at $C_o=4\%$. The 1.59 mmol/g CO_2 loading was realized at utmost examined pressure of 0.25 bars with $C_o=5\%$. As an outcome, it can be advocated that increased adsorbate gas in the feed mixture yields increased CO_2 uptake realistically.

4.4.5 MASS TRANSFER ZONE AND CAPACITY UTILIZATION FACTOR FOR AC-DS

The CO_2 concentration in fluid phase and solid phase vary with time and the position in the adsorption column. At initial stage, the CO_2 movement takes place in the neighborhood of the adsorption bed input and feed comes in contact with fresh adsorbent. The CO_2 amount in the feed bow out harshly with position effectually to zero before the end point of adsorption column is reached on condition that adsorbent has no CO_2 at the start of adsorption phenomenon. The segment of the bed wherever CO_2 essentially captured or the portion of the bed in which adsorbate concentration changes mostly is broadly known as zone of mass transfer (L_{MTZ}). The concentration limits are usually considered as $C = 5$ to $95\% C_o$ (vol.%). A thin MTZ characterizes an efficient utilization of the adsorbent leading to decreased regeneration cost. MTZ typically moves from the input to the output location signifying that an adsorbent adjacent to inlet position attained the state of saturation with CO_2 gas, consequently the MTZ moves towards the exit section of column.

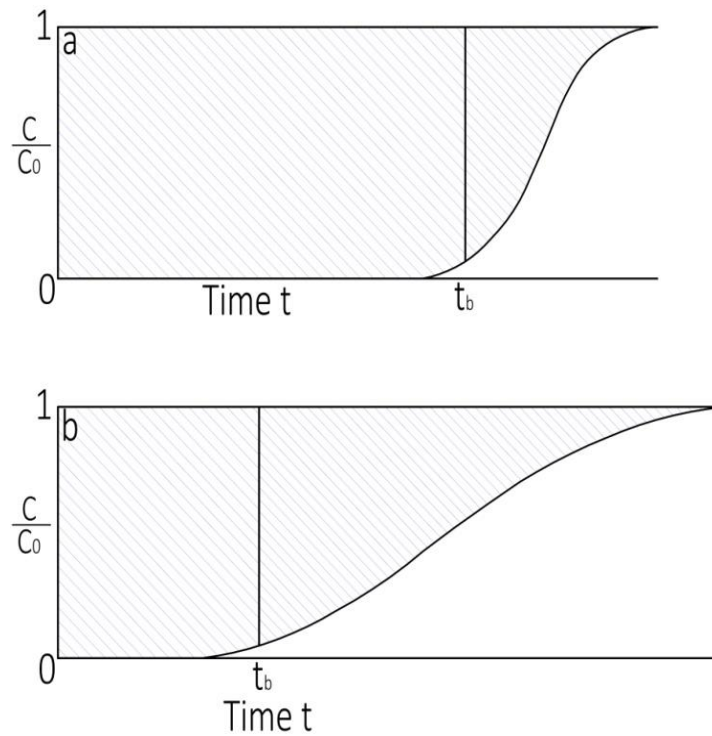


Fig. 37 (a) Breakthrough profile and narrow MTZ, and (b) breakthrough profile and wide MTZ

Fig. 4.37(a) – (b) demonstrates breakthrough curves with narrow and wide mass transfer zones. The narrow mass transfer zone corresponding to Fig.4.37 (a) is always desired for efficient utilization of bed capacity at breakthrough condition. The characteristics parameters for CO₂ adsorption determined for AC-DS have been presented in Table 4.20. The breakthrough period reduces with augmented temperatures in the investigated temperature range of 298 K to 328 K. The minimal L_{MTZ} of 1.20 cm for effective bed length of 25 cm was determined at 298 K yielding to improved utilization factor (f) of 0.974 cm with $F= 4$ L/min and $C_o= 5\%$. The factor f varies adversely with augmented temperature and highest value was determined at a temperature of 298 K. Smaller L_{MTZ} is always preferred for effectual adsorption of CO₂ from feed mixture causing an increase in utilization factor. The breakthrough and saturation periods decrease with increased feed flows in the range of 2 to 5 L/min. The variations in feed rate contribute slightly to L_{MTZ} and f as apparent from the results.

Table 4.20 Characteristic parameters of CO₂ adsorption for produced porous carbon

T(K)	F(L/min)	C _o (Vol.%)	t _b (s)	t _s (s)	L _{MTZ} (cm)	f
298	4	5	1524	1615	1.33	0.971
308	4	5	1265	1348	1.46	0.968
318	4	5	1059	1138	1.65	0.964
328	4	5	900	958	1.44	0.969
298	2	5	2603	2769	1.42	0.969
298	3	5	1833	1951	1.43	0.969
298	5	5	1401	1494	1.48	0.968
298	4	2	2280	2422	1.39	0.970
298	4	3	1884	2005	1.43	0.969
298	4	4	1875	1975	1.20	0.974

The closely the same L_{MTZ} and f were obtained at the feed flow of 2 and 3 L/min with fixed T= 298 and C_o = 5%. The CO₂ utilization factor of 0.696 is calculated at the similar feed flows. The saturation and breakthrough period also vary with initial adsorbate amount. The factor f assessed at different initial adsorbate volume do vary remarkably under constant operative conditions. The improved utilization factor of 0.974 was achieved with L_{MTZ} = 1.20 cm at adsorbate concentration of 4% at 298 K with 4 L/min feed flow. Mostly, an improved utilization factor is described by reduced mass transfer zone.

4.4.6 TEMPERATURE PROFILES AND REPEATABILITY MEASUREMENT FOR AC-DS

Fig. 4.38 represents the temperature profiles measured by thermocouples T1–T6 for adsorption-desorption cycle along the non-radial positions in the column. Temperature sensors T7 (308 K) relates to temperature of hot-water circulator and nearly remains equal to the set point.

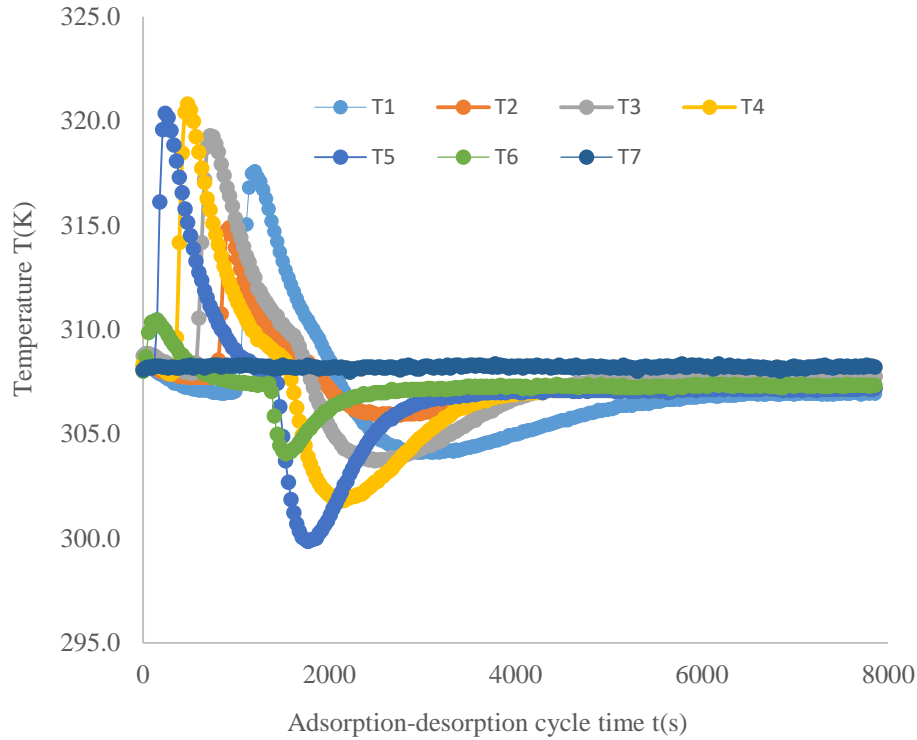


Fig. 4.38 Temperature profiles along axial positions inside column for AC-DS

All the temperature sensors are situated at various axial locations inside the column. Temperatures T6 and T1 relate to temperatures at extreme bottom and top positions, congruently. The temperatures T5 to T2 denote in-between temperatures from the bottom to top way. Each provided temperatures sensor is Type-K thermocouples with a precision of ± 0.15 K. The rise in temperature above the set value of 308 K during the adsorption period attributed to an exothermic nature of adsorption and related with the release of heat. Mass transfer front position is indicated by rise in temperature due to exothermic nature of adsorption and assisted by perceived profiles at different axial locations. Moreover, with increased concentration of CO_2 in feed mixture, the heat evolved due to adsorption process results in raised temperatures at various locations.

The re-applicability of the Date pits-derived activated carbon is studied by repeatability corresponding to Fig. 4.39. The data were collected at 298 K temperature, flow rate of 4 L/min with $C_o = 5\%$.

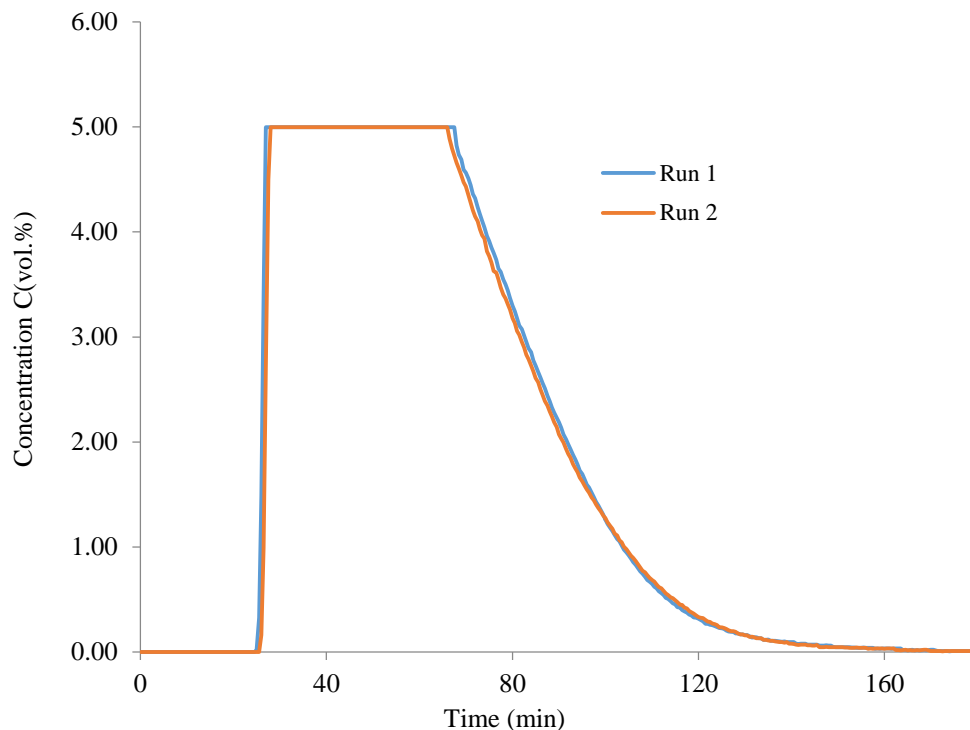


Fig. 4.39 Repeatability measurement of adsorption-desorption data of AC-DS

The strong relationship concerning the measurements is confirmed by $R^2 = 0.99$. The standard error for the data measured by sensor is gauged approximately equal to ± 0.20 L/min. The precision and supremacy of obtained data are confirmed satisfactorily by estimating the repeatability. The determined σ value explains exceptional conformity between the measurements and established that repeatability is good enough to trust on the obtained data.

4.5 ADSORPTION ISOTHERM STUDY

The adsorption isotherm study is conducted on the fixed bed continuous system filled with porous biomass derived adsorbent AC-DS. The temperature was controlled at 298 K with a total flow rate of 4 L/min. To fit the experimental adsorption equilibrium data of CO₂ adsorption on date derived adsorbent AC-DS, the Langmuir and Freundlich isotherm models are applied. From Figure 4.40(a), it is observed that the equilibrium CO₂ adsorption capacity of the AC-DS adsorbent at 298 K temperature continuously increases with the increase in partial pressure

of CO₂. The Langmuir adsorption isotherm seemed to be valid for the monolayer adsorption of adsorbate onto the limited identical adsorption active sites exist on the surface of the adsorbent. The adsorption capacity in this model is related to the adsorbent's specific surface area [69].

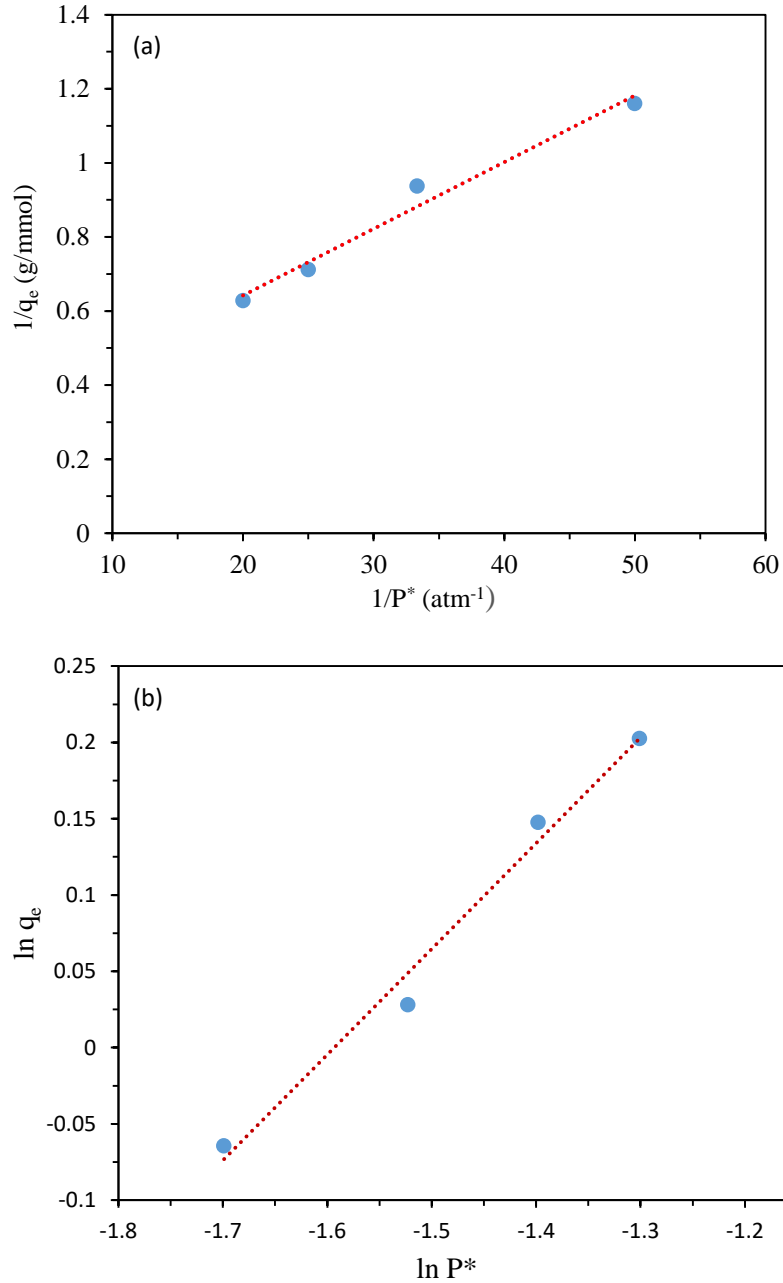


Fig.4.40 (a) Langmuir Isotherms (b) Freundlich Isotherm (Experimental conditions: T=298 K, Q = 4 L/min)

Table 4.21 summarizes the findings of Freundlich and Langmuir's model fitting, and the fitted model curves are depicted in Fig. 4.40 (a) – (b). From Table 4.21, the value of regression coefficients (R^2) larger than 0.95 for Langmuir isotherm suggested that the model fits reasonably well with the CO₂ adsorption data.

This also substantiated the hypothesis of monolayer coverage of adsorbate onto the surface of the AC-DS adsorbent. The separation factor (R_L) for the current experimental data is in the range of 0.01-0.1, demonstrating a favorable adsorption process ($0 < R_L < 1$). R_L 's low value implies that the adsorption on the date pits derived activated carbon is a physical and reversible process [81]. According to the Langmuir linear model, the maximum adsorption capacity of AC-DS adsorbent is obtained equal to 3.52 mmol/g. The equilibrium CO₂ adsorption data of AC-DS adsorbent is also analyzed according to the Freundlich isotherm. From Table 4.21, the R^2 (= 0.99) above the 0.95 for the Freundlich model indicates that the data fairly behaved according to the model. It can be suggested that CO₂ adsorption data under constant conditions of temperature and feed flow is very well fitted by Langmuir isotherm and Freundlich isotherm and is in agreement with the results reported by other authors [81].

Table 4.21 Langmuir and Freundlich isotherm constants for CO₂ adsorption on AC-DS adsorbent.

Langmuir isotherm				Freundlich isotherm			
q_L (mmol/g)	K_L (mmol/g.atm)	R_L	R^2	1/n	n	K_F (mmol/g) (atm) ^{-1/n}	R^2
3.52	15.62	0.01	0.97	0.67	1.47	0.34	0.99

4.6 COMPARATIVE ADSORPTION PERFORMANCES

4.6.1 ADSORPTION PERFORMANCES OF EXAMINED ADSORBENTS

The comparative analysis of CO₂ uptake determined for different class of adsorbents has been carried out under varied conditions of temperature, feed rate and initial adsorbate concentration as depicted in Table 4.22. The breakthrough time and adsorption capacity obtained for AC-Norit, MS-3Å, SG and AC-DS are summarized and depicted in Table. The breakthrough time varies substantially with temperature and inversely with temperature. The extended breakthrough period of 767 s is determined at 298 K and minimal value of 224 s for SG under constant conditions of F (= 4 L/min) and C_o (5%) is observed.

Table 4.22 Comparative breakthrough time and adsorption capacity obtained for various classes of adsorbents

T(K)	F (L/min)	C _o (vol.%)	AC-Norit		MS-3 Å		SG		AC-DS	
			t _b (s)	q (mmol/g)						
298	4	5	767	0.613	417	0.314	224	0.169	1524	1.436
308	4	5	705	0.519	388	0.265	183	0.124	1265	1.150
318	4	5	610	0.446	250	0.187	149	0.095	1059	0.942
328	4	5	523	0.377	210	0.153	121	0.092	900	0.752
298	2	5	1830	0.628	650	0.235	447	0.146	2603	1.234
298	3	5	1390	0.783	460	0.262	330	0.168	1833	1.308
298	5	5	1035	0.997	200	0.194	204	0.196	1401	1.661
298	4	2	1823	0.550	420	0.181	300	0.084	2280	0.862
298	4	3	1613	0.737	413	0.248	278	0.199	1844	1.067
298	4	4	1403	0.885	360	0.279	270	0.148	1875	1.405

Under same constant conditions of feed rate and initial concentration, a reduced breakthrough time of 417 s is obtained. It is also observed in case of all type of adsorbents examined for adsorption study, the capture capacity lessen with increased temperature from 298 K to 328 K. The adsorption capacity improved from 0.613 mmol/g to 0.519 mmol/g with an increased temperature from 298 K to

308 K. The improved capacity of 1.436 mmol/g is achieved at lowest studied temperature of 298 K for produced activated carbon AC-DS and reduced capture capacity of 0.752 mmol/g is obtained at elevated temperature of 328 K. An intermediate adsorption capacity in the range of 0.314 mmol/g to 0.153 mmol/g is observed for MS-3Å with varied temperatures from 298 K to 328 K. The lessening of adsorption capacity with increased temperature is in agreement with the adsorption exothermicity. When temperatures are increased, more excited adsorbent molecules are less susceptible to be trapped on the surface of adsorbent. As a consequence of this, at elevated temperature, the adsorbed molecule can transport back to gaseous phase easily since they have adequate energy to escape from attraction forces exercised by adsorbent surface and CO₂ molecule [81,106].

The breakthrough period reduces with increased flow rate in case of all examined adsorbents at constant temperatures and C_o, whereas the adsorption capacity improved with increased feed flow irrespective of adsorbent used. With increased flow, mass transfer zone moves faster attributing to high mass coefficient due to higher Reynolds number [56]. The Adsorption capacities of 0.997 mmol/g and 1.661 mmol/g have been observed at maximal flow of 5 L/min for AC-Norit and AC-DS, respectively. The capture capacity of CO₂ changes from 0.235 mmol/g to 0.262 mmol/g with an increased flow from 2 L/min to 3 L/min at fixed bed temperature and C_o for MS-3Å. The extended breakthrough period of 2603 s is observed for AC-DS at minimal flow of 2 L/min with 298 K and C_o=5%. The highest adsorption capacity of 1.66 mmol/g is determined at maximal flow of 5 L/min with C_o=5% at 298 K.

Capture capacity of CO₂ increases with increased initial CO₂ concentration in the range of 2 to 5% under fixed condition of temperature and feed rate for different examined adsorbents as depicted in the Table 4.22. The CO₂ uptake rises from 0.550 mmol/g to 0.885 mmol/g with an increased C_o from 2 to 4% at 298 K with a feed rate of 4 L/min. Similar trend of change of capacity with increased C_o is also observed for MS-3Å and a capacity of 0.279 mmol/g is observed at 4 % C_o and diminish with reduced initial concentration of adsorbate gas. The CO₂ adsorption

capacity is the amount of adsorbate CO₂ adsorbed once thermodynamic equilibrium is achieved, as CO₂ concentration (or CO₂ partial pressure) is increased, that is in accordance with the fact that P* is the adsorption driving force from thermodynamic perspective [81]. The CO₂ capture capacity for synthesized activated carbon follows increasing trend with higher values of initial concentration of adsorbate in feed and an improved capacity of 0.862 mmol/g is observed at C_o =2% with T=298 K and Q = 4 L/min. An adsorption capacity improved to 1.405 mmol/g on increasing the C_o to 4% by keeping constant temperature and feed rate.

The brief summary of adsorption capacity, efficiency and usable bed height determined for examined adsorbents is depicted in Table 4.23. The maximal and minimal adsorbent capacities of 0.997 mmol/g and 0.377 mmol/g are calculated for AC-Norit. The adsorbent MS-3Å contributes to lesser capacity of q_{max} = 0.314 mmol/g which is higher than that reported for silica gel under same operating conditions. The lowest and highest adsorption capacities equal to 0.752 mmol/g and 1.66 mmol/g are witnessed for AC-DS among all the examined adsorbents. Similarly, lowest efficiency (η_{max}= 72.75) based on column capacity is obtained for Silica gel. The bed filled with MS-3Å contributes to a maximal efficiency of 89.0%.

Table 4.23 Comparative analysis of adsorption capacity, column efficiency and usable bed height for different adsorbents

Adsorbent type	Adsorption capacity		Column efficiency		Usable bed height	
	q _{max} (mmol/g)	q _{min} (mmol/g)	η _{max} (%)	η _{min} (%)	L _{b,max} (cm)	L _{b,min} (cm)
AC-Norit	0.997	0.377	92.8	85.56	23.20	21.49
MS-3 Å	0.314	0.153	89.0	71.1	20.47	16.15
Silica gel	0.184	0.084	72.6	59.8	17.43	14.34
AS-DS	1.661	0.752	94.8	93.1	23.72	23.26

Among all the analyzed adsorbents, AC-DS performs well and improved efficiencies of $q_{\max} = 94.8\%$ and $q_{\min} = 93.1\%$ are achieved. The usable bed capacity signifies the capacity that can be effectively utilized upto the breakthrough point. The usable bed height equal to 21.49 cm is determined for a total bed height of 25 cm whereas minimum usable bed height corresponds to 14.34 cm for silica gel which is smallest among all the adsorbent examined. The maximum bed height nearly equal to 23.26 cm is obtained for produced activated carbon AC-DS.

The comparative analysis for adsorption performance parameters i.e. length of mass transfer zone and capacity utilization factor for analyzed adsorbents have been presented in Table. 4.24. The length of mass transfer zone is the section of column in which the CO_2 is actually adsorbed on the adsorbent. The MTZ is also referred as adsorption zone or critical bed depth [56]. The minimal mass transfer zone $L_{\text{MTZ}} = 1.87$ cm and maximal $L_{\text{MTZ}} = 3.88$ cm has been tabulated for commercial AC-Norit. The molecular sieve contributes to $L_{\text{MTZ, max}} = 8.04$ cm which is higher than the value obtained for AC-Norit. The longer mass transfer zone is undesired for economical separation of CO_2 from feed mixture. The longest mass transfer zone equal to 12.07 cm is determined for silica gel type adsorbent. The shorter mass transfer zones are obtained for AC-DS signifying the economical and efficient adsorption of CO_2 .

Table 4.24 Comparative analysis of length of mass transfer zone and capacity utilization factor for different adsorbents

Adsorbent type	Length of mass transfer zone		Utilization factor	
	$L_{\text{MTZ,max}}$ (cm)	$L_{\text{MTZ,min}}$ (cm)	f_{\max}	f_{\min}
AC-Norit	3.88	1.87	0.954	0.922
MS-3 Å	8.04	2.28	0.916	0.825
Silica gel	12.07	7.61	0.875	0.762
AS-DS	1.65	1.20	0.974	0.964

Also, minimal utilization factor is reported for Silica gel and it's value improved little further for MS-3Å adsorbent equal to $f_{\max} = 0.916$. The f_{\max} and f_{\min}

equivalent to 0.954 and 0.922 are obtained for AC-Norit nearly comparable to that AC-DS. Highest capacity utilization factor $f_{max} = 0.974$ has been determined for produced activated carbon from date pits–derived biomass. It can be recommended that produced activated carbon performs better in terms of performance parameters i.e. length of mass transfer zone and capacity utilization factor.

4.6.2 THE COMPARATIVE ADSORPTION PERFORMANCES OF CURRENT PROCESS WITH LITERATURE

The Table 4.25 summarized the operating conditions and adsorption capacities of current adsorption process with literature under batch and dynamic adsorption.

Table 4.25 Adsorption capacity of present study and reported in literature

Adsorbent	Temperature (K)	Pressure (bar)	Activation technique	Batch/dynamic adsorption	Adsorption capacity q (mmol/g)	Reference
Zeolite 13X	313	3.7	---	dynamic	4.70	[34]
Activated carbon	298	8	---	batch	4.10	[43]
Silica gel	298	6	---	dynamic	1.11	[47]
AC-white wood	298	1	physical, chemical	dynamic	1.80	[69]
AC-carbon black	291	1	physical & chemical	dynamic	0.57	[78]
AC-yellow tuff	298	0.25	---		0.71	[81]
AC-cherry stone	303	1	physical	dynamic	1.98	[84]
AC-olive stone	273	1	chemical & physical	batch & dynamic	4.81	[86]
AC-date stone	293	1	physical	batch	3.21	[101]
AC-date stone	298	2	physical	batch	2.94	[101]
AC-date sheets	273	1	chemical	batch	6.40	[101]
AC-Norit	298	1.25	physical	dynamic	0.99	current study
MS-3Å	298	1.25	physical	dynamic	0.31	current study
Silica gel	298	1.25	physical	dynamic	0.18	current study
AC-DS	298	1.25	physical	dynamic	1.66	current study

The activation method used in case of synthesized adsorbent is also provided in the table. An adsorption capacity of 4.7 mmol/g was obtained using commercial adsorbent 13X under dynamic adsorption study at 313 K [34]. Physically activated carbon based on cheery stone as biomass was examined for CO₂ adsorption using dynamic adsorption and CO₂ uptake of 1.98 mmol/g was achieved at 303 K with 1 bar [84]. Olive stone as biomass converted to porous adsorbent using physical and chemical activation techniques under batch and continuous mode achieving capture capacity of 3.21 mmol/g at 298 K and 1 bar [101]. In the present work, the data-pits derived activated carbon AC-DS produced by physical activation technique and examined in fixed bed column contributes a capture capacity of 1.66 mmol/g at 298K.

4.7 QUANTITATIVE ASSESSMENT OF ERROR

Quantitative assessment of error in terms of error bar for obtained results has been carried out. Standard error bars plays a decisive role in data analysis and interpretation, specifically by eliminating the sensors uncertainty or experimental uncertainty recorded in the final results. In the current study, the relationship between the adsorption parameters and temperature, error plots can be used to describe the uncertainty of the results present in the calculations of process performance parameters i.e. adsorption capacity, length of mass transfer zone, capacity utilization factor, efficiency and column capacity. Error bar is used to represent the quantitative assessment of error in the presented results as depicted in Fig. 4.41 and Fig.4.42. In Fig 4.41, x-axis represents the input as Temperature T (K) while y-axis represents output in terms of adsorption capacity q (mmol/g), length of mass transfer zone L_{MTZ} (cm) and capacity utilization factor (f). In Fig. 4.42, x-axis represents the input as Temperature T (K) while y- axis represent output as efficiency in terms of column capacity η (%) and usable bed height L_b (cm). Error bar is plotted using excel with an assumption of 0.05 significance level which states that the output (results) are reliable 95% with $\pm 5\%$ variation chances in the final output. In conclusion, standard error bars and error plots are

indications of uncertainty present in our data, giving valuable information on the level of uncertainty of the results.

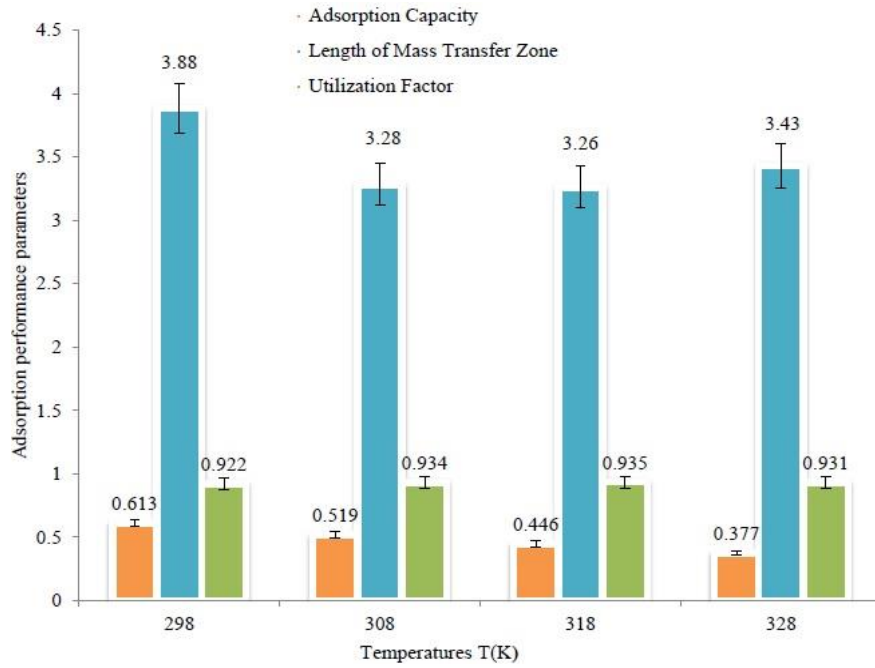


Fig.4.41 Error bar analysis of adsorption capacity, length of mass transfer zone and capacity utilization factor

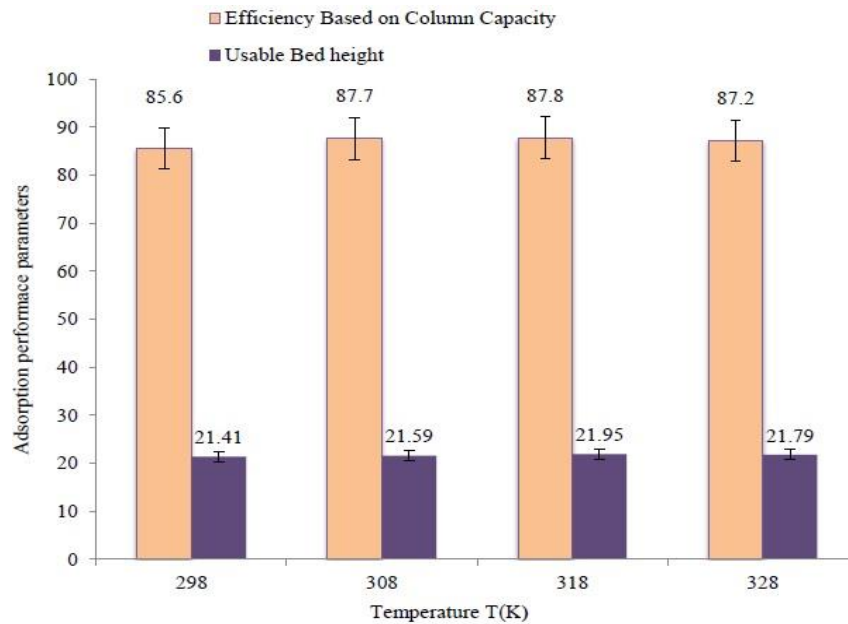


Fig.4.42 Error bar analysis of efficiency based on column capacity and usable bed height

CHAPTER 5: CONCLUSIONS AND FUTURE RECOMMENDATIONS

5.1 CONCLUSIONS

The improved surface and morphological characteristics have been observed for synthesized activated carbon (AC-DS) equated with other adsorbents i.e. activated carbon (Norit RB-2), Molecular sieve (MS-3Å) and Silica gel type-III (SG). The breakthrough and saturation periods reduce with increased temperature, feed rate adsorbate initial concentration in feed. The longer breakthrough period contributes to increased adsorption capacity under similar operating conditions. The prolonged breakthrough and saturation periods have been achieved for date pits derived activated carbon amongst all class of adsorbents. The vastly steep breakthrough curves for AC-DS signifies satisfactory exploitation of adsorbent ability under breakthrough condition. The maximal adsorption capacities of 1.66 mmol/g are determined for AC-DS and 0.196 mmol/g for Silica gel under similar operating conditions, respectively. The highest CO₂ capacity of 0.997 mmol/g and 0.314 mmol/g at 298 K with C₀=5% determined for Norit-RB2 and MS-3Å, respectively.

A thin mass transfer zone (L_{MTZ}) signifies an economic utilization of adsorbent material leading to the minimization of regeneration cost. The L_{MTZ} determined for all the adsorbents follow the order: 1.45 (AC-DS) < 1.87 (AC-Norit) < 2.28 (MS-3Å) < 7.61 (SG). The high capacity utilization factor is desired for good performance and the order is as: 0.974 (AC-DS) > 0.963 (AC-Norit) > 0.916 (MS) > 0.875 (SG). High efficiency based on column capacity ($\eta\%$) is determined for AC-DS equated with other class of adsorbents. The maximal column efficiency is determined for AC-DS whereas, the minimal is observed for Silica gel. The column efficiencies of investigated adsorbents are in the order as: 94.8% (AC-DS)

> 91.0 % (AC-Norit) > 89.0 % (MS-3Å) > 72.6 % (SG). The usable bed height, $L_b = 23.70$ cm is determined for AC-DS and minimal for SG (17.43 cm) for maximum effective bed height of 25 cm. The synthesized activated carbon performed better in terms of adsorption capacity, mass transfer zone, utilization factor for capacity, efficiency based on column capacity and usable bed height. The utilization of date pits-derived activated carbon may contribute to environmental pollution control by adsorption-based CO₂ capture. The outcomes of the study suggest that synthesized carbon based- adsorbent from date pits is significantly capable to capture CO₂ by adsorption under continuous mode in fixed bed column. The current target of protecting an environment will lead to an increase in the production of these biomass-derived materials in near future.

5.2 FUTURE RECOMMENDATIONS

An adoption which utilizes porous adsorbent is a favorable technology by reducing requirement for regeneration compared to widely used absorption technology. Relying on the results obtained from the study, the following recommendations are suggested for future work.

1. The effect of other emissions of combustion process such as moisture, N₂, CO, SO_x, NO_x on capture capacity and adsorption performances should be investigated.
2. Modeling and kinetics study of CO₂ adsorption using date pits derived activated carbons.
3. The study on the scale-up of CO₂ adsorption using date-pits derived activated carbon and necessary for implementing the capturing process on large scale.
4. The adsorption performances for CO₂ capture may be compared using date pits-derived porous adsorbents prepared by other activation techniques.
5. Better adsorbent structures [102] e.g. layer sheet having high mass transfer rate could be significant for enhanced adsorption.

REFERENCES

1. Rashidi, N.A.; Yusuf, S. (2016) An overview of activated carbons utilization for the post combustion carbon dioxide captures. *Journal of CO₂ utilization*. vol.13, pp.1–16.
2. Hester, R.E.; and Harrison, R.M. (2010) *Carbon capture, sequestration and storage*. 1st Edition, The Royal Society of Chemistry, Cambridge, 2010.
3. IEA (2003), *CO₂ capture at power stations and other major point sources*, Zero emission technologies for fossil fuels, OECD/IEA, Cedex.
4. Lee, S.Y.; Park, S.J. (2015) A review on solid adsorbents for carbon dioxide capture, *Journal of Industrial and Engineering Chemistry*. Vol. 23, pp.1-11.
5. Intergovernmental panel on climate change (2001) Climate Change synthesis report. Cambridge University Press, Cambridge.
6. Li, L.; Zhao, N.; Wei, W.; Sun, Y. (2013) A review of research progress on CO₂ capture, storage and utilization in Chinese Academy of Sciences. *Fuel*. Vol. 108, pp.112-130.
7. Choi, W.J.; Seo, J.B.; Jang, S.Y.; Jung, J.H.; Oh, K.J. (2009) Removal characteristics of CO₂ using aqueous MEA/AMP solutions in absorption and regeneration process. *Journal of Environmental Science*. Vol.21, pp.907-913.
8. Gupta, M.; Coyle, I.; Thambimuthu, K. (2003) Strawman document for CO₂ capture and storage technology roadmap. Canmet Energy Technology Centre, Natural Resources, Canada.
9. Brunetti, A.; Scura, F.; Barbieri, G.; Drioli, E. (2010) Membrane technologies for CO₂ separation. *Journal of Membrane Science*. Vol.359, pp.115-125.
10. Alabadi, A.; Razzaque, S.; Yang, Y.; Chen, S.; Tan, B. (2015) Highly porous activated carbon materials from carbonized biomass with high CO₂ capturing capacity. *Chemical Engineering Journal*. Vol.281, pp.606-612.

11. Figueroa, J.D.; Fout, T.; Plasynski, S.; Mcllcried, H.; Srivastava, R.D. (2008) Advances in CO₂ capture technology-The U.S. department of energy's carbon sequestration program. *International Journal of Greenhouse Gas Control*. Vol. 2, pp. 9-20.
12. Blomen, E.; Hendriksa, C.; Neele, F. (2009) Capture Technologies: improvement and promising developments. *Energy Procedia*. Vol. 1, pp.1505-1512.
13. Gibbins, J.; Chalmers, H. (2008) Carbon capture and storage. *Energy Policy*. Vol.36, pp. 4317-4322.
14. Garcia, S.; Gil, M.V.; Martin, C.F.; Pis, J.J.; Rubiera, F.; Pevida, C. (2011) Breakthrough adsorption study of a commercial activated carbon of a commercial activated carbon for pre-combustion carbon dioxide capture. *Chemical Engineering Journal*. Vol.17, pp.549-556.
15. Valverde, J.M.; Pontiga, F.; Soria-Hoyo, C.; Quintanlla, M.A.S.; Moreno, H.; Duran, H.; Espin, M.J. (2011) Improving the gas solids contact efficiency in a fluidized bed of carbon dioxide adsorbent fine particles. *Physical Chemistry Chemical Physics*. Vol.13, pp.14906-14909.
16. Yang, H.; Xu, Z.; Fan, M.; Gupta, R.; Slimane, R.B.; Bland, R.B.; Wright, I. (2008) Progress in carbon dioxide separation and capture: a review. *Journal of Environmental Science*. Vol. 20, pp.14-27.
17. MacDowell, N.; Florin, N.; Buchard, A.; Hallett, J.; Galindo, A.; Jackson, G.; Adjman, C.; Williams, C.K.; Shah, N.; Fannel, P. (2010) *An overview of carbon dioxide capture technologies*. *Energy and Environmental Science*. Vol.3, pp. 1645-1669.
18. Cohen, S.M.; Chalmers, H.L.; Webbe, M.E.; King, C.W. (2011) Comparing post-combustion carbon dioxide capture operations at retrofitted coal-fired power plants in the Texas and Great Britain electric grid. *Environmental Research Letters*. Vol.6, pp.1-14.
19. Li, J.; Ma, Y.; McCarthy, M.; Sculley, J.; Yu, J.; Jeong, H.; Balbuen, P. ; Zhou, H. (2011) Carbon dioxide-related gas adsorption and separation in

- metal-organic frameworks, *Coordination Chemistry Reviews*, Vol.255, pp.1791-1823.
20. Alonso, M.; Rodriguez, N.; Gonzalez, B.; Grasa, G.; Murillo, R.; Abanades, J.C. (2010) Carbon dioxide capture from combustion flue gases with a calcium oxide chemical loop: experimental results and process developments. *International Journal of Greenhouse Gas Control*. Vol.4, pp.167-173.
 21. Carapellucci, R.; Milazz, A. (2003) Membrane systems for CO₂ capture and their integration with gas turbine plants. Proceedings of the Institution of Mechanical Engineers Part A: *Journal of Power and Energy*. Vol. 217, pp.505-517.
 22. Stewart, S.; Hessami, M. (2005) A study of methods carbon dioxide capture and sequestration-the sustainability a photosynthesis bioreactor approach. *Energy conversion and management*. Vol.46, pp. 403-420.
 23. Ben-Mansour, R.; Habib, M.A.; Bamidele, O.E.; Basha, M.; Qasem, N.A.A.; Peedikakkal, A.; Laoui, T.; Ali, M. (2016) Carbon capture by physical adsorption: materials, experimental investigations and numerical modeling and simulations-A review. *Applied Energy*. Vol. 161, pp.225-255.
 24. Dong, R.; Lu, H.; Yu, Y.; Zhang, Z. (2012) A feasible process for simultaneous removal of CO₂, SO₂ and NO_x in cement industry by NH₃ scrubbing. *Applied Energy*. Vol. 97, pp. 185-191.
 25. Zhang, M.; Guo, Y. (2013) Rate based modeling of absorption and regeneration for CO₂ capture by aqueous ammonia solution. *Applied Energy*. Vol. 111, pp.142-152.
 26. Song, C.F.; Kitamura, Y.; Li, S.H. (2012) Evaluation of stirling cooler system for cryogenic CO₂ capture. *Applied Energy*. Vol.98, pp. 491-501.
 27. Nanada, S.; Reddy, S.N.; Mitra, S.K.; Kozinski, J.A. (2016) The progressive routes for carbon capture and sequestration. *Energy Science and Engineering*. Vol.4, No.2, pp.99-122.

28. Goetz, A.; Pupier, O.; Guillot, O. (2006) Carbon dioxide-methane adsorption on activated carbon. *Adsorption*. Vol.12, pp.55-63.
29. Rios, R.B.; Stragliotto, F.M.; Peixoto, H.R.; Torres, A.E.B.; Basto-Neto, M.; Azevedo, D.C.S.; Cavalcante Jr., C.L. (2013) Studies on the adsorption behavior of CO₂-CH₄ mixture using activated carbon. *Brazilian Journal of Chemical Engineering*. Vol.30, No.4, pp.939-951.
30. Raganati, F.; Ammendola, P.; Chirone, R. (2014) CO₂ adsorption on fine activated carbon in a sound assisted fluidized bed: effect of sound intensity and frequency. CO₂ partial pressure and fluidization velocity. *Applied Energy*. Vol. 113, pp.1269-1282.
31. Raganati, F.; Chirone, R.; Ammendola, P. (2020) CO₂ capture by temperature swing adsorption: working capacity as affected by temperature and CO₂ partial pressure. *Industrial and Engineering Chemistry Research*. Vol.59, No.8, pp.3593-3605.
32. Li, Y.; Yi, H.; Tang, X.; Li, F.; Yuan, Q. (2013) Adsorption separation of CO₂/CH₄ gas mixture on the commercial zeolites at atmospheric pressure. *Chemical Engineering Journal*. Vol.229, pp.50-56.
33. Mofarahi, M.; Gholipour, F. (2014) Gas adsorption separation of CO₂/CH₄ system using zeolite 5A. *Microporous and Mesoporous Materials*. Vol.200, pp.1-10.
34. Silva, J.A.C.; Cunha, A.F.; Schumann, K.; Rodrigues, A.E. (2014) Binary adsorption of CO₂/CH₄ in binderless beads of 13 X zeolite. *Microporous and Mesoporous Materials*. Vol.187, pp.100-107.
35. Gholipour, F.; Mofarahi, M. (2016) Adsorption equilibrium of methane and carbon dioxide on zeolite 13X: Equilibrium and the thermodynamic modeling. *The Journal of Supercritical Fluids*. Vol.111, pp.47-54.
36. Campo, M.C.; Ribeiro, A.M.; Ferreira, A.F.P.; Santos, J.C.; Lutz, C.; Loureiro, J.M.; Rodrigues, A.E. (2016) Carbon dioxide removal for methane upgrade by a VSA process using an improved 13X zeolite. *Fuel Processing Technology*. Vol.143, pp.185-194.

37. Garces-Polo, S.I.; Villarroel-Rocha, J.; Sapag, K.; Korili, S.A.; Gil, A. (2016) A comparative study of CO₂ diffusion from adsorption kinetic measurement on microporous materials at low pressures and temperature. *Chemical Engineering Journal*. Vol.302, pp.278-286.
38. Park, Y.; Ju, Y.; Park, D.; Lee, C. (2016) Adsorption equilibria and kinetics of six pure gases on pelletized zeolite 13X upto 1.0 MPa: CO₂, CO, N₂, CH₄, Ar and H₂. *Chemical Engineering Journal*. Vol.292, pp.348-365.
39. Jiang, N.; Shen, Y.; Liu, B.; Zhang, D.; Tang, Z.; Li, G.; Fu, B. (2020) CO₂ capture from dry gas by means of VPSA, TSA and TVSA. *Journal of CO₂ Utilization*. Vol.35, pp.153-168.
40. Wilkins, N.S.; Rajendran, A. (2019) Measurement of competitive CO₂ and H₂O adsorption on zeolite 13X for post-combustion CO₂ capture. *Adsorption*. Vol.25, pp.115-133.
41. Park, D.; Hong, S.H.; Kim, K.M.; Lee, C.H. (2020) Adsorption equilibria and kinetics of silica gel. *Separation Science and Technology*. Vol.251, pp.117326.
42. Sarkar, A.I.; Aroonwilas, A.; Veawab, A. (2017) Equilibrium and kinetic behavior of CO₂ adsorption onto zeolites, carbon molecular Sieve and activated carbons. *Energy Procedia*. Vol.114, 2450-2459.
43. Kacem, M.; Pellerano, M.; Delebarre, A. (2015) Pressure swing adsorption for CO₂/N₂ and CO₂/CH₄ separation: Comparison between activated carbon and zeolites performances. *Fuel Processing Technology*. Vol.138, pp. 271-283.
44. Wilson, S.M.W.; Kennedy, D.A.; Tezel, F.H. (2020) Adsorbent screening for CO₂/CO separation for applications in syngas production. *Separation and Purification Technology*. Vol. 235, pp.116268.
45. Zhao, R.; Deng, S.; Wang, S.; Zhao, L.; Zhang, Y.; Liu, B.; Li, H.; Yu, Z. (2018) Thermodynamic research of adsorbent materials on energy

- efficiency of vacuum-pressure swing adsorption cycle for CO₂ capture. *Applied Thermal Engineering*. Vol.128, pp.818-829.
46. Shi, W.; Yang, H.; Shen, Y.; Fu, Q.; Zhang, D.; Fu, B. (2018) Two-stage PSA/VSA to produce H₂ with CO₂ capture via steam methane reforming (SMR). *International Journal of Hydrogen Energy*. Vol.43, pp. 19057-19074.
47. Ferella, F.; Puca, A.; Taglieri, G.; Rossi, L.; Gallucci, K. (2017) Separation of carbon dioxide for biogas upgrading to biomethane. *Journal of Cleaner Production*. Vol.164, pp.1205-1218.
48. Li, J.-R.; Ma, Y.; McCarthy, M.C.; Scully, J.; Yu, J.; Jeong, H.-K.; Balbuena, P.B.; Zhou, H.-C. (2011) Carbon dioxide capture-related gas adsorption and separation in metal-organic frameworks. *Coordination Chemistry Reviews*. Vol.255, pp. 1791-1823.
49. Younas, M.; Rezakazemi, M.; Daud, M.; Wazir, M.B.; Ahmad, S.; Ullah, N.; Inamuddin.; Ramakrishna, S. (2020) Recent progress and remaining challenges in post-combustion CO₂ capture using metal-organic frameworks (MOFs). *Progress in Energy and Combustion Science*. Vol.80, pp.100849.
50. Song, G.; Zhu, X.; Chen, R.; Liao, Q.; Ding, Y.-D.; Chen, L. (2016) An investigation of CO₂ adsorption kinetics on porous oxide. *Chemical Engineering Journal*, Vol.283, pp.175-183.
51. Xu, X.; Zhao, X.; Sun, L.; Liu, X. (2008) Adsorption separation of carbon dioxide, methane, and nitrogen on H β and Na-exchanged β -zeolite. *Journal of Natural Gas Chemistry*. Vol.17. pp.391-396.
52. Sayari, A.; Belmabkhout, Y. (2010) Stabilization of Amine-Containing CO₂ adsorbents: dramatic effect of water vapor. *Journal of American Chemical Society*, Vol.132, pp.6312-6314.
53. Serna-Guerrero, R.; Sayari, A. (2010) Modeling adsorption of CO₂ on amine-functionalized mesoporous silica.2: kinetics and breakthrough curves. *Chemical Engineering Journal*. Vol.161, pp.182-190.

54. Sayari, A.; Belmabkhout, Y.; Da'na, E. (2012) CO₂ Deactivation of supported amines: does the nature of amine. *Langmuir*. Vol.28, pp.4241-4247.
55. Salmasi, M.; Fatemi, S.; Rad, M.D. (2013) Study of carbon dioxide and methane equilibrium adsorption on silicoaluminophosphate-34 zeotype and T-type zeolite. *International Journal of Environment Science and Technology*. Vol.10. pp.1067-1074.
56. Monazam, E.R.; Spenik, J.; Shadle, L.J. (2013) Fluid bed adsorption of carbon dioxide on immobilized polyethylenimine (PEI): kinetic analysis and breakthrough behavior. *Chemical Engineering Journal*. Vol.223, pp. 795-805.
57. Liu, D.; Yi, H.; Tang, X.; Zhao, S.; Wang, Z.; Gao, F.; Li, Q.; Zhao, B. (2016) Adsorption separation of CO₂/CH₄ mixture on carbon molecular sieve modified by potassium carbonate. *Journal of Chemical Engineering and Data*. Vol.61, No.7, pp.2197-2201.
58. Tiwari, D.; Goel, C.; Bhunia, H.; Bajpai, P.K. (2017) Dynamic CO₂ capture by carbon adsorbents: kinetic, isotherm and isotherm and thermodynamic studies. *Separation and Purification Technology*. Vol.181, pp.107-122.
59. Liu, X.; Zhai, D.; Sun, Y. (2017) Different CO₂ adsorbents-modified SBA-15 sorbent for highly selective CO₂ capture. *Chemical Physics Letter*. Vol.676, pp.53-57.
60. Sanz-Perez, E.S.; Dantas, T.C.M.; Arencibia, A.; Calleja, G.; Guedes, A.P.M.A.; Araujo, A.S.; Sanz, R. (2017) Reuse and recycling of amine-functionalized silica materials for CO₂ adsorption. *Chemical Engineering Journal*. Vol.308, pp.1021-1033.
61. Shahrom, M.S.R.; Wilfred, C.D.; Chong, F.K. (2018) Thermodynamics and kinetic studies on CO₂ capture with Poly[VBTMA][Arg]. *Journal of Physics and Chemistry of Solids*. Vol.116, pp.22-29.

62. Liu, Y.; Yu, X. (2018) Carbon dioxide adsorption properties and adsorption/desorption kinetics of amine-functionalized KIT-6. *Applied Energy*. Vol.211, pp.1080-1088.
63. Srensecek-Nazzal, J.; Narkiewich, U.; Morawski, A.W.; Wrobel, R.; Gesikiewicz-Puchalska, A.; Michalkiewicz, B. (2016) Modification of commercial activated carbons for CO₂ adsorption. *Acta Physica Polonica A*. Vol. 129.No. 3, pp.394-401.
64. Wang, X.; Guo, Q. (2016) CO₂ adsorption behavior of activated coal char modified with Tetraethylenepentamine. *Energy and Fuels*. Vol.30, No.4, pp.3281-3288.
65. Toprak, A.; Kopac, T. (2017) Carbon dioxide adsorption using high surface area activated carbons from local coals modified by KOH, NaOH and ZnCl₂ agents. *International Journal of Chemical Reactor Engineering*. Vol.15, No.3 pp.20160042.
66. Shen, C.; Grande, C.A.; Li, P.; Yu, J.; Rodrigues, A.E. (2010) Adsorption equilibria and kinetics of CO₂ and N₂ on activated carbon. *Chemical Engineering Journal*. Vol.160, pp.398-407.
67. Hao, W.; Bjorkman, E.; Lilliestrale, M.; Hedin, N. (2013) Activated carbon prepared from hydrothermally carbonized waster biomass used as adsorbent for CO₂ capture. *Applied Energy*. Vol.112, pp.526-532.
68. David, E.; Kopac, J. (2014) Activated carbons derived from residual biomass pyrolysis and their CO₂ adsorption capacity. *Journal of Analytical and Applied Pyrolysis*. Vol. 110, pp.322-332.
69. Shahkarami, S.; Azargohar, R.; Dalai, A.K., Soltan, J. (2015) Breakthrough CO₂ adsorption in bio-based activated carbons. *Journal of Environmental Science*. Vol.34, pp. 68-76.
70. Lira-Zuniga, S.; Sauz-Navarrete, C.; Rodriguez-Cordova, R.; Herrera-Zepelin, L.; Herrera-Urbina, R. (2016) CO₂ adsorption on agricultural biomass combustion ashes. *Madaras. Ciencia y Tecnologia*. Vol.18, No.4, pp.607-616.

71. Hong, S.-M.; Jang, E.; Dysart, A.D.; Pol, V.G.; Lee, K.B. (2016). CO₂ capture in the sustainable wheat-derived activated microporous carbon compartment. *Nature Reports*. Vol. 6, pp. 34690.
72. Calvo-Munoz, E.M.; Garcia-Mateos, F.J.; Rosas, J.M.; Rodriguez-Mirasol, J.; Cordero, T. (2016) Biomass waste carbon materials as adsorbents for CO₂ capture under post-combustion conditions. *Frontiers in Materials*. Vol.3, pp.23.
73. Geng, Z.; Xiao, Q.; Lu, H.; Li, B.; Wu, H.; Lu, Y.; Zhang, C. (2016) One step synthesis of microporous carbon monoliths derived from biomass with high nitrogen doping content for highly selective CO₂ capture. *Scientific Reports*. Vol.6, pp.30049.
74. Zhang, C.; Song, W.; Ma, Q.; Xie, L.-J.; Zhang, X. (2016) Enhancement of CO₂ capture on biomass-based carbon from Black locust by KOH activation and ammonia modification. *Energy and Fuels*. Vol.30, No.5, pp.4181-4190.
75. Serafin, J.; Narkiewicz, U.; Morawski, A.W.; Wrobel, R.J. (2017) Highly microporous activated carbons from biomass for CO₂ capture and effective microspores at different conditions. *Journal of CO₂ Utilization*. Vol.18, pp. 73-79.
76. Cai, W.; Zhang, S.; Hu, X.; Jaroniec, M. (2018) In situ synthesis of N-enriched activated carbons from *Procambarus Clarkii* shells with enhanced CO₂ adsorption performance. *Energy and Fuels*. Vol.32, No.9, pp. 9701-9710.
77. Peredo-Mancilla, D.; Ghouma, I.; Hort, C.; Ghimbeu, C.M.; Jeguirim, M.; Bessieres, D. (2018) CO₂ and CH₄ adsorption behavior of biomass-based activated carbon. *Energies*, Vol.22, pp.3136.
78. Raganati, F.; Alfe, M.; Gargiulo, V.; Chitone, R.; Ammendola, P. (2019) Kinetic study and breakthrough analysis of the hybrid physical/chemical CO₂ adsorption/desorption behavior of a magnetite-base adsorbent. *Chemical Engineering Journal*. Vol.372, pp.526-535.

79. Zhu, M.; Cai, W.; Verpoort, F.; Zhou, J. (2019) Preparation of pineapple-derived porous carbon with enhanced CO₂ capture performance by hydrothermal carbonation-alkali metal oxalates assisted thermal activation process. *Chemical Engineering Research and Design*. Vol.146, pp.130-140.
80. Kim, M.-J.; Choi, S.W.; Kim, H.; Mun, S.; Lee, K.B. (2020) Simple synthesis of spent coffee ground-based microporous carbons using K₂CO₃ as an activation agent and their application to CO₂ capture. *Chemical Engineering Journal*. Vol.397, pp. 125404.
81. Ammendola, P.; Ragnati, F.; Chirone, R.; Miccio, F. (2020) Fixed bed adsorption as affected by thermodynamics and kinetics: Yellow tuff for CO₂ capture. *Powder Technology*. Vol.373. pp. 446-458.
82. Sarwar, A.; Ali, M.; Khoja, A.H.; Nawar, A.; Waqas, A.; Liaquat, R.; Naqvi, S.R.; Asjid, M. (2021) Synthesis and characterization of biomass-derived surface-modified activated carbon for enhanced CO₂ adsorption. *Journal of CO₂ Utilization*. Vol.46, pp.101476.
83. Lewicka, K. (2017) Activated carbons prepared from hazelnut shells, walnut shells and peanut shells for high adsorption. *Polish Journal of Chemically Technology*. Vol. 19, No.2, pp.38-43.
84. Alvarez-Gutierrez, N.; Gil, M.V.; Rubiera, F.; Pevida, C. (2017) Kinetics of CO₂ adsorption on cherry stone-based carbons in CO₂/CH₄ separations. *Chemical Engineering Journal*. Vol.307, pp. 249-257.
85. Acevedo, S.; Giraldo, L.; Moreno-Pirajam, C. (2020) Adsorption of CO₂ on activated carbons prepared by chemical activation with cupric nitrate. *ACS Omega*. Vol.5, No.18, pp.10423-10432.
86. Balsamo, M.; Silvestre-Albero, A.; Silvestre-Albero, J.; Erto, A.; Rodriguez-Reinoso, F.; Lancia, A. (2014). Assessment of CO₂ adsorption capacity on activated carbons by a combination of batch and dynamics tests. *Langmuir*. Vol.30, pp.5840-5848.

87. Reddy, K.S.K.; Al Shoaibi, A.; Srinivasakannan, C. (2012) Activated carbon from date pits palm seed: process optimization using response surface methodology. *Waste and Biomass Valorization*. Vol.3, pp.149-156.
88. Reddy, K.S.K.; Al Shoaibi, A.; Srinivasakannan, C. (2015) Preparation of porous carbon from date palm seeds and process optimization. *International Journal of Environmental Science and Technology*. Vol. 12, pp.959-966.
89. Banat, F.; Al-Asheh, S.; Makhadmeh, L. (2003) Preparation and examination of activated carbons from date pits impregnated with potassium hydroxide for the removal of methylene blue from aqueous solution. *Adsorption Science and Technology*. Vol.21, No.6, pp.597-606.
90. Belhachemi, M.; Rios, R.V.R.A.; Addoun, F.; Silvestre-Albero, j.; Sepulveda-Escribano, A.; Rodrigues-Reinoso, F. (2009) Preparation of activated carbon from date pits: Effect of activation agent and liquid phase oxidation. *Journal of Analytical and Applied Pyrolysis*. Vo.86, pp.168-172.
91. Merzougui, Z.; Azoudj, Y.; Bouchemel, N.; Addoun F. (2011) Effect of activation method on the pore structure of activated carbon from date pits application to the treatment of water. *Desalination and water treatment*. Vo. 29, pp.236-240.
92. Pasalari, H.; Ghaffari, H.R.; Mahvi, A.H.; Pourshabani.; Azari, A. (2017) Activated carbon derived from data stone as natural adsorbent for phenol removal from aqueous solution. *Desalination and Water Treatment*. Vol.72, pp. 406-417.
93. Al-Saad, K.; EI-Azazy, M.; Issa, A.A.; Al-Yafie, A.; EI-Shafie,A.S.; Al-Sulaiti, M.; Shomar, B. (2019) Recycling of data pits into green adsorbent for removal of heavy metals: A fractional factorial design–based approach. *Frontiers in Chemistry*. Vol.7, pp.552.

94. Krishnamoorthy, R.; Govindan, B.; Banat, F.; Sagadevan, V.; Purushothaman, M.; Show, P.L. (2019) Date pits activated carbon for divalent ions removal. *Journal of Bioscience and Bioengineering*. Vol.128, No.1, pp.88-97.
95. Berber, M.R. (2020) Surface-functionalization of activated carbon with polyglucosamine polymer for efficient removal of cadmium ions. *Polymer Composite*. Vol.41, pp. 3074-3086.
96. Belhamdi, B.; Merzougli, Z.; Laksaci, H.; Belabed, C.; Boudiaf, S.; Trari, M. (2020) Removal of dissolved organic nitrogen amino acid from aqueous solutions using activated carbon based on date pits. *Water Practice and Technology*. Vol.15, No.4. pp.1158-1173.
97. Mansour, R.A.E.; Simeda, M.G., Zaatout, A.A. (2021) Removal of brilliant green dye from synthetic wastewater under batch mode using chemically activated date pit carbon. *RSC Advances*. Vol.22, pp.7851-7861.
98. Hussein, A.A.; Fadhil, A.B. (2021) Kinetics and isothermal evaluations of adsorptive desulfurization of dibenzothiophene over mixed bio-wastes derived activated carbon. *Energy Resources, Part A: Recovery, Utilization, and Environmental Effects*, doi:10.1080/15567036.2021.1895372.
99. Hijab, M.; Saleem, J.; Parthasarthy, P.; Mackey, H.R.; McKay, G. (2021) Two-stage optimization for malachite green removal using activated carbon date pits. *Biomass conversion and Biorefinery*. Vol.11, pp. 727-740.
100. Ogungbenro, A.E.; Quang, D.V.; Al-Ali, Khalid, Abu-Zahra, M.R.M. (2017) Activated carbon from date seeds for CO₂ capture applications. *Energy Procedia*. Vol.114, pp. 2313-2321.
101. Ogungbenro, A.E.; Quang, D.V.; Al-Ali, Khalid, Vega, L.F.; Abu-Zahra, M.R.M. (2018) Physical synthesis and characterization of activated carbon

- from date seeds for CO₂ capture. *Journal of Environmental Chemical Engineering*. Vol.8, pp.4245-4252.
102. Li, J.; Michalkiewicz, B.; Min, J.; Ma, C.; Chen, X.; Gong, J.; Mijowska, E.; Tang, T. (2019) Selective preparation of biomass-derived porous carbon with controllable pore sizes toward highly efficient CO₂ capture. *Chemical Engineering Journal*. Vol.360, pp.250-259.
103. Bahamon, D.; Ogungbenro, A.E.; Khaleel, M.; Abu-Zahra, M.R.M.; Vega, L.F. (2020) Performance of activated carbons derived from date seeds in CO₂ swing adsorption determined by combining experimental and molecular simulation data. *Industrial and Engineering Chemistry Research*. Vol.59, No.15, pp.7161-7173.
104. Al Mesfer, M.K.; Amari, A.; Danish, M.; Al Alwan, B.A.; Shah, M. (2021) Simulation study of fixed-bed adsorption from CO₂/N₂ mixture using activated carbon. *Chemical Engineering Communications*. Vol.208, No.9, pp. 1358-1367.
105. Pota, A.A.; Mathews, A.P. (1999) Effect of particles stratification on fixed bed adsorber performance. *Journal of Environmental Engineering*. 8, pp.705-711.
106. Zhou, X.; Yi, H.; Tang, X.; Deng, H.; Liu, H. (2012) Thermodynamics for the adsorption of SO₂, NO and CO₂ from flue gas on activated carbon fiber, *Chemical Engineering Journal*. Vol.200-202, pp.399-404.

Summary of research articles

1. Danish, M.; Vijay, Parthasarthy.; Al Mesfer, M.K. (2021) CO₂ capture using activated carbon synthesized date stone: breakthrough, equilibrium, and mass transfer zone. Carbon Letters. Vol.31, pp. 1261-1272.
<https://link.springer.com/article/10.1007/s42823-021-00249-y>
2. Danish, M.; Vijay, Parthasarthy.; Al Mesfer, M.K. (2021) CO₂ Capture by low-cost date pits-based activated carbon and silica gel. Materials. Vol.14, No.14, pp.3885.
<https://www.mdpi.com/1996-1944/14/14/3885>
3. Danish, M.; Vijay, Parthasarthy.; Al Mesfer, M.K. (2021) Comparative study of CO₂ capture by adsorption in sustainable date pits-derived porous activated carbon and molecular sieve. International Journal of Environmental Research and Public Health. Vol.18, No.16, pp.8497.
<https://www.mdpi.com/1660-4601/18/16/8497>
4. Danish, M.; Vijay, Parthasarthy.; Al Mesfer, M.K. (2022) Evaluating CO₂ capture performance by adsorption using synthesized and commercial activated carbon. Separation Science and Technology. Vol.57, No.9, 1392-1407.
<https://doi.org/10.1080/01496395.2021.1986070>

Turnitin Originality Report

PhD1 by Danish Md

From Quick Submit (Quick Submit)

- Processed on 24-Jul-2022 4:13 PM IST
- ID: 1874384008
- Word Count: 26558

Similarity Index

8%

Similarity by Source

Internet Sources:

2%

Publications:

7%

Student Papers:

N/A

sources:

- 1 < 1% match (publications)
[R. Ben-Mansour, M.A. Habib, O.F. Bamidele, M. Basha, N.A.A. Gasem, A. Peedikakkal, T. Laoui, M. Ali, "Carbon capture by physical adsorption: Materials, experimental investigations and numerical modeling and simulations – A review", Applied Energy, 2016](#)
- 2 < 1% match (publications)
[Qinglin Li, Halrong Zhang, Fen Peng, Can Wang, Hailong Li, Lian Xiong, Haijun Guo, Xinde Chen, " Monoethanolamine-Modified Attapulgite-Based Amorphous Silica for the Selective Adsorption of CO from Simulated Biogas ", Energy & Fuels, 2020](#)
- 3 < 1% match (publications)
[Qinglin Li, Halrong Zhang, Fen Peng, Can Wang, Hailong Li, Lian Xiong, Haijun Guo, Xinde Chen, " Monoethanolamine-Modified Attapulgite-Based Amorphous Silica for the Selective Adsorption of CO from Simulated Biogas ", Energy & Fuels, 2020](#)
- 4 < 1% match (publications)
[Qinglin Li, Halrong Zhang, Fen Peng, Can Wang, Hailong Li, Lian Xiong, Haijun Guo, Xinde Chen, " Monoethanolamine-Modified Attapulgite-Based Amorphous Silica for the Selective Adsorption of CO from Simulated Biogas ", Energy & Fuels, 2020](#)
- 5 < 1% match (Internet from 10-Oct-2021)
<https://www.science.gov/topicpages/c/capture+du+co2>
- 6 < 1% match (Internet from 13-Mar-2022)
<https://www.science.gov/topicpages/o/oas+technologies+co2cc>
- 7 < 1% match (publications)